1985ApJ...291..722T

THE ASTROPHYSICAL JOURNAL, 291:722–746, 1985 April 15
© 1985. The American Astronomical Society. All rights reserved. Printed in U.S.A.

PHOTODISSOCIATION REGIONS. I. BASIC MODEL

A. G. G. M. TIELENS AND DAVID HOLLENBACH
NASA/Ames Research Center, Moffett Field, California
Received 1984 June 20; accepted 1984 October 31

ABSTRACT

We have theoretically modeled the chemistry and heat balance of dense (10^3 cm^{-3} $< n_0 <$ 10^6 cm^{-3}) neutral gas illuminated by far-ultraviolet (FUV) (6 eV $< h\nu <$ 13.6 eV) fluxes 10^3–10^6 times more intense than the ambient interstellar field. The one-dimensional models extend $A_v \sim 10$ into the neutral gas, and are primarily intended to study the FUV illuminated neutral gas (photodissociation regions) between molecular clouds and H II regions. However, the models also apply to neutral shells around planetary nebulae, bright-rimmed molecular clouds, reflection nebulae, regions around protostars, and the center of the Galaxy, and to global studies of external galaxies. The models relate observed line and continuum emission from these regions to interesting physical parameters such as the gas density and temperature, the incident FUV flux, the elemental abundances, and the grain properties. The dense, highly illuminated photodissociation regions generally include a hot ($T > 100$ K) atomic region (H, O, and C^+) near the surface ($A_v \lesssim 3$) where trace H_2 is vibrationally excited by FUV pumping, a warm ($T \sim 100$ K) partially dissociated region (H_2, O, C, and CO) at about $A_v \sim 3$–5, and a cooler ($T < 100$ K) interior region ($A_v \sim 10$) where oxygen is still photodissociated to atomic form (H_2, CO, and O).

The FUV-induced photoelectric ejection of energetic ($\sim$1 eV) electrons from grains dominates the gas heating in the warm photodissociation regions, and the gas attains much higher temperatures than the grains. O I 63 μm and 145 μm and C II 158 μm dominate the gas cooling, and the ratios and peak intensities of these lines measure the gas density and temperature. The fraction of the FUV flux converted into flux in these lines, or, equivalently, the ratio of the flux in these lines to the integrated continuum infrared flux from the grains, is generally of order 10^{-2}–10^{-3}. This measured ratio is a function of the gas temperature, the electron density, and the FUV flux. The ratio decreases with increasing FUV flux and decreasing electron density because such changes in these parameters increase the positive grain charge and produce less efficient photoelectric heating.

The inclusion of sulfur and silicon chemistry, self-shielding of atomic carbon, and a high elemental abundance of carbon in the gas phase produces sufficient column densities of atomic carbon in our models to explain the intense and extended C I 609 μm emission observed near H II regions. We argue that the observed C I lies on the surfaces of molecular clouds, and does not exist in high abundance throughout the clouds as has been suggested elsewhere.

Subject headings: infrared: spectra — interstellar: molecules — molecular processes — nebulae: H II regions

I. INTRODUCTION

Observational studies directed toward H II regions and in galactic nuclei have revealed intense O I 63 μm and 145 μm and C II 158 μm fine-structure emission as well as luminous far-infrared continuum emission by the dust (see Werner *et al.* 1976; Melnick, Gull, and Harwit 1979; Storey, Watson, and Townes 1979; Furniss *et al.* 1982; Werner and Ellis 1985; Stacey *et al.* 1983; Russell *et al.* 1980, 1981; Crawford *et al.* 1985). Table 1 gives a partial survey of some of the regions observed, the luminosities in the lines, and the bolometric luminosity of each region (i.e., presumably the luminosities of the early-type stars which ionize the associated H II regions). Table 1 illustrates that the fine-structure emission, though luminous, is completely dwarfed by the luminosity of the ionizing source, and that a mechanism is required which transforms 0.1%–1% of the stellar radiation field into flux in these lines.

Motivated by these observations, we have constructed one-dimensional theoretical models of the surfaces of molecular clouds which are illuminated by intense far-ultraviolet (FUV) (6 eV $< h\nu <$ 13.6 eV) fluxes. We wish to model what lies between the ionized and molecular components of the interstellar medium. The intense FUV fluxes generally photodissociate the molecules and photoionize those heavy elements with ionization potentials less than the Lyman limit, leaving the gas mostly H, He, O, C^+, and N. We define "photodissociation regions" somewhat more generally to include regions where FUV radiation dominates the heating and/or some important aspect of the chemistry. Thus, photodissociation regions include most of the atomic gas in a galaxy, both in diffuse clouds and in the denser regions which are studied here. In addition, photodissociation regions extend to places where hydrogen is molecular and carbon is incorporated into CO, but where the residual oxygen remains in atomic form because of FUV photodissociation. In the Milky

TABLE 1

FINE-STRUCTURE LUMINOSITIES FROM SELECTED REGIONS

Source	O I 63 μm ($L_\odot$)	C II 158 μm ($L_\odot$)	L_{bol} ($L_\odot$)	References
M42	600	80	3×10^5	1, 2, 3
M17	3000	2000	6×10^6	1, 4
Sgr A	10^5	10^4	3×10^7	5, 6, 7
M82 (nucleus)	10^8	2.5×10^7	10^{10}	8, 6

REFERENCES.—(1) Melnick, Gull, and Harwit 1979; (2) Storey, Watson, and Townes 1979; (3) Russell *et al.* 1980; (4) Russell *et al.* 1981; (5) Genzel *et al.* 1984; (6) Genzel 1983; (7) Lester *et al.* 1981; (8) Watson *et al.* 1984.

© American Astronomical Society • Provided by the NASA Astrophysics Data System

1985ApJ...291..722T

Way these atomic regions may account for 0.2–0.5 of the neutral gas (see Solomon and Sanders 1980; Blitz and Shu 1980).

This paper focuses on photodissociation regions adjacent to H II regions, which are usually dense and which have incident FUV fluxes $\sim 10^3$–10^6 times as intense as the average ambient interstellar field. Previous theoretical models of photodissociation regions (Glassgold and Langer 1974, 1975, 1976; Langer 1976; Black and Dalgarno 1977; Clavel, Viala, and Bel 1978; de Jong, Dalgarno, and Boland 1980) have focused on gas of hydrogen nucleus density $n_0 < 10^3$ cm^{-3} illuminated by the ambient interstellar radiation field. Preliminary models have been reported for C II regions with $n_0 < 3 \times 10^3$ cm^{-3} by Brown, Lockman, and Knapp (1978) and Dewdney and Roger (1983). However, this paper presents the first theoretical models with full chemistry and heat balance of dense (10^3 cm$^{-3} < n_0 < 10^6$ cm^{-3}) gas illuminated by ultraviolet fluxes $G_0 = 10^3$–10^6, where G_0 is the FUV field measured in units of the equivalent Habing (1968) flux of 1.6×10^{-3} ergs cm^{-2} s^{-1} appropriate to the average interstellar medium.

Intense FUV fields have a dramatic effect on the structure and line emission from photodissociation regions. The models presented are not only relevant to the dust and gas between molecular clouds and H II regions but also apply to any neutral cloud illuminated by intense FUV fluxes. Such regions include the neutral gas near planetary nebulae, regions surrounding protostars (e.g., the BN object), bright-rimmed molecular clouds, and reflection nebulae. They also apply to neutral gas near unknown sources of FUV radiation, such as may exist in the galactic center and in the nuclei of external galaxies.

The goal of the theoretical models is to relate observed line and continuum emission from these regions to interesting physical parameters such as the gas density and temperature, the elemental and chemical abundances, the local radiation field, and the grain properties. These parameters are inherently of interest in what they reveal of the atomic phase of the interstellar medium and of the evolution and structure of the interstellar medium and the nature of molecular clouds. They also probe the physical environment of the nearby regions of massive star formation or galactic nucleus activity.

The relatively small number of chemical species and better understood reaction rates in photodissociation regions allows observation and theory to be linked in order to test theories of interstellar gas-phase chemistry, as has been done for diffuse clouds (see Black and Dalgarno 1977). The simple chemistry also means that elemental abundance information is relatively easy to extract, since much of an element will be tied in a single chemical species, such as C^+. Many previous gas-phase chemical models of dense molecular clouds have assumed that ultraviolet radiation can be ignored. However, the ultraviolet-dominated surface regions may contribute substantial column densities of some of the observed species (e.g., C I) and may help to explain some paradoxes which currently undermine the validity of the standard gas-phase chemistry models of molecular clouds (see Watson and Walmsley 1982).

In the following sections we present a theoretical parameter study of the temperature and chemical structure of dense photodissociation regions and their resultant spectrum. In § II we present an overview of the morphology of photodissociation regions, examine the density and temperature dependence of O I and C II cooling, and discuss why photoelectric heating is the most likely gas heating mechanism. Section III enumerates the various physical processes included in our thermochemical model, including the treatment of the FUV radiation field, the assumption of dynamical and chemical equilibrium, and the heating, cooling, and chemical processes. Section IV presents the results of our theoretical models, with special emphasis on the variations of line intensities with gas density and incident FUV flux. We discuss the results in § V, with a qualitative description of the important processes which govern chemistry, the energy balance, and the emitted line intensities. Section VI summarizes the main features of our theoretical parameter study. In a separate paper (Tielens and Hollenbach 1985, hereafter Paper II) we present an application of these results to the observational data from the OMC-1 region.

II. MAIN FEATURES OF DENSE PHOTODISSOCIATION REGIONS

a) Overview of the Global Morphology of Dense Photodissociation Regions

The one-dimensional theoretical models to be described in this paper assume that the photodissociation region hydrogen nucleus density n_0 and the incident FUV flux G_0 are independent parameters. This allows application to a variety of geometries, such as the photodissociation regions adjacent to "blister" H II regions. We note, however, that around spherical, ionization-bounded H II regions produced by O stars, the density and FUV field are related by $G_0 \approx 3 \times 10^5 (n_4/C)^{1.33}$, where $n_4 = n_0/10^4$ cm^{-3}, $C = n_0/n_{\rm II}$, and $n_{\rm II}$ is the electron density in the H II region (see Spitzer 1978). We restrict ourselves to sufficiently late times after the onset of the ultraviolet flux that the photodissociation region is in pressure equilibrium with the H II region and, therefore $C \approx 10$–100 (there will be further discussion of this assumption in § III). We study the range 10^3 cm$^{-3} < n_0 < 10^6$ cm^{-3}, which corresponds roughly to H II region densities of 10 cm$^{-3} < n_{\rm II} < 10^5$ cm^{-3}. Typically, an FUV source ($T_{\rm eff} > 3 \times 10^4$ K) of luminosity 10^4–10^5 $L_\odot$ lies some 0.1–1.0 pc from the atomic region. The incident flux is therefore in the range $G_0 \sim 10^2$–10^5. The photodissociation region behind the Trapezium stars in OMC-1 has $G_0 \sim 10^5$ and $n_0 \sim 10^5$ cm^{-3}. Reflection nebulae illuminated by early-type B stars, such as NGC 2023 and NGC 7023, can have $G_0 \sim 10^3$ and $n_0 \sim 10^3$–10^4 cm^{-3}.

Figure 1 schematically shows the overall morphology of dense clouds illuminated by ultraviolet radiation from nearby sources. We shall show in § IV that under these conditions, the ultraviolet flux can heat, through photoelectric heating, a neutral column of gas near the cloud surface of 8×10^{21} hydrogen nuclei cm^{-2} to high temperatures: 100 K $< T <$ 1000 K. The high-temperature gas is predominantly atomic, with some singly ionized elements such as C^+, S^+, Si^+, and Fe^+ whose ionization potentials lie below the Lyman limit. Cooling is primarily by O I 63 μm and C II 158 μm. An appreciable amount of vibrationally excited H_2 (by ultraviolet pumping) is also found in this gas. Somewhat farther into the cloud ($A_v \sim 5$), we find large quantities of atomic carbon and warm CO as C^+ makes the transition to CO. Finally, at $A_v \sim$ 10–20, photodissociation of OH, H_2O, and O_2 ceases to be important, and a chemical equilibrium appropriate to opaque molecular clouds dominated by cosmic-ray ionization becomes relevant.

We ignore ionization by soft X-ray or XUV photons. Photons with energies >0.5 keV are required to penetrate the substantial column density of neutral gas which comprises the photodissociation region. With sufficient flux, these X-rays

© American Astronomical Society • Provided by the NASA Astrophysics Data System

1985ApJ...291..722T

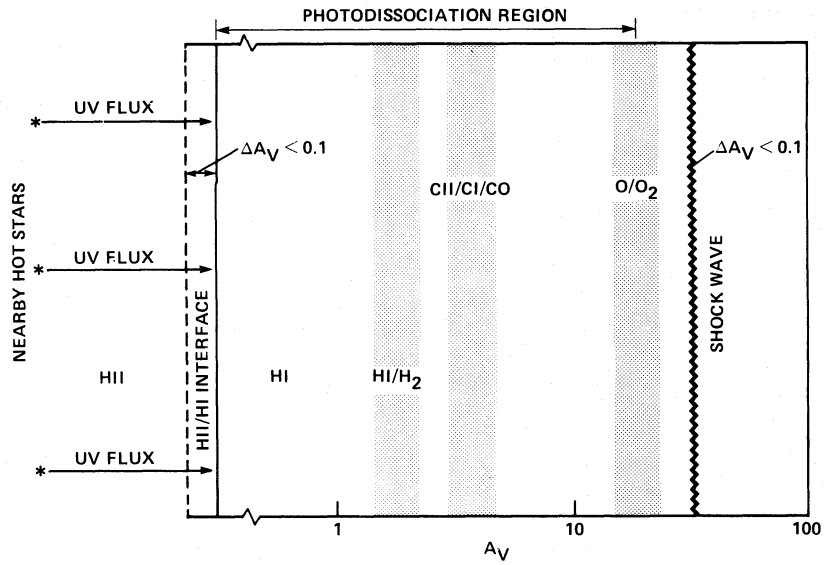

FIG. 1.—A schematic drawing of a photodissociation region. Our one-dimensional theoretical models extend from the predominantly atomic region to the point where O_2 is not appreciably photodissociated. Hence, the photodissociation region includes gas whose hydrogen is mostly H_2 and whose carbon is mostly in CO. The above diagram is roughly for Orion-like conditions with intense FUV fields incident upon the cloud. Large columns of warm O, C, C^+, and CO and vibrationally excited H_2 are produced in the photodissociation region.

could dominate the FUV ionization of atomic carbon. Therefore, our models hold only if X-ray sources with luminosity L (in >0.5 keV photons) lie at least 0.1 pc $L_{32}^{0.5}$ from the photodissociation region, where $L_{32} = L/10^{32}$ ergs s^{-1}. This condition nearly always applies (see Lepp and McCray 1983).

b) Temperature and Density Dependence of O I 63 μm, O I 145 μm, *and* C II 158 μm *Emission*

The relative integrated strengths of the O I 63 μm and O I 145 μm lines provide constraints on the density n_0 and temperature T of the gas if these lines are optically thin. Figure 2 plots the ratio of these two lines as a function of temperature for a range of assumed neutral gas densities. We take the collisional rate coefficients from Launay and Roueff (1977*a*) and assume the colliding partners to be H atoms. The dotted line in Figure 2 shows the ratio of the two lines in an optically thick approximation where the peak line intensities are the blackbody values and the line widths are assumed equal. We find that in photodissocation regions the O I 63 μm line is usually optically thick so that the O I 145 μm/O I 63 μm ratio lies above the optically thin value for the relevant n_0 and T. Therefore, this line ratio does not set a simple constraint on n_0 and T. However, the peak O I 63 μm line intensity, if resolved, provides a measure of gas temperature. The O I 145 μm line, which is thin, provides a measure of the column density of O I if the density and temperature are known.

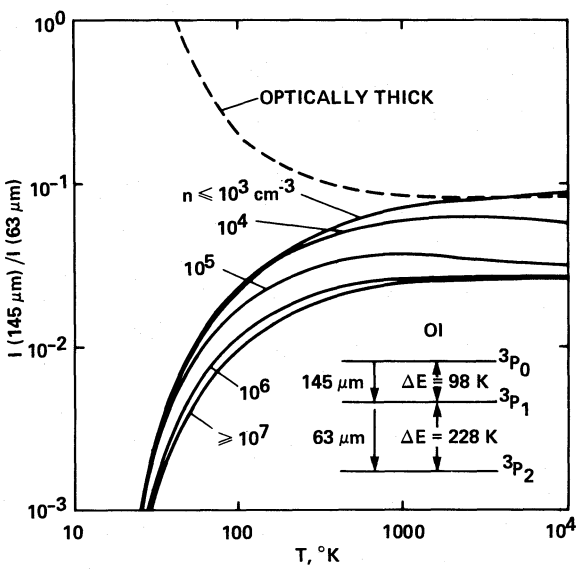

FIG. 2.—The ratio of the intensity in the O I 145 μm line to that in the O I 63 μm line is shown as a function of temperature. The solid lines give this ratio for different densities in the optically thin case. The broken line gives the ratio for optically thick lines of equal line width. A schematic energy diagram of the fine-structure states of O are shown in the lower right-hand corner. Collisions with atomic hydrogen are assumed.

Assuming that the gas-phase elemental abundances of O and C are relatively well known, the C II 158 μm/O I 63 μm ratio also constrains gas temperature and density (see Fig. 3, which assumes abundances of 3.7×10^{-4} for C^+ and 6.7×10^{-4} for O). Collision rates for O are taken from Launay and Roueff (1977*a*). Collision rates for C^+ are taken from Launay and Roueff (1977*b*) for H atom collisions, from Flower and Launay (1977) for H_2 collisions, and from Osterbrock (1974) for electron collisions (the electron abundance is taken to be equal to the carbon abundance in Figure 3, and the hydrogen is assumed to be atomic). C II 158 μm dominates for $n_0 < 10^3$ cm^{-3} and $T < 10^4$ K, while O I 63 μm dominates for $n_0 > 10^4$ cm^{-3} and $T > 100$ K. The observation that the C II 158 μm/O I 63 μm ratio observed in Orion is about 0.1 (see Table 1) suggests that the gas temperature is about 500 K and the density about 10^5 cm^{-3}. Since these two lines generally dominate the atomic gas cooling in photodissociation regions, we have also plotted in Figure 4 the absolute C II 158 μm cooling rate per C^+ ion as a function of temperature for various hydrogen atom gas densities.

In a homogeneous slab with constant density, temperature, and C^+ abundance, the emergent intensity in the C II 158 μm line can be calculated analytically as a function of the total

© American Astronomical Society • Provided by the NASA Astrophysics Data System

1985ApJ...291..722T

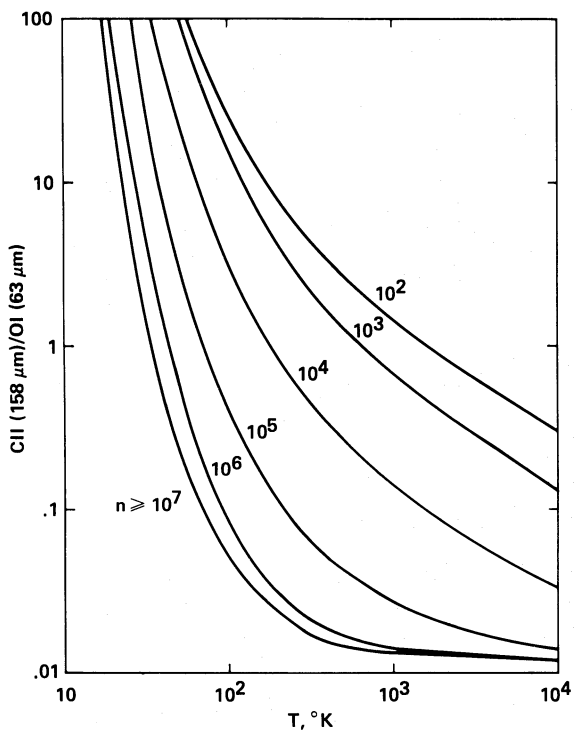

FIG. 3.—The ratio of the intensity in the C II 158 μm line to that in the O I 63 μm line is shown as a function of temperature and density. The C^+/O abundance ratio is taken to be 0.55, the cosmic abundance ratio of C to O. Collisions with atomic hydrogen are assumed.

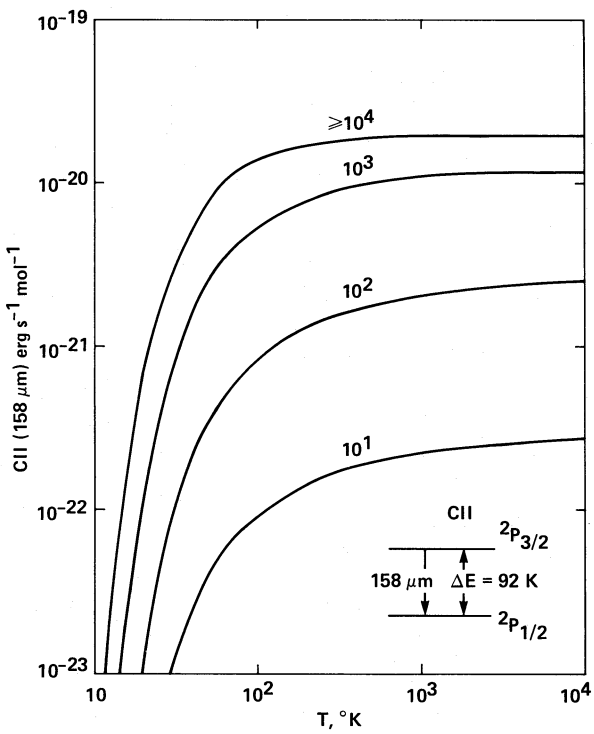

FIG. 4.—Cooling in the C II 158 μm line per carbon ion is plotted as a function of temperature and density. A schematic energy diagram of C^+ is given in the lower right-hand corner. Collisions with atomic hydrogen are assumed.

column density of C^+, $N(C^+)$. Figure 5 plots the C II 158 μm intensity against $N(C^+)$ for different temperatures, where it is assumed that the fine-structure levels are in LTE ($n_0 > 2 \times 10^3$ cm^{-3}), a safe approximation for photodissociation regions around H II regions. For low column densities the integrated intensity is directly proportional to the column density, as expected for an optically thin line. For very large column densities the integrated intensity is given by

$$I_\nu = B_\nu(T)\nu(\delta v_d/c)f(\tau) , \quad (1)$$

where B_ν is the Planck function at the frequency of the line ν, δv_d is the turbulent Doppler width, and $f(\tau)$ is a factor which takes optical-depth effects into account (see Appendix B). For large optical depths $f(\tau)$ is proportional to the logarithm of the column density (i.e., the line is on the logarithmic part of the curve of growth). The curves in Figure 5 are calculated for $\delta v_d = 2.7$ km s^{-1}, appropriate for Orion (Paper II). Comparing this curve with the observed surface brightness of the C II 158 μm line in Orion ($\sim 4 \times 10^{-3}$ ergs cm^{-2} s^{-1} sr^{-1}) implies again that the gas is warm (~ 500 K) and that the column density of C II is of the order of 4×10^{18} cm^{-2}.

c) *Gas Heating Mechanisms in Photodissociation Regions*

The absolute strengths of the observed O I 63 μm and C II 158 μm lines in Table 1 are at least an order of magnitude larger than those predicted by Hill and Hollenbach (1978) to emerge from the H II/H I transition zone (the thin neutral region where Lyman continuum photons dominate the heating and ionization) or from the neutral shock wave driven by the pressure of the expanding H II region. Both of these regions have dimensions of order $\Delta A_v \sim 10^{-2}$–10^{-1} (see Fig. 1). The photodissociation region has a dimension ΔA_v of the order of several, and we shall show in §§ III and IV that the photoelectric mechanism heats these regions to sufficient temperatures ($T > 100$ K) to appreciably excite both O I 63 μm and C II 158 μm.

Simple physical arguments demonstrate that the photoelectric mechanism can convert up to about 4% of the FUV radiation flux into gas heating. Since 10 eV is an average FUV photon energy and 6 eV is a typical work function of a neutral

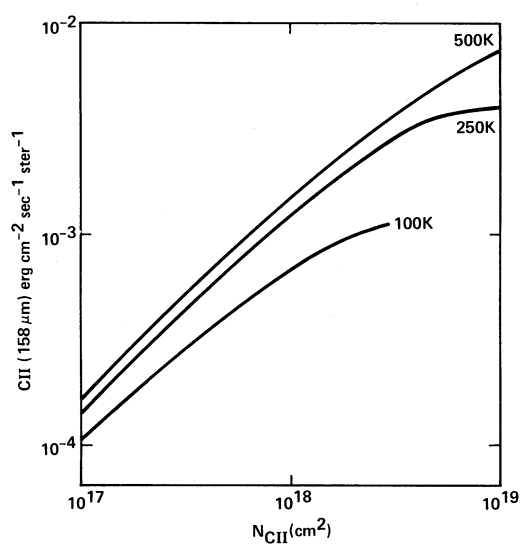

FIG. 5.—The intensity in the C II 158 μm line as a function of the total C^+ column density in a homogeneous slab model is plotted (see text).

© American Astronomical Society • Provided by the NASA Astrophysics Data System

1985ApJ...291..722T

interstellar grain (see de Jong 1980), electrons ejected from neutral grains carry about 4 eV of kinetic energy which heats the neutral gas. The probability that an absorbed photon ejects an electron (the "photoelectric yield") is of order 0.1 (see de Jong 1980). Therefore, the fraction ϵ of the absorbed FUV flux which is converted to gas heating, or the "heating efficiency," is approximately $(4/10) \times 0.1 = 0.04$ for neutral grains. When comparing with, for example, Table 1, one must multiply ϵ by the fraction of the O star bolometric luminosity which falls into the FUV band ($\sim$0.5). Typically, the heating efficiency is perhaps an order of magnitude smaller than this value because the FUV flux positively charges the grains, which results in a larger effective work function. We note that the efficiency of the photoelectric mechanism depends on the microscopic parameters of the grain such as the photoelectric yield and the neutral work function and not on the global grain parameters such as the gas-to-dust ratio. The efficiency is also insensitive to the FUV albedo and absorption cross sections of the grains.

Figure 6 shows a more quantitative analysis of the photoelectric mechanism which includes the effect of grain charging. Using the formalism derived by de Jong (1980) (see § I of Appendix A), we can calculate ϵ as a function of the parameter

$$\gamma = 2.9 \times 10^{-5} G_0 T^{0.5} n_e^{-1} . \quad (2)$$

The parameter γ is a measure of the ratio of the rate at which FUV photons strike grains to the rate at which electrons recombine with grains. Thus, $\gamma \ll 1$ implies neutral or negatively charged grains where ϵ is expected to be high (>0.01), while $\gamma \gg 1$ implies positively charged grains. Figure 6 plots ϵ against γ. Typically, in photodissociation regions which lie between H II regions and molecular clouds, $G_0 \sim 10^4$, $n_e \sim 10$ cm^{-3}, and $T \sim 100$ K, so that $\gamma \approx 0.3$ and $\epsilon \approx 4 \times 10^{-3}$. Therefore, photoelectric heating is a promising mechanism to explain the extended and luminous O I 63 μm and C II 158 μm emission.

Our models are intended for regions such as those listed in Table 1 where the energy input to the gas is >100–$1000\ L_\odot$; this eliminates in most cases the possibility that X-ray heating could account for a substantial fraction of the gas heating. The number density and luminosity of X-ray sources (see Lepp and McCray 1983) are insufficient to account for the widespread observations of O I 63 μm and C II 158 μm emission. Furthermore, as will be discussed in Paper II, the observations in Orion show that the emission is luminous in the ionization bar, as would be expected for photodissociation regions but not for X-ray–heated gas.

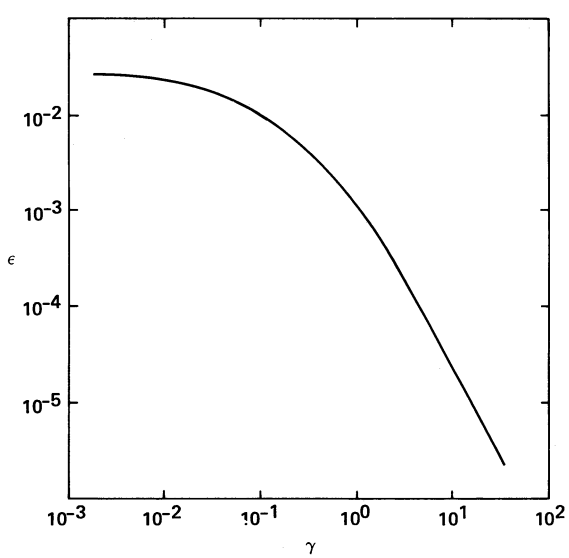

FIG. 6.—The efficiency of the photoelectric heating of the gas as a function of γ is shown.

III. PHYSICAL PROCESSES

a) The Far-Ultraviolet Radiation Field

The penetration of FUV radiation into dense molecular clouds is a sensitive function of the rather unknown scattering properties of the interstellar dust (Sandell and Mattila 1975; Whithworth 1975; Flannery, Roberge, and Rybicki 1980). Accurate calculations of the radiative transfer equations for plane-parallel semi-infinite slabs show that the mean intensity is proportional to $\exp(-k_\lambda A_v)$, provided that the total visual extinction of the cloud is large (Flannery, Roberge, and Rybicki 1980). A_v here is the visual extinction into the slab measured from the H II/H I transition zone. The constants k_λ for the different ionization, dissociation, and heating processes are taken from the numerical results of Roberge, Dalgarno, and Flannery (1981) for their model 2 dust properties, and from Black and Dalgarno (1977) when not available from Roberge *et al.* The values of k_λ range from $\sim$1 to $\sim$3.5 for the different processes considered.

Because the penetration of FUV radiation has such an influence on the chemical and heat balance, we have examined the importance of varying k_λ. This was done by treating two limiting cases: (1) the standard case discussed above, and (2) a low attenuation case where $k_\lambda = 1$ for all λ.

The penetration of FUV radiation is also influenced by absorption by neutral carbon atoms (Werner 1970) and by absorption by molecular hydrogen (Black and Dalgarno 1977). This is particularly important for the C^+/C/CO and the H I/H_2 transition (see Appendix A).

The wavelength dependence of the incident FUV flux is set equal to the theoretical estimate for the interstellar FUV radiation field (Habing 1968), except for some of the photodissociation and photoionization reactions which were calculated using Draine's (1978) estimate of the interstellar FUV field (see Roberge, Dalgarno, and Flannery 1981). The differences between the two estimates are only small.

b) Dynamical Equilibrium

In our model the atomic region, which separates an H II region from its parent molecular cloud, is represented by a constant-density plane-parallel slab. We adopt a Gaussian turbulent velocity field in the cloud, and this turbulence is assumed to dominate the pressure. Quantitatively, $P = 0.5\rho\delta v_d^2$, or

$$P/k = 5.8 \times 10^6 (n_0/10^5\ \mathrm{cm}^{-3})(\delta v_d/1\ \mathrm{km\ s}^{-1})^2\ \mathrm{cm}^{-3}\ \mathrm{K}\ , \quad (3)$$

where P, ρ, and n_0 are the gas pressure, mass density, and number density and where δv_d is the Gaussian velocity width. Apart from a factor of 2 associated with the H I/H_2 transition, our constant-density plane-parallel slab is therefore also in pressure equilibrium. The neglect of dynamical effects (e.g., shocks) limits the applicability of our models to the later stages ($t > t_p = 10^5 n_4^{-1}$ yr) of the dynamical evolution of H II regions, when global pressure equilibrium between the atomic gas and the ionized gas has been reached for $A_v < 10$ (Hill and Hollenbach 1978).

© American Astronomical Society • Provided by the NASA Astrophysics Data System

1985ApJ...291..722T

Dynamical equilibrium, in the sense of a static pressure-confined H II region, is not required. The models hold as long as the gas density and pressure are roughly constant inside the photodissociation region, or, equivalently, no strong shocks exist inside the photodissociation region. Therefore, the models may apply to the expanding shells of planetary nebulae if these shells have column densities $> 10^{22}$ cm^{-2}.

c) *Heating and Cooling Processes*

The photodissociation region is predominantly heated by ultraviolet photons longward of 912 Å. Various mechanisms convert FUV radiation into gas heating: (1) photoelectric emission from dust grains, (2) neutral carbon ionization, (3) H_2 photodissociation, (4) the FUV pumping followed by collisional de-excitation of vibrationally excited H_2, (5) H_2 formation from FUV-produced hydrogen atoms, and (6) collisions between gas particles and FUV-heated or radiatively accelerated dust grains. In addition, (7) cosmic-ray heating may also contribute deep in the cloud, and (8) O I may heat the gas through the collisional de-excitation of the (dust) continuum radiation-excited $^3P_1$ fine structure level. These eight heating mechanisms are well-known, with the possible exception of the O I mechanism, and we briefly describe the rates incorporated into our model in Appendix A.

The gas is generally cooled by infrared fine-structure lines from atoms and by low-lying rotational lines from molecules. Which of these two classes of cooling processes dominates depends on the chemical composition of the gas phase. We include the infrared fine-structure lines of C, C^+, O, S, Si, Si^+, Fe, and Fe^+; the first 20 rotational levels of CO; and the rotational cooling of H_2, CH, OH, and H_2O. At temperatures of a few thousand degrees, vib-rotational transitions in H_2 and excitation of the metastable ^1D level of atomic oxygen are of importance. At even higher temperatures (10^4 K) Lyα cooling will become dominant. Our treatment of radiative cooling includes line opacity effects and basically follows that of de Jong, Dalgarno, and Boland (1980) and Hollenbach and McKee (1979). We summarize our radiative transfer scheme and the derived cooling rates in Appendix B.

d) *Chemistry*

The heating and cooling in the H II/H I/H_2 transition region depend sensitively on the molecular composition of the gas. We have constructed a chemical network of 165 reactions between 41 species consisting of the elements hydrogen, helium, carbon, oxygen, silicon, sulfur, magnesium, and iron. The species and their reactions are listed in Appendix C. The photoreactions are taken from Roberge, Dalgarno, and Flannery (1981) and, where not available there, from Black and Dalgarno (1977). Unless otherwise noted, the rest of the reactions are from Prasad and Huntress (1980). For a few typical models the calculated abundances were checked against the results from a more extensive chemical code in order to ensure that all the important reactions are included in the model calculations. The abundance of H_2, C^+, e^-, and CO are of particular importance. In the remainder of this section we will discuss the hydrogen chemistry, the C^+/C/CO transition, the electron abundance, and the assumption of chemical equilibrium.

i) *The Hydrogen Chemistry*

Molecular hydrogen is formed on grain surfaces (Hollenbach and Salpeter 1971) probably through H abstraction from molecules like H_2S, H_2CO, N_2H_2, N_2H_4, and the metal hydrides (Tielens and Hagen 1982). The rate of this reaction is given by

$$R = 0.5 n_H n_d \sigma_d \bar{v} S(T)$$
$$\approx 6 \times 10^{-17} (T/300)^{0.5} n_H n S(T) \text{ cm}^{-3} \text{ s}^{-1} , \quad (4)$$

where n_d and σ_d are the number density and cross section of dust grains and n_H, $\bar{v}$, and $S(T)$ are the number density, mean velocity, and thermally averaged sticking coefficient of hydrogen atoms. The latter is given by (Hollenbach and McKee 1979)

$$S(T) = [1 + 0.4(T + T_d)^{0.5} + 2 \times 10^{-3} T + 8 \times 10^{-6} T^2]^{-1} , \quad (5)$$

where T_d is the dust temperature.

Not considered in equations (4) and (5) is the thermal evaporation of H atoms from grains. Above a certain critical grain temperature, T_{cr}, the rate at which H_2 is formed on a grain surface drops rapidly because of this evaporation. As discussed in Appendix C, this critical grain temperature is about 75 K. To simplify the calculations, and since grain temperatures are generally < 75 K in photodissociation regions, it is assumed that H_2 formation on grain surfaces is always given by equations (4) and (5). The importance of this assumption will be discussed.

If H_2 is not formed on grain surfaces, then the important mechanism for H_2 formation is by the radiative association reaction (de Jong 1972)

$$H + e^- \rightarrow H^- + h\nu ,$$

followed by the associative detachment reaction

$$H^- + H \rightarrow H_2 + e^- .$$

Molecular hydrogen is electronically excited by absorption of FUV photons in the Lyman-Werner bands. Subsequent fluorescence leads to dissociation in about 10% of the cases and to an H_2 molecule in a vibrationally excited state of the ground electronic state in the remaining 90% of the cases (Black and Dalgarno 1976). Vibrationally excited H_2^* can react with no activation energy with many chemical species and will emit (2 μm) vibrational emission. The forbidden nature of the vibrational decay means that a large abundance of H_2^* can be maintained. Therefore, as discussed in Appendix B, we have lumped the vibrational levels of ground state H_2 into a single pseudolevel at $v \approx 6$, and we treat the vibrationally excited H_2^* as a separate chemical species in the chemical equilibrium. It is formed by the above FUV pumping mechanism and destroyed by FUV pumping to Lyman and Werner bands followed by dissociation, by direct FUV dissociation, by radiative decay or collisional de-excitation to $v = 0$, and by the chemical reactions discussed below.

At low densities in an intense FUV field, the vibrational excitation temperature of H_2 may be quite different from the gas temperature. Part of the internal energy of vibrationally excited H_2^* can be used to overcome activation energy barriers in chemical reactions. It has been suggested that the reaction of vibrationally excited H_2^* with C^+ is a major pathway for the synthesis of interstellar CH^+ (Stecher and Williams 1972). Although interstellar CH^+ generally seems to be formed behind low-velocity shocks (Elitzur and Watson 1980; Federman 1982), for some lines of sight (e.g., the stars in the Pleiades) reactions of vibrationally excited H_2^* may be dominant (Freeman and Williams 1982). Laboratory data and theoretical

© American Astronomical Society • Provided by the NASA Astrophysics Data System

1985ApJ...291..722T

calculations indicate that the reduction of the activation energy for vibrationally excited H_2^* depends on the height, width, and location of the activation barrier (Schatz 1981; Light 1978; Schinke and Lester 1979; Lee *et al.* 1982). We will assume that all of the available vibrational energy can be used to overcome an activation barrier. For the important reactions

$$H_2^* + C^+ \rightarrow CH^+ + H$$

and

$$H_2^* + O \rightarrow OH + H ,$$

this is a reasonable assumption, since the activation barrier ($\sim$0.5 eV) is much less than the average vibrational excitation energy ($\sim$2.6 eV). For the collisional dissociation reactions

$$H_2^* + H \rightarrow H + H + H$$

and

$$H_2^* + H_2 \rightarrow H + H + H_2 ,$$

this may overestimate the rates considerably. However, FUV dissociation always dominates.

ii) *The* C^+/C/CO *Transition*

The C^+/C/CO transition is of prime importance for the calculation of the energy balance and line intensities of photodissociation regions. At the edge of dense molecular clouds, carbon is photoionized to C^+. Partly as a result of self-shielding (Werner 1970) and partly because of dust shielding, the C^+ will be transformed to C and CO at greater depths into the cloud. This transition has been studied in detail by Glassgold and Langer (1975), Oppenheimer and Dalgarno (1975), Langer (1976, 1977), Bally and Langer (1982), and Frerking, Langer, and Wilson (1982).

a) C I.—At the edge of the cloud, neutral carbon is mainly formed by

$$C^+ + e \rightarrow C + h\nu$$

and

$$CH + h\nu \rightarrow C + H .$$

Deeper in the cloud, where the electron abundance drops, the charge exchange reactions

$$C^+ + S \rightarrow C + S^+$$

and

$$C^+ + SiO \rightarrow C + SiO^+$$

are the main formation mechanisms for C. These two reactions have generally been ignored in studies of the chemistry in photodissociation regions. They are, however, of prime importance.

For $A_v < 7$, C is destroyed mainly through photoionization. It should be noted that dust, C, and H_2 compete for the same photons (Black and Dalgarno 1977; Werner 1970). All three absorption processes must be included in calculating the photoionization rate of C. Deep in the cloud C cycles to CO through

$$C + OH \rightarrow CO + H ,$$

$$C + O_2 \rightarrow CO + O .$$

The OH formation is initiated by cosmic-ray ionization of H, followed by charge exchange with O, ion reactions with H_2, and finally ion dissociative recombination with electrons. The O_2 results from

$$O + OH \rightarrow O_2 + H .$$

b) CO.—There are three different chemical pathways for forming CO. First, CO formation is initiated by the radiative association of C^+ with H_2, which ultimately leads to CH and CH_2, which react with O to form CO. This is generally the most important pathway at the edge of the cloud ($A_v < 5$). A second path, which is important for $A_v > 5$, is initiated by the radiative association of Si^+ with H, which ultimately leads to SiO, which reacts with C^+ to form CO. A third involves the production of H_2O which reacts with C^+, or OH which reacts with C or C^+, to ultimately form CO. However, the high FUV fields in photodissociation regions limit the abundance of OH and H_2O, and this third pathway is generally unimportant in our models.

In the interiors of the clouds CO is destroyed by reactions with He^+ and H_3^+ ions, which result from cosmic-ray ionization of He and H_2:

$$CO + He^+ \rightarrow C^+ + O + He ,$$

$$CO + H_3^+ \rightarrow HCO^+ + H_2 .$$

The latter reaction merely recycles the CO through dissociative electron recombination. At the edge of the cloud CO destruction is dominated by photodissociation. It has been suggested that the FUV photodissociation of CO occurs through absorption in discrete lines rather than a continuum. In that case CO self-shielding will be important. This might explain the observed changes in the $C^{18}O/C^{16}O$ ratios with visual extinction (Bally and Langer 1982, Chu and Watson 1983). These isotope observations may, however, also be due to differences in excitation (Leung 1983). In effect, the photon observed to come from the edge of the cloud may actually be generated inside the cloud. Upon diffusing outward these photons may be scattered into the observers beam. Because of its higher abundance the scattered intensity in $C^{16}O$ will extend farther outward than that in $C^{18}O$. Observations of the polarization in these millimeter lines could settle this question. There are no clear laboratory data supporting or refuting CO self-shielding. Generally, we will ignore CO self-shielding, but we also treat cases with self-shielding included. The adopted rates are given in Appendix C.

iii) *The Electron Abundance*

The electron abundance is of some importance for the chemistry (see above) and particularly for the heating balance, since it affects the grain charge, which determines the efficiency of the often dominant photoelectric heating. At the edge of the cloud the electron density is governed by photoionization and radiative recombination of C and S. Deep in the cloud the degree of ionization is determined by the cosmic-ray ionization of H_2 and He and by photoionization of the metals Mg and Fe. The charge resulting from cosmic-ray ionization is also quickly passed on to the metals through charge exchange reactions. Because these metals do not form molecular ions at low temperatures and because radiative recombination of metal ions proceeds very slowly, all the positive charge will be locked up in the metals deep in the cloud (Oppenheimer and Dalgarno 1974).

iv) *Chemical Equilibrium*

The molecular composition of the photoelectrically heated region is assumed to be in chemical equilibrium. The lifetimes

© American Astronomical Society • Provided by the NASA Astrophysics Data System

1985ApJ...291..722T

of these regions are, however, so short ($< 10^6$–10^7 yr, the lifetime of a massive star) that nonequilibrium effects might be important. Time-dependent calculations of the H I/H_2 transition around H II regions show that H_2 reaches equilibrium after about $10^5 n_4^{-1}$ yr (Hill and Hollenbach 1978). This is comparable to the time scale to reach global pressure equilibrium. For heavier molecules the situation is slightly more complicated. Consider, for example, the cycle $C^+ \rightarrow CH_2^+ \rightarrow CO \rightarrow C \rightarrow C^+$, which is the dominant formation and destruction pathway of CO at the edge of the molecular cloud. The neutral carbon ionization time scale is very short at the edge of a molecular cloud ($\tau_{C^+} \sim 10^2 G_0^{-1}$ yr). The longest time scale in the CO cycle in atomic regions is that controlling the formation of CH_2^+ through radiative association, $\tau_{CH_2^+} \sim 10^4 n_4^{-1}$ yr, again short compared with the global pressure equilibrium time scale. Further into the cloud where the gas is molecular, carbon ionization will become the limiting process in CO formation. The time scale is then $\tau_{C^+} \sim 10^2 G_0^{-1} \exp(2.6 A_v)$ yr, where A_v is the visual extinction to the cloud surface. Therefore, for $A_v < 7.1 + 0.4 \ln(G_{05}/n_4)$, where $G_{05} = G_0/10^5$, the FUV–dominated CO cycle chemistry is in equilibrium. Likewise, the FUV dissociates all oxygen not incorporated in CO into atomic oxygen on a time scale $\tau_0 \sim 10^2 G_0^{-1} \exp(1.4 A_v)$, so that oxygen equilibrium applies for $A_v < 13 + 0.7 \ln(G_{05}/n_4)$.

Our equilibrium calculations extend to $A_v \approx 10$. Although the deeper regions may be somewhat out of equilibrium, we shall show that regions of high extinction $A_v \approx 5$–10 contribute little to the O I and C II emission, and that most of the carbon is tied up in CO in these regions—a result valid for nonequilibrium models, since the gas prior to the onset of the FUV source is assumed to be molecular. The main discrepancy introduced by our equilibrium assumption is in the calculation of C I intensities. These we may somewhat underestimate, since, in a time scale t_p, the gas has been compressed by the H II region pressure and the previous lower density gas had a higher C I abundance (see Prasad and Huntress 1980; Graedel, Langer, and Frerking 1982).

IV. RESULTS

The equations of energy balance and chemical equilibrium are solved simultaneously to determine the temperature and molecular abundances as functions of cloud depth (see Appendix D). The emergent line intensities are then calculated from each model cloud. Free parameters in the calculations are the number density of hydrogen nuclei n_0 (which is equivalent to turbulent gas pressure according to eq. [3], once δv_d is specified) and the incident FUV radiation field G_0. Other parameters which are constrained but which, because of their uncertainty, are varied to determine the sensitivity of our results include the turbulent Doppler width δv_d, the ratio of the dust abundance to that in the diffuse interstellar medium δ_d, the ratio of the dust absorption efficiency in the FUV to the dust extinction efficiency in the visual, δ_{uv}, and the elemental abundances $\mathscr{A}_i$ for species i.

For the elemental abundances $\mathscr{A}_i$, the values obtained for the heavily depleted line of sight toward ζ Oph are chosen (Morton 1974; de Boer 1981; Jenkins, Jura, and Loewenstein 1983). Note that for the carbon abundance the upper limit has been chosen (see Table 2). This value is equal to the measured carbon abundance in the Orion Nebula (Peimbert 1982) and therefore is probably more appropriate for models of the Orion photodissociation region (see Paper II). The derived lower limit to the carbon abundance toward ζ Oph is half the upper limit (Jenkins, Jura, and Loewenstein 1983).

TABLE 2

STANDARD MODEL PARAMETERS

Parameter	Standard Model
n_0 (cm^{-3})	2.3(5)
G_0	1.0(5)
δv_d (km s^{-1})	2.7
$\mathscr{A}_C$	3.0(−4)
$\mathscr{A}_O$	5.0(−4)
$\mathscr{A}_{Si}$	7.9(−7)
$\mathscr{A}_S$	7.9(−6)
$\mathscr{A}_{Fe}$	2.5(−7)
$\mathscr{A}_{Mg}$	1.3(−6)
F_{IR} (ergs cm^{-2} s^{-1})	5.0(2)
T_0 (K)	75
$\tau_{100\,\mu m}$	3.0(−1)
δ_d	1.0
δ_{uv}	1.8
k_{uv}	1.8
Y	1.0(−1)
E_d (eV)	6.0

NOTE.—Numbers in parentheses: 2.3(5) = 2.3×10^5.

The infrared flux from the cloud, F_{IR}, the emission optical depth at 100 μm, $\tau_{100\,\mu m}$, and the dust color temperature, T_0, are set from far-infrared continuum observations. The cosmic-ray ionization rate ζ (see Table 10) is held fixed. In addition, the yield Y and the threshold E_d of the photoelectric effect are not free parameters in the model calculations. They are chosen in such a way as to balance the observed cooling in the diffuse interstellar medium (Pottasch, Wesselius, and van Duinen 1979; de Jong 1980).

In Table 2 we list the values chosen for the parameters in the standard model. This standard model reproduces the observations of Orion reasonably well (Paper II). Figures 7, 8, and 9 give the temperature, the heating and cooling processes, and the molecular abundances as a function of depth for the standard model. The calculated line intensities perpendicular to the slab are given as a function of n_0 and G_0 in Figures 10 and 11. The effects of varying the other parameters are described in the following section.

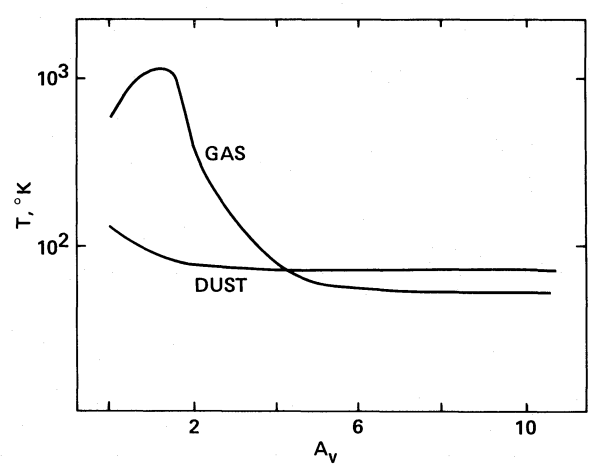

FIG. 7.—The calculated gas and dust temperature in the standard model is plotted as a function of the visual extinction A_v into the cloud.

© American Astronomical Society • Provided by the NASA Astrophysics Data System

1985ApJ...291..722T

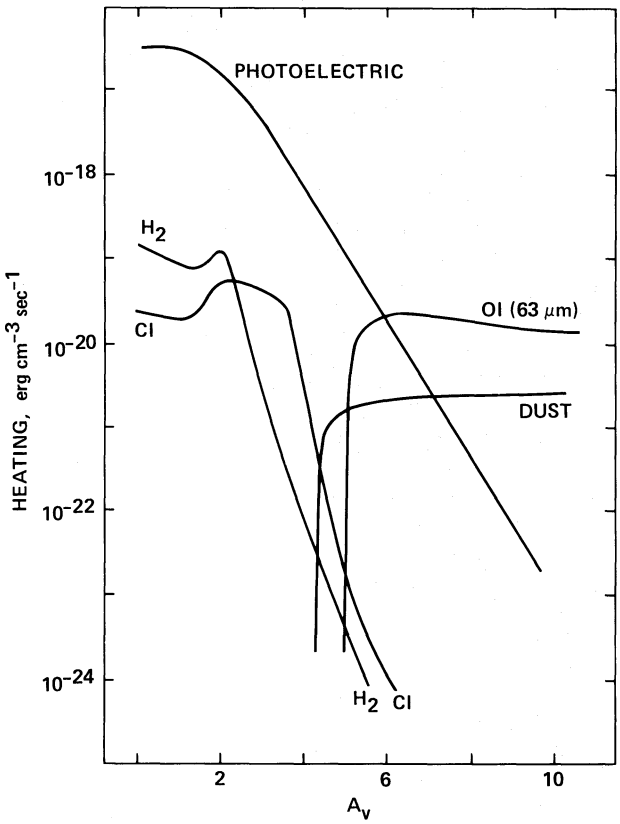

FIG. 8*a*

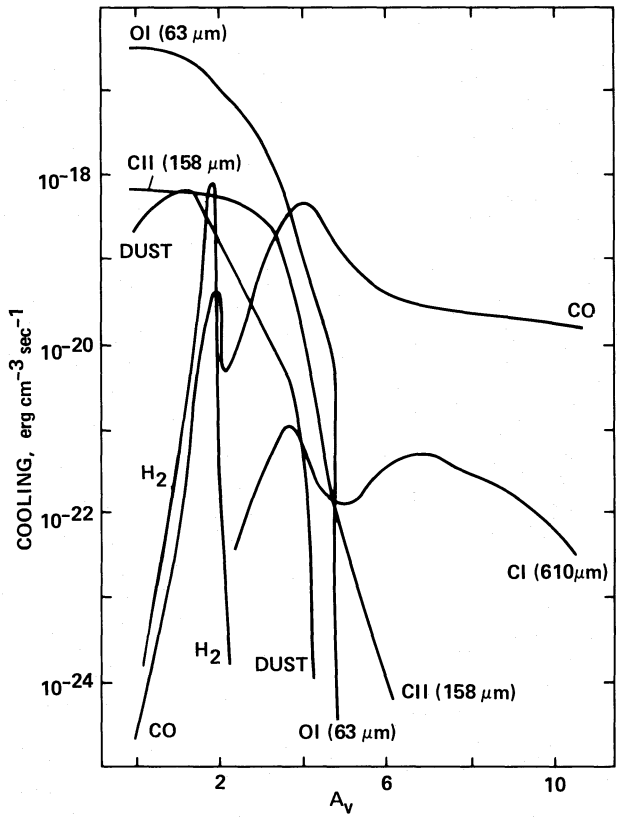

FIG. 8*b*

FIG. 8.—(*a*) The different heating terms in the energy balance are given as a function of visual extinction A_v into the cloud for the standard model (see text). (*b*) The different cooling terms in the energy balance are shown as a function of visual extinction A_v into the cloud for the standard model (see text).

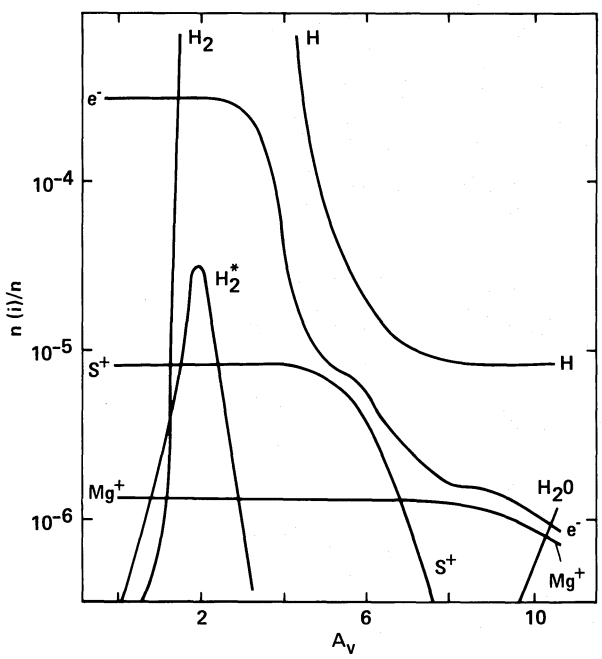

FIG. 9*a*

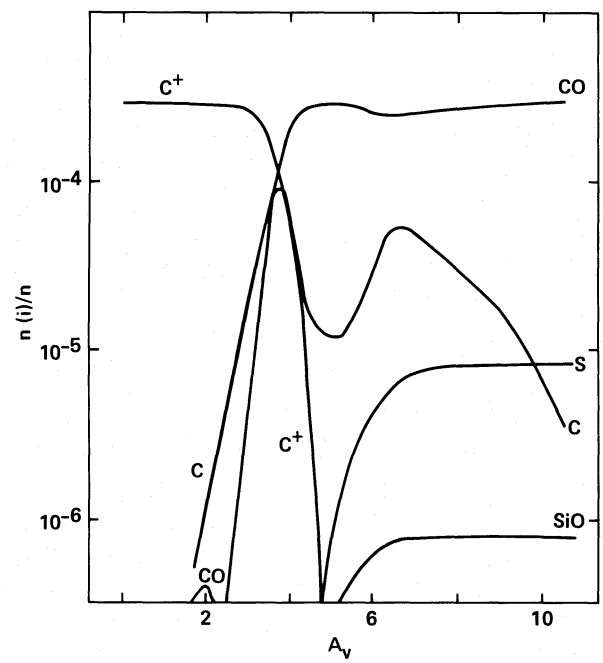

FIG. 9*b*

FIG. 9.—The molecular abundances of species *i*, $n(i)/n_0$, are plotted as a function of visual extinction A_v into the cloud for the standard model

© American Astronomical Society • Provided by the NASA Astrophysics Data System

1985ApJ...291..722T

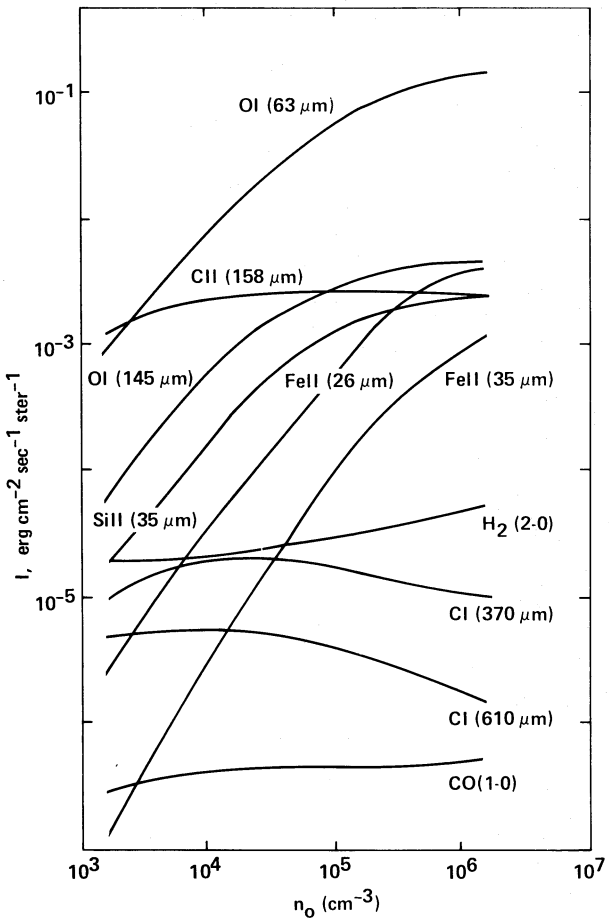

FIG. 10.—The emergent intensities I in the cooling lines are given as a function of density n_0 in the slab. All other parameters have the standard values of Table 2.

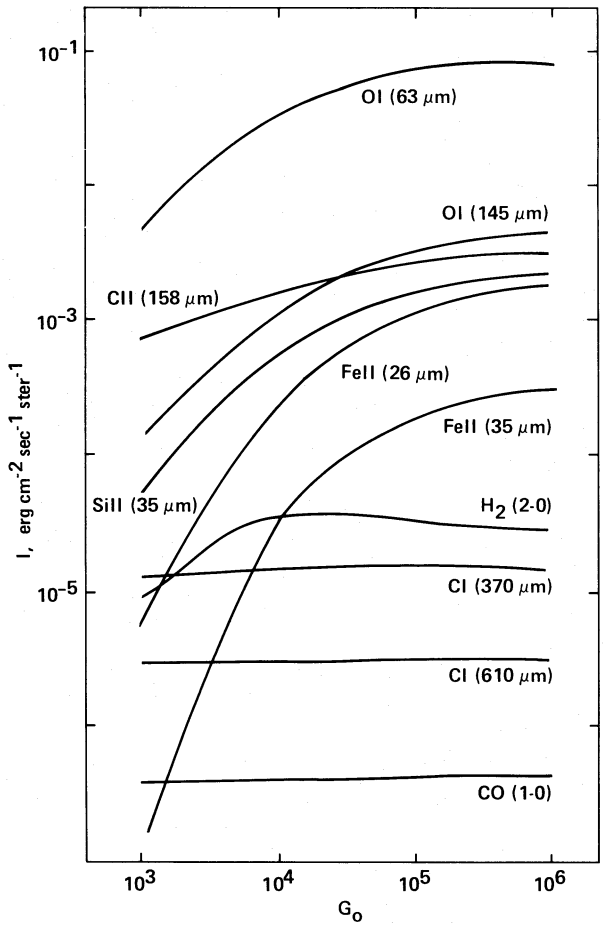

FIG. 11.—The emergent intensities I in the cooling lines are given as a function of the mean intensity of the incident FUV field G_0. All other parameters have the standard values of Table 2.

V. DISCUSSION

In this section the general characteristics of the photodissociation regions will be described, with emphasis on the results of the standard model (Table 2, Figures 7–9). We will first discuss the molecular composition, then the energy balance, and finally the intensities of the atomic fine-structure and molecular rotational lines.

a) The Molecular Composition

i) *The Abundance of Vibrationally Excited* H_2^*

At the cloud edge hydrogen is mainly in atomic form. Because of self-shielding, the abundance of H_2 increases with increasing depth into the cloud. For $A_v > 2$, hydrogen is mainly in molecular form in the standard model (see Fig. 9*a*).

At the cloud edge the few existing H_2 molecules are in vibrationally excited states. The abundance of vibrationally excited H_2^* is important because H_2^* may be observable in 2 μm vibrational emission (see Paper II) and can dominate the chemical production of some species (see below). The collisional de-excitation of H_2^* is second only to the photoelectric mechanism as a heat source for the gas.

The abundance of H_2^* is set by the equilibrium between FUV pumping, radiative decay, and collisional de-excitation. Because of the decrease in the FUV pumping rate, the fraction of H_2 in vibrationally excited states decreases with increasing depth into the cloud. The abundance of H_2^* increases, however, until $A_v = 2$ as a result of the increase in the total H_2 abundance. The column density of H_2^* in all levels with $v \geq 1$ is 4.5×10^{16} cm^{-2} in the standard model. This is in good agreement with the detailed results of Shull (1978), who included all vibrational levels of H_2 in his calculations.

The column density of H_2^* increases by a factor of 20 as the density is increased from 10^3 to 10^6 cm^{-3}. A higher density results in a higher H abundance for $A_v < 2$. As a result, H_2 can compete more effectively with the dust for the FUV photons capable of pumping it to the $B\,^1\Sigma_u^+$ and $C\,^1\Pi_u$ electronic states. It should be noted that in the standard model the FUV dust optical depth is about 2 at the position where the optical depths in the H_2 lines reach unity. Therefore, a considerable fraction of the photons shortward of 1100 Å wind up heating the dust rather than pumping H_2 molecules to the electronically excited states.

The column density of H_2^* is also sensitive to the turbulent Doppler width of the H_2 absorption lines. Lowering the Doppler width from 5 to 1 km s^{-1}, while keeping the density constant, results in a 30% decrease in the H_2^* column density. A smaller Doppler width results in significant self-shielding at smaller column densities of the ground state H_2. Consequently, the column density of H_2^* will also be smaller.

The H_2^* column density is only slightly sensitive to G_0. As expected, for $G_0 < 10^4$, the column density of H_2^* increases slightly with G_0 (a factor of 2 for a factor of 10 change in G_0).

© American Astronomical Society • Provided by the NASA Astrophysics Data System

1985ApJ...291..722T

For $G_0 > 10^4$, however, the H_2^* column density decreases slightly with G_0 (a factor of 2 for a factor of 100 increase in G_0). This decrease in $N(H_2^*)$ for large G_0 is caused by the increased gas temperature, which leads to greater collisional de-excitation of H_2^*.

Finally, $N(H_2^*)$ also depends on the absorption cross section of the dust. A smaller FUV ($\lambda < 1100$ Å) dust absorption cross section implies that H_2 competes more effectively with the dust for H_2 pumping photons. This results in a larger column density of H_2^*. For $k_\lambda = 1$ (see § III*a*) the H_2^* column density increases by a factor of 3 as compared with the standard model.

ii) *The* C^+/C/CO *Transition*

The abundance of C^+, C, and CO show a complex behavior as a function of A_v (Fig. 9*b*). At the cloud edge most of the carbon is in the form of C^+. The abundance of C^+ decreases steadily with depth into the cloud. The neutral carbon abundance generally shows two peaks. In the standard model these occur at a visual extinction of 3.7 and 6.5 mag, respectively. The CO abundance reaches a first maximum around 2 mag. Beyond 4 mag most of the carbon is in the form of CO.

This complex behavior is the result of the many competing processes which transform C^+ into either C or CO. At the cloud edge, $A_v < 4$ in the standard model, ionized carbon is formed through photoionization of C. C^+ is destroyed mainly through radiative recombination. The first small peak in the CO abundance, around $A_v \approx 2$, is initiated by reactions of H_2^* with O which produce OH. Reactions with C^+ then ultimately produce CO. Beyond $A_v > 3$ the CO abundance starts to rise again, because of reactions of O with the CH and CH_2 which originated from the radiative association of C^+ with ground state H_2. The dip in the CO abundance around 6.5 mag corresponds to the second peak in the C abundance and will be discussed below.

For $A_v < 2$ neutral carbon results mainly from radiative recombination of C^+, with some contribution from CO photodissociation. The abundance of neutral carbon rises in this region because of the decrease in the photoionization rate of C. For $A_v > 2$ an increasing amount of C^+ is channeled to CH and CH_2 by the radiative association with H_2. These molecules may flow to neutral carbon through photodissociation or may flow to CO through reactions with O (see above). The latter channel becomes increasingly important at higher A_v. This produces the decline in the C abundance for $4 < A_v < 5$. Beyond a visual extinction of 5 mag the C abundance rises again because of charge exchange reactions of C^+ with S and, to a lesser extent, SiO. Once the C^+ abundance falls below that of S^+, the charge exchange of S with C^+ produces more C than direct recombination of C^+. This can be understood by realizing that the more abundant S^+ recombines more rapidly than C^+, and every S^+ recombination leads to an S which charge-exchanges to produce a C.

The main destruction mechanism for neutral carbon is photoionization for $A_v > 7$. The carbon abundance drops beyond $A_v > 7$ because of the reaction of C with OH to form CO. The OH abundance increases in this region because of the decrease in the photodissociation rate of OH.

The neutral carbon column density is about 4.5×10^{17} cm^{-2} in the standard model, a value which is insensitive to G_0. Although for smaller G_0 fewer C atoms are photoionized, also fewer molecules like CH, CH_2, and CO are photodissociated to produce C. The C column density is somewhat more sensitive to the gas density n_0. At $n_0 = 2.3 \times 10^3$ cm^{-3} the C column density is about 1.6×10^{18} cm^{-2}. This increase in the C column density for decreasing density is a result of the competition between the different loss channels of C^+. For decreasing density relatively more C^+ is transformed to C rather than to CO, because the C^+-produced CH and CH_2 photodissociate rather than react with O to form CO.

The column density of C^+ is typically about 2×10^{18} cm^{-2}. It is quite insensitive to the density n_0 and the intensity of the incident FUV field G_0. Varying n_0 or G_0 by a factor of 10^2 changes the C^+ column density by only a factor of 2, because the extent of the C^+ region is limited by dust absorption of FUV photons.

The C^+/C/CO transition is somewhat dependent on the assumed FUV absorption properties of the dust, and the assumed elemental abundances of oxygen and carbon. Decreasing the FUV cross section of the dust per H nucleus increases the column densities of C^+ and C. For $k_\lambda = 1$ (see § III*a*) the C^+ and C column densities increase by about a factor of 2. For a fixed oxygen abundance the column densities of C, C^+, and CO scale linearly with the carbon abundance. For a fixed carbon abundance the column densities of C and C^+ increase, while that of CO decreases, for a decreasing oxygen abundance. This O dependence arises because of the increased importance of photodissociation of CH and CH_2 forming C and ultimately C^+ relative to the CH and CH_2 reactions with O to form CO. In the limiting case, when the carbon abundance is larger than the oxygen abundance, neutral carbon can become important throughout the whole cloud.

iii) *The Electron Abundance*

The electron abundance is coupled to the C^+, S^+, and Mg^+ abundances (see Fig. 9*a*). At the cloud edge the electron abundance is equal to the carbon abundance. For increasing visual extinction the electron abundance decreases because the attenuation of the UV flux allows C^+ to recombine. The electron abundance drops until it reaches the sulfur abundance at about $A_v \sim 4$. Sulfur has a slightly lower ionization potential than carbon and is therefore photoionized to somewhat greater depth into the cloud. For $A_v > 5$, S^+ recombines and the electron abundance drops to that of the (depleted) metals. The metals have a low ionization potential and are photoionized until $A_v \approx 10$. Beyond that depth the ionization is dominated by cosmic-ray ionization of H_2 and He. This charge flows quickly to molecular ions and finally metal ions through charge transfer reactions (Oppenheimer and Dalgarno 1974).

iv) *Other Molecules*

The abundances of CH^+, CH_2^+, and CH_3^+ show a distinct maximum around $A_v \approx 2$ in the standard model, as O and C^+ react with H_2^* to produce the intermediate CH^+ which leads to these molecules. In Table 3 we present column densities of those molecules which result from reactions of H_2^*. These column densities depend quite strongly on the rather uncertain rate assumed for the initiating reactions of H_2^*. Measurements of the column density of these species can be used to derive the rate of these reactions. This is especially true since these molecules generally have a very low abundance inside dense molecular clouds, although care should be excercised to avoid contributions from shocked gas.

The abundance of the neutral oxygen–bearing molecules, OH, H_2O and O_2, increases at great depth in the clouds. These molecules are dissociated to much greater depth than CO because lower energy (more penetrating) FUV photons can cause their destruction.

© American Astronomical Society • Provided by the NASA Astrophysics Data System

1985ApJ...291..722T

TABLE 3

EFFECTS OF VIBRATIONALLY EXCITED H_2 IN THE STANDARD MODEL

Species	Maximum Abundance[a]	Column Density (cm^{-2})
H_2^*	3.0(−5)	4.4(16)
CH^+	3.6(−9)	1.8(12)
CH_2^+	1.1(−9)	1.1(12)
CH_3^+	1.1(−9)	3.2(12)

NOTE.—Numbers in parentheses: see Table 2.

[a] The abundances are fractional number densities relative to hydrogen nuclei.

b) *The Energy Balance*

i) *Dominant Heating and Cooling Mechanisms*

The outer cloud layers, $A_v < 6$ for the standard model, are predominantly heated by the photoelectric effect on dust grains. The contribution to the heating by FUV pumping of H_2 and by photoionization of C is small (see Fig. 8*a*). The cooling in the standard model is dominated by O I 63 μm emission (see Fig. 8*b*). The cooling due to C II 158 μm emission is small because of the high density and temperature in this model (see § II and Fig. 3).

The cooling through the O I 63 μm line (Fig. 8*b*) decreases with increasing depth into the cloud because of the increased optical depth in the O I 63 μm line (in Appendix B we describe the escape probability formalism, which treats optical-depth effects). The photoelectric heating drops with increasing A_v because of the increased FUV optical depths of the dust. This is, however, partly offset by an increase in the efficiency of the photoelectric effect. At the edge of the cloud the grains are highly positively charged and the photoelectric efficiency is only about 0.1%. At the position of the maximum temperature the efficiency is 0.7% because of the decreased grain charge resulting from the lower intensity of the FUV radiation field (see § II, Fig. 6). The tendency for the heating to drop less than the cooling results in a temperature maximum around $A_v \sim 1.2$.

Deeper into the cloud the gas temperature drops again because of the increased cooling through the rotational lines of CO and H_2 and because of decreased heating caused by the dust extinction of FUV radiation. For $A_v > 4$ the rotational transitions of CO dominate the cooling.

For $A_v > 6$ the gas is heated mainly by the continuum infrared radiation field produced by the dust. Once the gas temperature drops below the equivalent radiation temperature of the infrared background (about 50 K in the standard model; see Appendix B), radiative excitation of the O I $^3P_1$ level by a 63 μm photon, followed by collisional de-excitation, will heat the gas. This tends to couple the gas and dust temperatures to each other. Other species such as H_2O are unimportant because all O not bonded in CO remains atomic to $A_v \sim 10$. The CO transitions lie at submillimeter wavelengths and ineffectually couple the gas to the radiation field.

Gas-grain collisions can also be of some importance in the energy balance of the gas. At the cloud edge the gas is hotter than the dust and the gas is cooled by gas-grain collisions. Deeper into the cloud the gas temperature drops below the dust temperature and gas-grain collisions heat the gas. In the standard model the gas-grain collision mechanism is never the dominant gas heating or cooling source. For higher densities ($n_0 > 10^6$ cm^{-3}), however, it is the most important gas cooling source at the cloud edge and the dominant gas heating source deeper in the cloud.

ii) *The Gas Temperature at Cloud Edge and the Maximum Temperature of the Gas*

The temperature of the gas initially increases with depth for the standard model from a value of about $T_{edge} \approx 600$ K at the edge to a maximum value of about $T_{max} \approx 1100$ K at $A_v \approx 1.2$. Comparison of the temperature structure of the different models is understood primarily by examining the effects of grain charge. When the grains at cloud edge are highly positively charged ($G_0 T_{edge}^{0.5}/n_e > 3 \times 10^3$ K$^{0.5}$ cm^3), T_{edge} increases with increasing density because photoelectric heating increases more rapidly with density than the cooling. Similarly, T_{edge} decreases with increasing G_0 for positively charged grains because of the decreased heating efficiency (recall that most of the FUV is reradiated as infrared continuum by the grains).

If the grains at cloud edge are highly positively charged, then the gas temperature will increase with depth into the cloud and a temperature maximum T_{max} will be reached where the grains are more neutral. This temperature inversion depends on the gas density and the intensity of the incident FUV field. For a constant incident FUV field T_{max} increases with increasing density, as the enhanced grain-electron recombination rate leads to higher photoelectric heating efficiencies. Increasing the incident FUV field while keeping the density constant decreases T_{edge} as discussed above. At the same time it increases T_{max} because the O I cooling is suppressed by the increased optical depth into the cloud at which T_{max} is reached. The largest temperature inversions occur for high incident FUV fields and low densities.

The observed emission from photodissociation regions is very sensitive to T_{max}, and therefore we have run cases where the constrained parameters have been varied. If the Doppler width is increased while n_0 and G_0 are kept constant, then T_{max} drops because of the greater escape probabilities of the cooling transitions. In particular, using the standard model, we find $T_{max} = 1900$ K for $\delta v_d = 1$ km s^{-1}, while $T_{max} = 850$ K for $\delta v_d = 5$ km s^{-1}. T_{edge} is not influenced by δv_d, since the cooling is optically thin at cloud edge.

The carbon and oxygen abundance also have some influence on the temperature of the cloud. A lower carbon abundance implies a lower electron abundance. The lower grain-electron recombination rate results in a higher grain positive charge and thus a lower photoelectric efficiency. As a consequence, the gas temperature is lower. A lower oxygen abundance implies a lower cooling rate and hence a higher temperature.

Finally, for smaller FUV absorption cross sections of the dust per H nucleus, the gas temperature will be lower because of the decrease in photoelectric heating.

c) *Line Intensities*

The emergent intensities of the cooling lines generally increase monotonically with the gas density and the intensity of the incident FUV field, with the exception of the C I 370 μm and 609 μm and the C II 158 μm lines (see Figs. 10 and 11). The atomic infrared and submillimeter fine structure lines are all optically thin except for the O I 63 μm line, which reaches an optical depth of a few in the photoelectrically heated region, and the C I lines, which may reach an optical depth of about unity at $A_v \sim 10$. The low rotational lines of CO are optically thick.

The O I 63 μm and 145 μm, the C II 158 μm, the Si II 35 μm,

© American Astronomical Society • Provided by the NASA Astrophysics Data System

1985ApJ...291..722T

the Fe II 26 μm and 35 μm, and the H_2(2–0) [the $S(0)$ pure rotational transition at 28 μm] lines originate in the warm photoelectrically heated region ($A_v < 5$). The C I 370 μm and 609 μm lines are produced deeper into the standard cloud ($A_v > 4$). In the absence of large-scale velocity gradients, the CO rotational lines originate mainly from the C^+/C/CO transition region ($A_v \sim 5$), with a small contribution from the region with vibrationally excited H_2^* ($A_v \sim 2$).

In interpreting Figures 10 and 11, it should be kept in mind that the maximum gas temperature in the photodissociation region increases with increasing n_0 and G_0. The differences in the behavior of the intensities of the different lines as a function of n_0 and G_0 can then be easily understood in terms of the critical densities and excitation energies of the levels involved (see Appendix B and Table 4). Thus, despite their similar abundances in photodissociation regions, C II 158 μm dominates at low densities ($n_0 < 10^3$ cm^{-3}), while O I 63 μm dominates at high densities ($n_0 > 10^4$ cm^{-3}) and high temperatures ($T > 100$ K; see Fig. 3). Similarly, the Fe II and Si II fine-structure lines rise somewhat more steeply with n_0 and G_0 than the O I 63 μm line because of their higher excitation energies.

The C I 370 μm and 609 μm lines behave somewhat differently from the other lines. They originate in the region heated by infrared radiation and by gas-dust collisions. The temperature in this region depends only slightly on the density. The C I column density increases with decreasing density (see § V*a*[ii]). The C I lines reach an optical depth of unity around $n_0 \approx 10^5$ cm^{-3}. The rise of the temperature with n_0 then produces a maximum in the line intensities around $n_0 \sim 10^4$ cm^{-3} (see Fig. 10). The column density of neutral carbon in the photodissociation region model is about 10 times larger than previous calculations indicated (Glassgold and Langer 1975; Langer 1976, 1977; de Jong, Dalgarno, and Boland 1980). Part of this difference is due to improvements in the chemical modeling, especially the inclusion of charge exchange reactions between C^+ and S, and to a lesser extent SiO, and self-shielding of neutral carbon. The rest of this difference in the column density of atomic carbon arises because of the higher elemental abundance of carbon in our models compared with previous models. In recent years the elemental abundance of gas-phase carbon, derived from UV observations of the diffuse interstellar medium, has been revised upward (Jenkins and Shaya 1979; Jenkins, Jura, and Loewenstein 1983). Although inside dense molecular clouds gas-phase species may condense out on cold dust grains in the form of icy grain mantles, it is unlikely that this will occur in a photodissociation region illuminated by an intense FUV field. Furthermore, pre-existing grain mantles would not likely survive such a harsh environment (Tielens and Hagen 1982). The carbon depletion in photodissociation regions around H II regions is therefore not expected to be larger than in the diffuse interstellar medium or in the H II regions themselves. In our standard model we have chosen to use the measured carbon abundance in the Orion Nebula (Peimbert 1982). The C I column density in the photodissociation region (i.e., the cloud surface) is sufficiently large to explain the intensities of the observed C I 609 μm emission toward molecular clouds (see Phillips and Huggins 1981). Paper II and Tielens and Hollenbach (1984) discuss the C I emission from OMC-1 in detail.

Besides their sensitivity to n_0 and G_0, the emergent intensities depend also on the Doppler width of the lines, the FUV opacity of the dust, and the abundances of the elements. We examine these three parameters below.

Changing the Doppler width from 1 to 5 km s^{-1} in the standard model, while keeping n_0 and G_0 fixed, produces variations in the emergent intensities of the O I 63 μm and 145 μm, the C II 158 μm, and the C I 370 μm and 609 μm lines of less than 30%. Changing the Doppler width influences mainly the temperature of the gas. The O I 63 μm line measures the total photoelectric heating of the gas, which is only weakly dependent on the gas temperature. The other lines are optically thin and relatively temperature-insensitive, so that they vary little with δv_d. The Si II and Fe II infrared fine-structure lines are somewhat more sensitive to the Doppler width, because their relatively high excitation energies make them temperature-sensitive. Their computed line intensities change by less than a factor of 2 from $\delta v_d = 5$ km s^{-1} to $\delta v_d = 1$ km s^{-1}.

We have also calculated a model with reduced FUV absorption cross sections for the dust. Assuming a gray dust opacity ($k_\lambda = 1$) from the visual to the far-ultraviolet instead of the mean interstellar extinction curve changes the emergent intensities up to 50%. The O I 63 μm intensity increases slightly (10%) owing to the lower gas temperature, which produces an overall higher efficiency of the photoelectric effect. The effect on the intensity of the C I and C II lines is somewhat larger ($\sim$50%). This increase is caused by the increased extent of the photodissociation region for lower FUV absorption cross sections of the dust. This results in larger C and C^+ column densities and therefore larger optical depths and line intensities.

Decreasing the elemental carbon abundance from 3×10^{-4} to 10^{-4} in the standard model, while keeping all other parameters constant, decreases the intensity in the C I 370 μm and 609 μm and the C II 158 μm lines by a factor of 3. This is because the grains control FUV absorption so that the column densities of C I and C II are proportional to the carbon abundance. The elemental carbon abundance also influences the O I 63 μm intensity, because it supplies electrons in the photoelectrically heated region. A decrease in the elemental carbon abundance therefore reduces the photoelectric efficiency, although this is partly offset by the lower gas temperature. A decrease in the elemental carbon abundance by a factor of 3 produces a change in the O I 63 μm intensity of less than a factor of 2. The decreased temperature also produces lower (less than a factor of 2) intensities in the Si II and Fe II lines.

Changing the oxygen abundance has little influence on the emergent intensities. The O I 145 μm line forms an exception, because this line is optically thin and therefore measures the column density of O I. A lower oxygen abundance implies that the equilibrium between C and CO shifts toward C (see § V*a*[ii]), and the C I line intensities increase slightly. The Si II and Fe II line intensities increase somewhat for lower O abundance because of the higher gas temperature.

d) *Uncertainties in the Chemical Network*

Because the computed results of our rather restricted chemical network differ considerably from the results of previous studies, it is of particular interest to assess the accuracy of our network. Such an evaluation is, of course, also of interest for the comparison of the computed line intensities with the observations.

Following the "thermal" model calculations, which compute the thermal balance, the chemical equilibrium (using a restricted chemical network), and the radiative transfer in the lines, we have recalculated, using the temperature structure from the thermal model, the chemical abundances as a function

© American Astronomical Society • Provided by the NASA Astrophysics Data System

1985ApJ...291..722T

of depth in a number of model clouds with a more extended chemical network. This network is based on the compilation of Prasad and Huntress (1980). It includes 1533 reactions between 145 species. Self-shielding by C and H_2 has been taken into account. Reactions of H_2^* have been excluded. A more extensive discussion of the equilibrium chemical model is provided in Tielens and Hagen (1982). The input parameters for these calculations (e.g., n_0, G_0, T_0, A_v, the carbon column density, and the self-shielding factor β for photodissociation of H_2) are taken from the thermal model calculations. In the subsequent discussion we will concentrate mainly on the C^+/C/CO transition, where differences from previous calculations are most important, but we will also discuss H_2 formation and CO self-shielding.

i) C^+/C/CO *Chemistry*

In the standard model the abundances of C^+, C, and CO in the extensive chemical model generally agree to $\pm 20\%$ accuracy with their respective values in the thermal model. They never differ by more than a factor of 2 in the regions of interest, with the exception of the region around $A_v \sim 2$, where reactions of H_2^* dominate the chemistry. These reactions are not included in the extensive chemical scheme. The calculated column densities agree to within 10%, since differences between the two models tend to cancel as a function of depth.

This assessment of the accuracy of the calculated abundances and column densities in the standard model does not take into account the uncertainties in the rates of the key reactions involved. It should be emphasized that the chemistry is dominated by photoionization and dissociation of atoms and molecules. The column densities of many species therefore depend directly on the penetration depth of FUV photons into a cloud, i.e., on the FUV extinction properties of the dust and the self-shielding of H_2 and C (photoionization of C is important to $A_v \sim 7$).

ii) H_2 *Formation on Grains*

If the grain temperature is higher than a critical temperature (~ 75 K), then H_2 formation on grain surfaces will be inhibited (§ III*d* and Appendix C). In that case an H atom on a grain surface evaporates before it can react to form H_2. In order to assess the importance of H_2 formation on grains, we have recalculated the standard model, excluding H_2 formation on grains. Because the H^--initiated gas-phase H_2 formation mechanism is less effective than the grain-surface reaction rate assumed in the standard calculation, the H_2 abundance is suppressed and the hydrogen becomes molecular deeper into the cloud. This has, however, no major consequences for the emergent intensities in the infrared atomic fine-structure lines. It is reflected only in $N(H_2^*)$. $N(H_2^*)$ decreases by more than 2 orders of magnitude, basically because the dust absorbs most of the photons capable of exciting H_2. Because $N(H_2^*)$ inferred from the observations of the H_2 1–0 $S(1)$ line in Orion is in reasonable agreement with the model calculations with grain-surface formation of H_2 (Paper II), we conclude that H_2 formation on grain surfaces in the parameter space studied here proceeds at a rate comparable to that in diffuse clouds.

iii) CO *Self-shielding*

We have recalculated the standard model including CO self-shielding in the manner described in Appendix C. As expected, the major change occurs in the CO and C abundances. Relatively more C^+ is converted to CO rather than to C. As a result, the emergent intensity in the C I 609 μm line decreases by a factor of 2. This would make it somewhat difficult to explain the intensity of this line observed toward Orion (Paper II). The emergent intensities of the other infrared fine-structure lines do not change by more than $\sim 20\%$.

VI. SUMMARY

We have theoretically modeled the chemistry and heat balance of dense (10^3 cm$^{-3} < n_0 < 10^6$ cm^{-3}) neutral gas illuminated by FUV flux $G_0 = 10^3$–10^6 times as intense as the ambient interstellar field. The intense FUV fields have a dramatic effect on the structure and line emission from these regions. The FUV dominates the chemistry and heating as deep as $A_v \sim 10$ into the molecular clouds. Molecular clouds typically have column densities in the range 2×10^{22} cm^{-2} ($A_v \approx 10$) to 2×10^{23} cm^{-2} ($A_v \approx 100$) and, therefore, photodissociation regions include a significant volume and mass of the dense opaque clouds. They also lie adjacent to possibly shock-compressed molecular regions ($A_v \sim 20$) where massive star formation may be proceeding (Elmegreen and Lada 1977). More important, a major fraction of the FUV photons emitted by the stars are absorbed by dust in photodissociation regions and transformed into infrared radiation. A small fraction of this energy is tapped by the gas through the photoelectric ejection of electrons from grains, and is reradiated in infrared fine-structure lines.

The models are intended primarily for the FUV–illuminated neutral gas between H II regions and molecular clouds like those in Orion (Paper II), but they also apply to neutral shells around planetary nebulae, bright-rimmed molecular clouds, reflection nebulae, regions around protostars, and the center of the Galaxy, and to global studies of external galaxies. The models relate line and grain continuum emission from these regions to interesting physical parameters such as gas density, turbulent line widths, FUV flux, dust FUV opacity, and elemental abundances.

The main conclusions and results for one-dimensional models of intense FUV flux incident on plane-parallel photodissociation regions are as follows.

1. Although the bulk of the FUV flux is absorbed by grains and reradiated as infrared continuum, a fraction $\epsilon \sim 10^{-2}$–10^{-3} heats the gas through the photoelectric heating mechanism and emerges as C II 158 μm or O I 63 μm line flux. This value is consistent with observations of photodissociation regions near H II regions (Table 1). The heating efficiency ϵ decreases with increasing G_0 and decreasing n_0 because of the effect of positive grain charge on the photoelectric heating mechanism. As an application of this result, we note that many stellar photons in dusty spiral galaxies are absorbed by the interstellar gas and dust, and most of this absorption occurs in atomic photodissociation regions. The absorption is primarily by dust, and more than 99% of the absorbed FUV radiation is converted into far-infrared continuum. The remaining ($<1\%$) FUV energy flux is converted into gas heating and thereby far-infrared and submillimeter line radiation such as O I 63 μm and 145 μm, C II 158 μm, C I 370 μm and 609 μm, and low-lying rotational transitions of CO (see recent observations by Crawford *et al.* 1985).

2. At the cloud surface (A_v less than a few) the dominant gas heating mechanism is photoelectric heating, and the gas temperature greatly exceeds the grain temperature (for example, for Orion-like conditions, $T_{gas} \sim 100$–1000 K and $T_{gr} \sim 75$ K). Heating by the collisional de-excitation of vibrationally excited H_2 is also significant at high densities. The H_2 vibrational excitation arises from an FUV pumping mechanism. Deeper in

© American Astronomical Society • Provided by the NASA Astrophysics Data System

1985ApJ...291..722T

the cloud, where the FUV flux is greatly attenuated and the gas temperature drops below the grain temperature, the collisional deexcitation of O I excited by the absorption of 63 μm continuum from dust grains is an important heating mechanism, as are direct H_2-grain collisions.

3. We predict approximately an order of magnitude greater column density of warm C I in the photodissociation region as compared with previous models. This result is due to the inclusion of a higher gas-phase elemental abundance of carbon, sulfur and silicon chemistry, and self-shielding of atomic carbon. This result is rather insensitive to the FUV flux and gas density. For example, $N(\text{C I}) = 2 \times 10^{18}$ and 5×10^{17} cm^{-2} for $n_0 = 10^3$ and 10^5 cm^{-3}, respectively. A future paper will treat C I abundances for $n_0 < 10^3$ cm^{-3}, where a more complicated sulfur chemistry is required. The large C I column densities which emerge from our models strongly suggest that the observed C I 609 μm emission may generally arise from molecular cloud surfaces, and not from their interiors as has been previously suggested.

4. Photodissociation regions adjacent to H II regions glow brilliantly in the infrared and radio. The observed far-infrared continuum (see Werner *et al.* 1976), and such lines as O I 63 μm and 145 μm, C II 158 μm (see Table 1 and § I), C I 609 μm (see Phillips and Huggins 1981), low-lying CO rotational transitions (see Loren 1979; Phillips *et al.* 1979; Thronson and Lada 1983), extended H_2 1–0 $S(1)$ (Treffers 1983), C I 9850 Å (Münch and Hippelein 1982), and C II recombination transitions (see Palmer *et al.* 1967; Dupree 1974; Boughton 1978; Brown, Lockman, and Knapp 1978) all may originate in the photodissociation region (see Paper II for explicit model of OMC-1).

5. The line and grain continuum intensities constrain interesting physical parameters and test chemical reaction schemes in the interstellar medium. (*a*) The grain continuum measures the FUV flux G_0. (*b*) The O I 63 μm, C II 158 μm, and the grain continuum fluxes probe n_e, T, n_0, and the carbon abundance. The O I 63 μm is moderately optically thick, so that the peak intensity provides a measure of the gas temperature. The ratio O I 63 μm/C II 158 μm is sensitive to gas density and temperature; in particular, large values of this ratio ($\gg 1$) indicate high densities, $n_0 \gg 10^3$ cm^{-3}, and temperature $T > 100$ K. The ratio (O I 63 μm + C II 158 μm)/F_{IR} measures ϵ and is sensitive to the parameter $\gamma \propto G_0 T^{0.5}/n_e$. The C II 158 μm intensity, taken with the C I 370 μm and 609 μm intensities, probes the carbon abundance and the FUV opacity of the dust grains. (*c*) The Fe and Si fine-structure lines, as yet unobserved, are sensitive to temperature and to the gas-phase abundances of these elements. (*d*) Line emission from photodissociation regions provides interesting constraints on chemistry in the interstellar medium. The FUV–pumped 1–0 $S(1)$ emission from H_2 probes the formation rate of H_2 on warm dust grains. The detection of CH^+, CH_2^+ or CH_3^+ will determine the reaction rate of H_2^* with C^+. As discussed in item 3 above, the interpretation of the C I 609 μm observations affects our understanding of the chemistry of molecular clouds.

We have benefited from discussions with R. Genzel, D. Watson, and M. Werner. We would like to thank the Astronomy/Relativity Branch at NASA Headquarters for their support under NASA RTOP 188-41-53.

APPENDIX A

GAS HEATING MECHANISMS

I. PHOTOELECTRIC EMISSION FROM DUST GRAINS

Absorption of a FUV photon by a dust grain can give rise to the emission of an electron. The energy difference between the photon energy and the work function of the grain will be carried away in the form of kinetic energy by the electron. The difference between this heat input to the gas and the effective cooling when an electron with energy $\sim kT$ recombines with a grain usually results in a net heating of the gas.

Because the work function of the grain depends on its charge, the calculation of the net photoelectric heating rate is somewhat involved. Following de Jong (1977, 1980), we write for the net photoelectric heating rate

$$\Gamma_1 = 0.5\langle n_d \sigma_d \rangle Y \lambda_{\text{H}} \langle F \rangle e^{-\tau}[(1-x)^2/x + x_k(x^2-1)/x^2] , \tag{A1}$$

where n_d, σ_d, and Y are the number density, FUV cross section, and photoelectric yield of the dust grains, λ_{H} is the wavelength corresponding to the hydrogen ionization limit, and $\langle F \rangle$ is the mean ultraviolet flux per unit wavelength incident on our slab. The exponential factor describes the attenuation of the radiation field by dust absorption. The factor in brackets takes into account the effect of the neutral work function of the grain, the grain charging, and the electron recombination. The charge parameter x is discussed below. Inserting numerical values in equation (A1), we find

$$\Gamma_1 = 2.7 \times 10^{-25} \delta_{uv} \delta_d n_0 Y G_0 e^{-k_{uv} A_v}[(1-x)^2/x + x_k(x^2-1)/x^2] \text{ ergs cm}^{-3} \text{ s}^{-1} . \tag{A2}$$

Here δ_{uv} is the ratio of the geometrical cross section of the grains that absorb in the FUV to that of the grains that absorb in the visual, δ_d is the ratio of the dust abundance in these regions to that in the diffuse interstellar medium (we assume that $\langle n_d \sigma_d \rangle = 5 \times 10^{-22} n \delta_{uv} \delta_d$), n_0 is the hydrogen nucleus number density, G_0 is the mean FUV flux incident on the slab in terms of that in the diffuse interstellar medium (Habing 1968), and k_{uv} is the effective ratio of FUV optical depth to A_v (see § III*a*).

Equating the photoelectric emission rate with the electron recombination rate of the grain yields an equation for the grain charge parameter x (de Jong 1977):

$$x^3 + (x_k - x_d + \gamma)x^2 - \gamma = 0 , \tag{A3}$$

© American Astronomical Society • Provided by the NASA Astrophysics Data System

1985ApJ...291..722T

where $x = \nu_0/\nu_H$, $x_k = kT/h\nu_H$, and $x_d = \nu_d/\nu_H$. Here T is the gas temperature, $h\nu_d$ is the photoelectric threshold energy for the neutral grain material, and $h\nu_0$ is the energy barrier which an electron has to overcome, including the grain-charge effect. The grain charge, Z_d, is then given by

$$Z_d = (x - x_d)h\nu_H a/e^2 , \tag{A4}$$

where a is the grain radius.

The unitless parameter γ is given by

$$\gamma = 2.9 \times 10^{-4} Y T^{0.5} G_0 e^{-k_{uv} A_v} n_e^{-1} , \tag{A5}$$

where n_e is the electron density in cm^{-3} and T is in K.

The photoelectric yield Y and threshold energy $h\nu_d$ depend on the grain material and the size of the grain particle (Watson 1972). Following de Jong (1980), we will assume $Y = 0.1$ and $h\nu_d = 6$ eV. These values give a photoelectric heating rate of the diffuse interstellar medium in agreement with the cooling rate derived from observations of FUV resonance lines of C^+ (Pottasch, Wesselius, and van Duinen 1979).

II. CARBON IONIZATION

The heating rate due to photoionization of neutral carbon atoms is given by

$$\Gamma_2 = 2.2 \times 10^{-22} n(C) G_0 \exp(-2.4A_v - \tau_c - \tau b/\pi v_1^2)(1 + \tau b/\pi v_1^2)^{-1} \text{ ergs cm}^{-3} \text{ s}^{-1} , \tag{A6}$$

where $n(C)$ is the neutral carbon density. The first exponential factor in this equation describes the attenuation by dust absorption (Black and Dalgarno 1977), the second describes attenuation by self-absorption of C (Werner 1970), and the last describes attenuation by H_2 (de Jong, Dalgarno, and Boland 1980). The unitless parameters in this expression are given by

$$\tau_c = 10^{-17} N(C) , \qquad \tau = 1.2 \times 10^{-14} N(H_2) \delta v_d^{-1} , \qquad b = 9.2 \times 10^{-3} \delta v_d^{-1} , \qquad v_1 = 5 \times 10^2 \delta v_d^{-1} , \tag{A7}$$

where $N(C)$ and $N(H_2)$ are the column densities of neutral carbon and H_2, and δv_d is the turbulent Doppler line width in km s^{-1}.

III. H_2 PHOTODISSOCIATION

The pumping of H_2 molecules by photons in the Lyman and Werner bands can heat the gas through photodissociation. This occurs for about 10% of the pumps, when the radiative decay from the excited electronic state leads to the vibrational continuum of the ground electronic state, as originally suggested by Solomon (see Field, Somerville, and Dressler 1966) and calculated by Stecher and Williams (1967). The total FUV pumping rate R_{pump} and the heating rate associated with photodissociation are given by

$$R_{pump} = 3.4 \times 10^{-10} \beta(\tau) G_0 e^{-2.5A_v} \text{ s}^{-1} , \tag{A8}$$

and

$$\Gamma_3 = 1.36 \times 10^{-23} n(H_2) \beta(\tau) G_0 e^{-2.5A_v} \text{ ergs cm}^{-3} \text{ s}^{-1} , \tag{A9}$$

where $n(H_2)$ is the number density of H_2 molecules in the ground state, and the exponential factors take dust absorption of FUV photons into account.

When photon absorption is dominated by the Doppler cores or the Lorentz wings ($\tau > 10$), then the self-shielding factor is given by

$$\beta(\tau) = \{\tau^{-1}[\ln(\tau/\sqrt{\pi})]^{-0.5} + (b/\tau)^{0.5}\} \operatorname{erfc}(\tau b \pi^{-1} v_1^{-2})^{0.5} , \tag{A10}$$

where τ, b, and v_1 are given by equations (A7). In this expression line overlap has been taken into account (de Jong, Dalgarno, and Boland 1980). On the linear part of the curve of growth, the self-shielding factor is given by (Shull 1978)

$$\beta(\tau) = \sum_{n=0}^{\infty} \frac{(-1)^n \tau^n}{n!(n+1)^{1/2} \pi^{n/2}} . \tag{A11}$$

The latter equation for $\beta(\tau)$ is used for $\tau \leq 10$.

In our calculation we have treated the ground electronic state of H_2 as having a ground vibrational and a single excited vibrational state. The effective quantum number of this pseudolevel is $v = 6$, and the effective energy is $E_* = 2.6$ eV (London 1978). This vib-rotationally excited level is treated as a separate molecule in the chemical equilibrium. Vib-rotationally excited H_2^* can be FUV pumped and dissociated. The rate for this process is also given by equation (A8). The optical depth in this case is evaluated by assuming that the H_2^* is divided equally over all vibrational levels. H_2^* can also be dissociated directly by absorption of a FUV photon with a rate (Shull 1978)

$$R = 10^{-11} G_0 e^{-2.5A_v} \text{ s}^{-1} . \tag{A12}$$

IV. FUV PUMPING OF H_2 MOLECULES

About 90% of the Lyman-Werner band absorptions are followed by decay to vib-rotationally excited levels in the ground electronic state. Collisional de-excitation then leads to heating of the gas. We approximate the complicated cascade process with our single excited pseudovibrational level. The heating rate associated with this process is given by

$$\Gamma_4 = [n(H)\gamma_{*0}^{H} + n(H_2)\gamma_{*0}^{H_2}] n(H_2^*) E_* , \tag{A13}$$

© American Astronomical Society • Provided by the NASA Astrophysics Data System

1985ApJ...291..722T

where $n(H_2^*)$ is the number density of H_2^* molecules. The collisional de-excitation rate coefficients (for transitions from the pseudo-$v = 6$ to $v = 0$ which, in reality, tend to occur in steps of $\Delta v = 1$) γ_{*0}^{H} and $\gamma_{*0}^{H_2}$ are assumed to be equal to one-sixth of the $v = 1$ to $v = 0$ rate coefficients γ_{10}^{H} and $\gamma_{10}^{H_2}$ (London 1978). These rates are given by (Hollenbach and McKee 1979)

$$\gamma_{10}^{H} = 10^{-12} T^{0.5} \exp(-1000/T) \text{ cm}^3 \text{ s}^{-1} ,$$
$$\gamma_{10}^{H_2} = 1.4 \times 10^{-12} T^{0.5} \exp\{-[18{,}100/(T + 1200)]\} \text{ cm}^3 \text{ s}^{-1} . \quad \text{(A14)}$$

The H_2^* can also radiatively decay to the ground state with an effective rate $R = 2 \times 10^{-7} \text{ s}^{-1}$ (London 1978).

V. H_2 FORMATION

The chemical energy stored in the gas upon photodissociation of H_2 becomes available as heat when two hydrogen atoms recombine. Formation of H_2 molecules on a grain surface will result in a molecule in a highly excited rotational and vibrational state. Part of the formation energy may flow into center-of-mass translational motion which can cause ejection of the vib-rotationally excited molecule into the gas phase. The excess kinetic energy of the H_2 molecule will heat the gas. Collisional de-excitation of the vib-rotationally hot H_2^* molecule will also heat the gas (see above).

Theoretical calculations indicate that this latter process may be important (Hollenbach and Salpeter 1970; Hunter and Watson 1978). However, these calculations minimize the transfer of energy to the grain surface. Recent matrix isolation studies on energy transfer in low-temperature solids (Legay 1978; Bondeybey and Brus 1980) suggest that most of the vib-rotational energy will be transferred to neighboring molecules through multipolar-multipolar interactions or will flow into local rotational modes (Tielens and Hagen 1984). It is therefore possible that the H_2 molecule will thermally evaporate in the ground vibrational state. Since, in equilibrium, nine molecules are pumped for every molecule formed or destroyed, the formation heating must in any case be small compared with the sum of UV pumping and photodissociation heating. To be conservative, we have not included the ejection of H_2^* after formation on grain surfaces as a heating source or a source of H_2^* in our calculations.

VI. HEATING DUE TO GAS-GRAIN COLLISIONS

There are two ways in which the FUV radiation field can heat the gas through the grains. First, radiation pressure will accelerate the grains relative to the gas and produce a viscous heating term due to gas drag. We find that the grain acceleration time scale is short compared with other time scales, and the grains are moving at their local drift velocity v_d. Basically, all the momentum gained by the grains through radiation pressure is transferred to the gas by, mainly Coulomb drag. Typically, the steady state drift velocities v_d (see Spitzer 1978) are small ($< 10^3$ cm s^{-1}) in our calculations, and no significant gas-grain separation will occur. The heating due to the grain drift is then

$$\Gamma_{6a} = 8\pi e^4 n_d Z_d^2 (kT)^{-1} (\ln \Lambda) v_d [n(C^+) G(y_{C^+}) + n_e G(y_e)] , \quad \text{(A15)}$$

where n_d is the grain number density, Z_d is the grain charge, $n(C^+)$ and n_e are the C^+ and electron number densities, and the functions Λ and G are given by

$$\Lambda = 1.5 Z_d^{-1} e^{-3} (kT)^{1.5} (\pi n_e)^{-0.5} , \quad \text{(A16)}$$

$$G(y) = \frac{1}{2y^2} \left[\text{erf}(y) - \frac{2}{\pi^{0.5}} y e^{-y^2} \right] , \quad \text{(A17)}$$

where $y = v_d/v_{\text{th}}$, and v_{th} is the thermal velocity of the ion or electron.

The second method of energy exchange between gas and dust is through the difference in their temperatures. For the heating rate of the gas we can write (Hollenbach and McKee 1979; Burke and Hollenbach 1983)

$$\Gamma_{6b} = [n(H) + n(H_2)] n_d \delta_d \bar{v}_H \bar{\alpha}_T (2kT_d - 2kT) , \quad \text{(A18)}$$

where $\bar{v}_H$ is the thermal speed of H atoms and $\bar{\alpha}_T$ measures the accommodation effects. We have used $\bar{\alpha}_T = 0.3$, appropriate for molecular gas at $T \sim 100$ K colliding with grains at $T_d \sim 100$ K. Inserting numerical values, we find

$$\Gamma_{6b} = 3.5 \times 10^{-34} n^2 \delta_d T^{0.5} (T_d - T) \text{ ergs cm}^{-3} \text{ s}^{-1} . \quad \text{(A19)}$$

Note that the gas is cooled by this process when $T > T_d$.

The dust temperature follows from the balance between photon absorption and emission.

$$4\pi a^2 \int_0^\infty Q_a(\nu) \pi B(\nu, T_d) d\nu = \pi a^2 \int_0^\infty Q_a(\nu) F(\nu) e^{-\tau(\nu)} d\nu + 4\pi a^2 \int_0^\infty Q_a(\nu) \pi J_d(\nu) d\nu . \quad \text{(A20)}$$

The last term describes absorption from the infrared emission of the dust. In this equation $Q_a(\nu)$ is the absorption efficiency of the dust and $J_d(\nu)$ is the mean radiation field due to dust. We will assume that

$$Q_a(\nu) = \nu/10^{15} \text{ s}^{-1} , \qquad \nu < 10^{15} \text{ s}^{-1}$$
$$= 1 , \qquad \nu > 10^{15} \text{ s}^{-1} , \quad \text{(A21)}$$

and that the dust emission is characterized by a constant temperature T_0 and a total emission optical depth $\tau_d = \tau_{100\,\mu\text{m}}(100\ \mu\text{m}/\lambda)$, where $\tau_{100\,\mu\text{m}}$ is the 100 μm emission optical depth. This yields the following equation for the dust temperature:

$$T_d = (5.6 \times 10^7 G_0 e^{-1.8 A_v} + 3.4 \times 10^2 T_0^6 \tau_{100\,\mu\text{m}})^{0.2} \text{ K} . \quad \text{(A22)}$$

© American Astronomical Society • Provided by the NASA Astrophysics Data System

1985ApJ...291..722T

VII. COSMIC-RAY HEATING

Ionization by cosmic rays produces energetic electrons. About 8 eV of heat is deposited per primary ionization in a molecular gas (Glassgold and Langer 1973; Cravens and Dalgarno 1978). In the atomic gas cosmic-ray heating is of no importance. Including helium ionization, we find for the heating rate

$$\Gamma_7 = 1.5 \times 10^{-11} \zeta n(\mathrm{H}_2) \text{ ergs cm}^{-3} \text{ s}^{-1} , \tag{A23}$$

where ζ is the cosmic-ray ionization rate per H_2 molecule.

VIII. HEATING BY O I

The heating by the collisional de-excitation of the infrared-pumped $^3P_1$ fine-structure level of O I is treated in Appendix B, under the discussion of atomic cooling.

APPENDIX B

RADIATIVE COOLING

I. BASIC EQUATIONS

The radiative cooling rate due to a transition from level i to level j of some species x is given by

$$\Lambda_x(\nu_{ij}) = n_i A_{ij} h\nu_{ij} \beta_{\mathrm{esc}}(\tau_{ij})\{[S_x(\nu_{ij}) - P(\nu_{ij})]/S_x(\nu_{ij})\} , \tag{B1}$$

where n_i is the population density of species x in level i, A_{ij} is the spontaneous transition probability, $h\nu_{ij}$ is the energy difference between levels i and j, τ_{ij} is the optical depth averaged over the line, and $\beta_{\mathrm{esc}}(\tau_{ij})$ is the escape probability at optical depth τ_{ij} of the line. The source function $S_x(\nu_{ij})$ is given by

$$S_x(\nu_{ij}) = \frac{2h\nu_{ij}^3}{c^2}\left(\frac{g_i n_j}{g_j n_i} - 1\right)^{-1} , \tag{B2}$$

where g_i and g_j are the statistical weights of the levels. The background radiation $P(\nu_{ij})$ consists of two terms, the 2.7 K microwave background and the infrared emission of dust at a temperature T_0 and with an emission optical depth $\tau_d(\nu_{ij})$.

$$P(\nu_{ij}) = B(\nu_{ij}, T = 2.7 \text{ K}) + \tau_d(\nu_{ij}) B(\nu_{ij}, T_0) . \tag{B3}$$

The level populations follow from solving the equations of statistical equilibrium (see de Jong, Dalgarno, and Boland 1980).

$$n_i \sum_{j \neq i}^{l} R_{ij} = \sum_{j \neq i}^{l} n_j R_{ji} , \tag{B4}$$

where l is the total number of levels included and

$$\begin{aligned} R_{ij} &= A_{ij} \beta_{\mathrm{esc}}(\tau_{ij})(1 + Q_{ij}) + C_{ij} , \qquad i > j \\ R_{ij} &= (g_j/g_i) A_{ji} \beta_{\mathrm{esc}}(\tau_{ji}) Q_{ji} + C_{ij} , \qquad i < j . \end{aligned} \tag{B5}$$

Here C_{ij} is the collisional rate from level i to level j. The background radiation is contained in the Q_{ij},

$$Q_{ij} = \frac{c^2}{2h\nu_{ij}^3} P(\nu_{ij}) . \tag{B6}$$

The set of l statistical equilibrium equations is not independent, and one of the equations has to be replaced by the conservation equation

$$n_x = \sum_{j=0}^{l} n_j , \tag{B7}$$

where n_x is the number density of species x in all levels.

The optical depth averaged over the line is given by

$$\tau_{ij}(z) = \frac{A_{ij} c^3}{8\pi\nu_{ij}^3} \int_0^z n_i(z')\left[\frac{n_j(z') g_i}{n_i(z') g_j} - 1\right] \frac{dz'}{\delta v_d} , \tag{B8}$$

where the integration is carried out from the surface of the plane-parallel cloud ($z = 0$) to depth z. Following de Jong, Dalgarno, and Boland (1980), the probability that a photon escapes through the nearest boundary is approximated by

$$\begin{aligned} \beta_{\mathrm{esc}}(\tau) &= \frac{1 - \exp(-2.34\tau)}{4.68\tau} , \qquad \tau < 7 \\ &= \left\{4\tau\left[\ln\left(\frac{\tau}{\sqrt{\pi}}\right)\right]^{0.5}\right\}^{-1} , \qquad \tau \geq 7 . \end{aligned} \tag{B9}$$

© American Astronomical Society • Provided by the NASA Astrophysics Data System

1985ApJ...291..722T

TABLE 4

ATOMIC FINE-STRUCTURE DATA

Species	Level g	Level u	E (K)	λ (μm)	A (s^{-1})	a[a]	b[a]	n_{cr} (cm^{-3})	N_τ[b] (cm^{-2})	Reference
				Two-Level Species						
C^+	$^2P_{1/2}$	$^2P_{3/2}$	92	157.7	2.4(−6)	5.8(−10)	0.02	2.8(3)	1.2(21)	1, 2
Si^+	$^2P_{1/2}$	$^2P_{3/2}$	414	34.8	2.2(−4)	6.5(−10)	...	3.4(5)	4.6(23)	3
				Three-Level Species						
C	$^3P_0$	$^3P_1$	23.6	610	7.93(−8)	1.3(−10)	0.045	4.7(2)	4.2(20)	4
	$^3P_1$	$^3P_2$	38.9	370	2.68(−7)	7.8(−11)	0.035	2.8(3)	1.0(21)	4
	$^3P_0$	$^3P_2$	62.5	230	2.0(−14)	2.0(−10)	0.084	6.3(−5)	1.9(28)	4
O	$^3P_2$	$^3P_1$	228	63.2	8.95(−5)	4.2(−12)	0.67	4.7(5)	1.0(21)	4
	$^3P_1$	$^3P_0$	98	145.6	1.70(−5)	1.5(−10)	0.44	9.5(4)	7.8(20)	4
	$^3P_2$	$^3P_0$	326	44.0	1.0(−10)	1.1(−12)	0.8	9.7(−1)	8.0(27)	4
Si	$^3P_0$	$^3P_1$	111	129.6	8.25(−6)	3.5(−10)	...	2.4(4)	1.6(23)	3
	$^3P_1$	$^3P_2$	210	68.5	4.21(−5)	5.0(−10)	...	8.4(4)	3.8(23)	3
	$^3P_0$	$^3P_2$	321	44.8	3.56(−10)	1.7(−10)	...	2.1(0)	4.5(29)	3
S	$^3P_2$	$^3P_1$	571	25.2	1.39(−3)	7.5(−10)	...	1.9(6)	6.4(22)	3
	$^3P_1$	$^3P_0$	255	56.6	3.02(−4)	4.2(−10)	...	7.2(5)	4.7(22)	3
	$^3P_2$	$^3P_0$	826	17.4	6.71(−8)	7.1(−10)	...	9.5(1)	1.2(28)	3
Fe[c]	$^5D_4$	$^5D_3$	595	24.2	2.5(−3)	8.0(−10)	...	3.1(6)	9.9(23)	3
	$^5D_3$	$^5D_2$	415	34.7	1.6(−3)	5.3(−10)	...	3.0(6)	5.7(23)	3
	$^5D_4$	$^5D_2$	1010	14.3	1.0(−10)[d]	6.9(−10)	...	1.4(−1)	1.7(32)	3
Fe^+[c]	$^6D_{9/2}$	$^6D_{7/2}$	554	26.0	2.13(−3)	9.5(−10)	...	2.2(6)	9.1(23)	3
	$^6D_{7/2}$	$^6D_{5/2}$	407	35.4	1.57(−3)	4.7(−10)	...	3.3(6)	5.2(23)	3
	$^6D_{9/2}$	$^6D_{5/2}$	961	15.0	1.5(−9)	5.7(−10)	...	2.6(0)	9.0(30)	3

NOTE.—Numbers in parentheses: see Table 2.

[a] Collisional de-excitation rate coefficients for atomic hydrogen collisions given by $\gamma_H = aT^b \mathrm{cm}^3\ \mathrm{s}^{-1}$.

[b] N_τ is the column density of hydrogen nuclei required for unit optical depth in the line, assuming abundances from Table 2 and that all of the given element is in the lower level (see text).

[c] Only the lowest three fine-structure levels were taken into account.

[d] Our estimate.

REFERENCES.—(1) Launey and Roueff 1977*a*; (2) Flower and Launay 1977; (3) this work; (4) Launay and Roueff 1977*b*.

In these formulae it is implicitly assumed that half of the photons, those that are emitted into the semi-infinite slab, do not escape. Because all opacity is assumed to be local in the escape probability formalism, these inwardly directed photons do not contribute to the cooling. This is incorrect if the optical depth is small inward through the cloud, and, as a consequence, the cooling rate will be underestimated. This has, however, no serious consequences for the calculated models because the cooling is dominated by the O I 63 μm and CO lines. These lines are optically thick through the cloud, and the assumption that the opacity is local should give reasonable results.

Given n_x, T_0, $\tau_d(\nu)$, and τ_{ij}, we can solve the statistical equilibrium equations (B4) and (B7) iteratively for the level population densities. These can then be used to calculate the source function (eqs. [B2]) and the cooling rate (eq. [B1]).

Note that if the source function is less than the background radiation field, the transition heats the gas. For an infrared transition in a two-level species, this occurs for

$$T \lesssim T_0\left[1 - \frac{kT_0}{h\nu_{21}} \ln(\tau_d)\right]^{-1} . \tag{B10}$$

Inserting $T_0 = 75$ K, $\tau_d = 0.3$, and $\nu_{21} = 4.8 \times 10^{12}\ \mathrm{s}^{-1}$ ($\lambda = 63\ \mu$m), we find $T < 53$ K. For submillimeter lines this inequality is given by $T < T_0 \tau_d$. Inserting $T_0 = 75$ K and $\tau_d = 0.3$ yields $T < 23$ K.

II. COOLING BY ATOMIC FINE-STRUCTURE LINES

A predominantly atomic gas is cooled by atomic infrared fine-structure lines for temperatures less than about 1000 K. Table 4 lists the transitions included in the models. The collisional de-excitation rate coefficients γ_H for collisions with atomic hydrogen are given. We assume $\gamma_H = \gamma_{H_2}$, except for C^+, where we take $\gamma_{H_2} = 3.1 \times 10^{-10} T^{0.1}\ \mathrm{cm}^3\ \mathrm{s}^{-1}$. We also give the critical density n_{cr} above which collisional de-excitation becomes important, calculated assuming that the upper and lower levels form a two-level system, so that

$$n_{cr} = A_{21}/\gamma_H . \tag{B11}$$

In order to estimate when optical-depth effects become important, we have calculated the equivalent column density of hydrogen nuclei $N_\tau(\nu_{ij})$ needed to reach a line-center optical depth of unity in the fine-structure transition $i \rightarrow j$ for species x. This calculation is performed using the abundances in Table 2 and assuming that all of the given element is in the j-level of the respective atomic or ionic species. The column density $N_\tau(\nu_{ij})$ is then given by

$$N_\tau(x_{ij}) = \frac{8\pi\delta\nu_d}{A_{ij}\lambda_{ij}^3}\frac{g_j}{g_i}\frac{1}{\mathscr{A}_x} = \frac{6.8 \times 10^{18}}{A_{ij}\mathscr{A}_x}\frac{g_j}{g_i}\left(\frac{1\ \mu\mathrm{m}}{\lambda_{ij}}\right)^3\left(\frac{\delta\nu_d}{2.7\ \mathrm{km\ s}^{-1}}\right) \mathrm{cm}^{-2} , \tag{B12}$$

© American Astronomical Society • Provided by the NASA Astrophysics Data System

1985ApJ...291..722T

where $\mathscr{A}_x$ is the elemental abundance of species x and A_{ij} is in s^{-1}. Note that N_τ is about the same for O I 63 μm and C II 158 μm, but that O I 63 μm becomes optically thick more readily because the high statistical weight of the ground state ensures a high fraction of O I in this lower level.

Some insight into the analysis of the intensity of the fine-structure lines can be gained by considering a two-level atom in a plane-parallel, uniform density and temperature slab. For simplicity assume that $n_0 \gg n_{cr}$, so that the level populations are in LTE. The optical depth $\tau(z)$ can be found by integrating equation (B8) to yield

$$\tau(z) = A_{21}\, c^3 n_2\, z[\exp\,(h\nu_{21}/kT) - 1]/(8\pi\nu_{21}^3\, \delta v_d)\,. \tag{B13}$$

The emergent intensity on the front surface of the slab, perpendicular to the slab and integrated over the line, is given by

$$I = (2\pi)^{-1} \int_0^z \Lambda(z')dz'\,. \tag{B14}$$

The factor 2π takes into account the fact that the photons escape only into one hemisphere. If background radiation is neglected and equation (B1) is used, this becomes

$$I = B(T)\nu(\delta v_d/c)f(\tau)\,, \tag{B15}$$

where $f(\tau)$ is given by

$$f(\tau) = 2\int_0^\tau \beta(\tau')d\tau'\,. \tag{B16}$$

For $\tau \leq 7$ this can be integrated using equation (B9), to yield

$$f(\tau) = 0.428[E_1(2.34\tau) + \ln\,(2.34\tau) + 0.57721]\,, \tag{B17}$$

where E_1 is the exponential integral tabulated by Abramowitz and Stegun (1973). For $\tau \ll 1$ this becomes $f(\tau) = \tau$, and the intensity is given by

$$I = A_{21}N_2\, h\nu_{21}/(4\pi)\,, \tag{B18}$$

where N_2 is the column density in the upper state. For large optical depth the logarithm in equation (B17) dominates (the logarithmic part of the curve of growth).

III. COOLING BY MOLECULAR ROTATIONAL LINES

For temperatures less than a few hundred degrees, a molecular gas is cooled mainly by infrared and millimeter rotational lines. For CO, the dominant molecular coolant, we have solved the equation of statistical equilibrium for the first 20 rotational levels. We have used the analytical formula of de Jong, Chu, and Dalgarno (1975) for the collisional de-excitation rates.

The rotational cooling of the molecules CH, OH, and H_2O and the vib-rotational cooling of H_2 are calculated using the analytical formulae of Hollenbach and McKee (1979). The collisional de-excitation cross sections for OH, CH, and H_2O are assumed to be equal to 3×10^{-16} cm^2 (McKee *et al.* 1982). It should be noted that in these analytical formulae the background radiation field is neglected. This tends to overestimate the actual cooling rate by about a factor of 2, which is about the level of accuracy of the analytical approximations. There are no serious consequences for the energy balance, because the contribution of these molecules to the total cooling rate is small.

IV. O I 6300 Å AND H I Lyα COOLING

At high temperatures ($T > 5000$ K) an atomic gas is mainly cooled by excitation of the metastable ^1D level of atomic oxygen and the 2 ^2P level of atomic hydrogen. The cooling rate due to O I 6300 Å emission is given by

$$\Lambda(\text{O I}) = 1.8 \times 10^{-24} n(\text{O})[n(\text{H}) + n(\text{H}_2)]e^{-22{,}800/T}\ \text{ergs cm}^{-3}\ \text{s}^{-1}\,, \tag{B19}$$

where n(O) is the density of atomic oxygen and the de-excitation cross section has been taken from Federman and Shipsey (1983). The cooling by Lyα is given by (Spitzer 1978)

$$\Lambda(\text{H I}) = 7.3 \times 10^{-19} n_e\, n(\text{H})e^{-118{,}400/T}\ \text{ergs cm}^{-3}\ \text{s}^{-1}\,. \tag{B20}$$

APPENDIX C

CHEMISTRY

In our chemical network we have included reactions between 41 species: H, He, C, O, Si, S, Mg, Fe, H_2, CH, OH, SiH, CO, O_2, SiO, CH_2, H_2O, e^-, H^+, He^+, C^+, O^+, Si^+, S^+, Mg^+, Fe^+, H_2^+, CH^+, OH^+, CO^+, SiO^+, H_3^+, CH_2^+, H_2O^+, SiH_2^+, HCO^+, $HOSi^+$, CH_3^+, H_3^+, H^-, and H_2^*. We have taken into account photodissociation and ionization reactions (Table 5), ion-molecule reactions (Table 6), radiative and dissociative electron recombination reactions (Table 7), neutral-neutral reactions (Table 8), reactions of H_2^* (Table 9), cosmic-ray ionization reactions (Table 10), charge exchange reactions (Table 11), radiative association reactions (Table 12), reactions of negative ions (Table 13), reactions with activation energies (Table 14), and H_2 formation on grain surfaces. The

© American Astronomical Society • Provided by the NASA Astrophysics Data System

1985ApJ...291..722T

TABLE 5

PHOTOIONIZATION AND DISSOCIATION REACTIONS[a]

Reaction				a	b
C	$\rightarrow C^+$	$+ e^-$	.....	2.1(−10)	2.6
Mg	$\rightarrow Mg^+$	$+ e^-$	.....	4.4(−11)	1.4
S	$\rightarrow S^+$	$+ e^-$	.....	3.9(−10)	2.5
Si	$\rightarrow Si^+$	$+ e^-$	.....	1.2(−9)	1.6
Fe	$\rightarrow Fe^+$	$+ e^-$	.....	1.0(−10)	2.3
CH	$\rightarrow CH^+$	$+ e^-$	.....	3.2(−10)	3.0
CH	$\rightarrow C$	$+ H$	.....	2.7(−10)	1.3
CH_2	$\rightarrow CH$	$+ H$	.....	5.0(−11)	1.7
CH_2	$\rightarrow CH_2^+$	$+ e^-$	.....	1.0(−9)	2.3
CH^+	$\rightarrow C^+$	$+ H$	.....	1.8(−10)	2.8
CH_2^+	$\rightarrow CH^+$	$+ H$	.....	1.7(−9)	1.7
CH_3^+	$\rightarrow CH_2^+$	$+ H$	.....	1.0(−9)	1.7
CH_3^+	$\rightarrow CH^+$	$+ H_2$	.....	1.0(−9)	1.7
H_2^+	$\rightarrow H$	$+ H^+$	.....	2.6(−10)	1.8
H_3^+	$\rightarrow H_2^+$	$+ H$	.....	7.9(−9)	2.3
H_3^+	$\rightarrow H_2$	$+ H^+$	.....	2.0(−8)	1.8
H_2	$\rightarrow H$	$+ H$	.....	3.4(−11)	2.5
O_2	$\rightarrow O$	$+ O$	.....	3.3(−10)	1.4
OH	$\rightarrow O$	$+ H$	.....	2.2(−10)	2.0[b]
CO	$\rightarrow C$	$+ O$	.....	1.4(−11)	3.2
H_2O	$\rightarrow OH$	$+ H$	.....	5.1(−10)	1.8
SiO	$\rightarrow Si$	$+ O$	.....	1.0(−10)	2.3

NOTE.—Numbers in parentheses: see Table 2.

[a] Reactions from Roberge, Dalgarno, and Flannery 1981 and Black and Dalgarno 1977, except where noted.

[b] Van Dishoeck and Dalgarno 1984.

reaction rates are given in these tables in the format

$$k = a(T/300)^b \exp(-c/T) \text{ cm}^3 \text{ s}^{-1} , \tag{C1}$$

where T is the gas temperature. The exceptions are the photodissociation and ionization reactions, which are given in the format

$$k = aG_0 \exp(-bA_v) \text{ s}^{-1} , \tag{C2}$$

where A_v is the visual extinction. For those species with an ionization or dissociation energy larger than 11.3 eV (1100 Å), we have taken into account absorption of FUV photons by H_2 and by neutral carbon (see eqs. [A6] and [A7]).

In order to study the effects of CO self-shielding, the CO photodissociation rate is multiplied by the factor $[1 + \alpha\beta(\tau_{CO})]/(1 + \alpha)$, where the CO optical depth is given by

$$\tau_{CO} = 1.1 \times 10^{-14} N(\text{CO}) \left(\frac{1 \text{ km s}^{-1}}{\delta v_d} \right) . \tag{C3}$$

The self-shielding factor $\beta(\tau_{CO})$ is given by equations (A10) and (A11). The parameter α measures the importance of CO photodissociation in discrete lines. Generally, we ignore self-shielding ($\alpha = 0$).

We have ignored grain-surface reactions, except for the formation of H_2. Although some gas-phase species (e.g., H_2CO and NH_3) may be mainly synthesized on grain surfaces (Tielens 1983), it is generally believed that the "simple" molecules and ions (e.g., CO and OH) are formed mainly in the gas phase (Watson and Walmsley 1982). Furthermore, it should be noted that grain-surface reactions will proceed only for grain temperatures less than a critical temperature. This inequality guarantees that the evaporation time scale of a radical will be longer than the time scale for collisions between gas-phase radicals and a grain. For species like O, C, and CO this critical temperature is about 30 K (Tielens and Hagen 1982).

The critical grain temperature for the formation of H_2 is somewhat more difficult to estimate. Recent calculations of interstellar grain-surface chemistry show that H_2 can be formed by H abstraction from molecules such as H_2S, N_2H_2, N_2H_4, and H_2CO rather than by direct H atom recombination. In a sense, these molecules act as enhanced binding sites for H atoms (Tielens and Hagen 1982). The critical grain temperature for H_2 formation by H abstraction on a perfect surface is given by

$$T_{cr} \approx \frac{E_B/k}{2wh^{-1}(2mE_a)^{0.5} - 0.5 \ln(N) - \ln(f_s)} , \tag{C4}$$

where E_B is the physical adsorption binding energy of a hydrogen atom to the surface, E_a and w are the height and width, respectively, of the energy barrier associated with the H abstraction, m is the hydrogen mass, f_s is the fraction of sites from which H abstraction can take place, and N is the total number of sites on the grain surface. Inserting $E_B/k = 750$ K, $E_a/k = 1000$ K, $w = 1$ Å, $N = 10^6$, and $f_s = 10^{-2}$, we find $T_{cr} \approx 75$ K.

For an imperfect grain surface, migrating H atoms will be scattered by surface imperfections. This will increase the surface

© American Astronomical Society • Provided by the NASA Astrophysics Data System

1985ApJ...291..722T

TABLE 6

ION-MOLECULE REACTIONS[a]

Reaction	a
$H^+ + CH \rightarrow CH^+ + H$	1.9(−9)
$H^+ + OH \rightarrow OH^+ + H$	2.1(−9)
$H^+ + H_2O \rightarrow H_2O^+ + H$	8.2(−9)
$H^+ + CH_2 \rightarrow CH^+ + H_2$	1.4(−9)
$H^+ + CH_2 \rightarrow CH_2^+ + H$	1.4(−9)
$He^+ + H \rightarrow H^+ + He$	1.9(−15)
$He^+ + H_2 \rightarrow H^+ + H + He$	1.5(−13)
$He^+ + O_2 \rightarrow O^+ + O + He$	1.0(−9)
$He^+ + CO \rightarrow C^+ + O + He$	1.6(−9)
$He^+ + CH \rightarrow C^+ + H + He$	1.1(−9)
$He^+ + CH_2 \rightarrow CH^+ + H + He$	7.5(−10)
$He^+ + CH_2 \rightarrow C^+ + H_2 + He$	7.5(−10)
$He^+ + H_2O \rightarrow OH^+ + H + He$	3.7(−10)
$He^+ + H_2O \rightarrow H_2O^+ + He$	7.0(−11)
$He^+ + OH \rightarrow O^+ + H + He$	1.1(−9)
$C^+ + O_2 \rightarrow O^+ + CO$	4.1(−10)
$C^+ + O_2 \rightarrow CO^+ + O$	7.5(−10)
$C^+ + OH \rightarrow CO^+ + H$	7.7(−10)
$C^+ + H_2O \rightarrow HCO^+ + H$	2.7(−9)
$C^+ + CH \rightarrow CH^+ + C$	3.8(−10)
$C^+ + CH_2 \rightarrow CH_2^+ + C$	5.2(−10)
$C^+ + SiO \rightarrow Si^+ + CO$	5.4(−10)
$C^+ + SiO \rightarrow SiO^+ + C$	5.4(−10)
$O^+ + H \rightarrow O + H^+$	7.0(−10)
$O^+ + H_2 \rightarrow OH^+ + H$	1.6(−9)
$OH^+ + H_2 \rightarrow H_2O^+ + H$	1.1(−9)
$CO^+ + H \rightarrow CO + H^+$	1.0(−10)
$CO^+ + H_2 \rightarrow HCO^+ + H$	2.0(−9)
$H_2O^+ + H_2 \rightarrow H_3O^+ + H$	6.1(−10)
$HCO^+ + C \rightarrow CH^+ + CO$	1.1(−9)
$HCO^+ + CH \rightarrow CH_2^+ + CO$	6.3(−10)
$HCO^+ + OH \rightarrow H_2O^+ + CO$	6.2(−10)
$HCO^+ + CH_2 \rightarrow CH_3^+ + CO$	8.6(−10)
$HCO^+ + H_2O \rightarrow H_3O^+ + CO$	2.7(−9)
$H_3O^+ + C \rightarrow HCO^+ + H_2$	1.0(−11)
$H_3O^+ + CH \rightarrow CH_2^+ + H_2O$	6.8(−10)
$H_3O^+ + CH_2 \rightarrow CH_3^+ + H_2O$	9.4(−10)
$H_2^+ + H \rightarrow H^+ + H_2$	1.0(−10)
$H_2^+ + H_2 \rightarrow H_3^+ + H$	2.1(−9)
$H_3^+ + C \rightarrow CH^+ + H_2$	2.0(−9)
$H_3^+ + O \rightarrow OH^+ + H_2$	8.0(−10)
$H_3^+ + CH \rightarrow CH_2^+ + H_2$	1.2(−9)
$H_3^+ + OH \rightarrow H_2O^+ + H_2$	1.3(−9)
$H_3^+ + CO \rightarrow HCO^+ + H_2$	1.7(−9)
$H_3^+ + H_2O \rightarrow H_3O^+ + H_2$	5.9(−9)
$H_3^+ + CH_2 \rightarrow CH_3^+ + H_2$	1.7(−9)
$CH^+ + H \rightarrow C^+ + H_2$	9.4(−12)[b]
$CH^+ + H_2 \rightarrow CH_2^+ + H$	1.0(−9)
$CH^+ + O \rightarrow CO^+ + H$	7.6(−10)
$CH_2^+ + H_2 \rightarrow CH_3^+ + H$	7.2(−10)
$CH_3^+ + O \rightarrow HCO^+ + H_2$	4.4(−10)
$SiO^+ + H_2 \rightarrow HOSi^+ + H$	1.5(−9)
$SiH_2^+ + O \rightarrow HOSi^+ + H$	6.3(−10)

[a] Reactions for Tables 6–8 and 10–14 are from Prasad and Huntress 1980, unless otherwise noted.

[b] This reaction has a rate given by $k = a(T/300)^{1.25}$.

TABLE 7

ELECTRON RECOMBINATION REACTIONS

Reaction	a	b
$H^+ + e^- \rightarrow H$	3.5(−12)	−0.70
$C^+ + e^- \rightarrow C$	4.4(−12)	−0.61
$S^+ + e^- \rightarrow S$	3.9(−12)	−0.63
$Si^+ + e^- \rightarrow Si$	4.9(−12)	−0.60
$Mg^+ + e^- \rightarrow Mg$	2.8(−12)	−0.86
$Fe^+ + e^- \rightarrow Fe$	3.7(−12)	−0.65
$OH^+ + e^- \rightarrow O + H$	2.0(−7)	−0.50
$CO^+ + e^- \rightarrow C + O$	1.8(−7)	−0.50
$H_2O^+ + e^- \rightarrow OH + H$	2.0(−7)	−0.50
$H_2O^+ + e^- \rightarrow O + H_2$	2.0(−7)	−0.50
$HCO^+ + e^- \rightarrow CO + H$	2.0(−7)	−0.75
$H_3O^+ + e^- \rightarrow H_2O + H$	6.5(−7)	−0.50
$H_3O^+ + e^- \rightarrow OH + H + H$	6.5(−7)	−0.50
$H_3^+ + e^- \rightarrow H_2 + H$	1.1(−7)	−0.50
$H_3^+ + e^- \rightarrow H + H + H$	1.1(−7)	−0.50
$CH^+ + e^- \rightarrow C + H$	1.0(−7)	−0.50
$CH_2^+ + e^- \rightarrow CH + H$	1.5(−7)	−0.50
$CH_2^+ + e^- \rightarrow C + H_2$	1.5(−7)	−0.50
$CH_3^+ + e^- \rightarrow CH_2 + H$	1.5(−7)	−0.50
$CH_3^+ + e^- \rightarrow CH + H + H$	1.5(−7)	−0.50
$SiH_2^+ + e^- \rightarrow Si + H + H$	2.0(−7)	−0.50
$SiH_2^+ + e^- \rightarrow SiH + H$	2.0(−7)	−0.50
$HOSi^+ + e^- \rightarrow SiO + H$	1.5(−7)	−0.50
$HOSi^+ + e^- \rightarrow Si + OH$	1.5(−7)	−0.50

NOTE.—Numbers in parentheses: see Table 2.

TABLE 8

NEUTRAL-NEUTRAL REACTIONS

Reaction	a	b
$C + OH \rightarrow CO + H$	1.10(−10)	0.50
$C + O_2 \rightarrow CO + O$	3.3(−11)	0.50
$O + OH \rightarrow O_2 + H$	4.0(−11)	0.50
$O + CH \rightarrow CO + H$	4.0(−11)	0.50
$O + CH \rightarrow HCO^+ + e^-$	2.0(−11)	0.44
$O + CH_2 \rightarrow CO + H + H$	2.0(−11)	0.50
$O + SiH \rightarrow SiO + H$	4.0(−11)	0.50

NOTE.—Numbers in parentheses: see Table 2.

TABLE 9

REACTIONS OF VIBRATIONALLY EXCITED HYDROGEN

Reaction	a	b	c
$H_2^* \rightarrow H + H$	[a]	...	...
$H_2^* + H \rightarrow H_2 + H$	1.9(−12)	0.50	1.0(3)
$H_2^* + H_2 \rightarrow H_2 + H_2$	[b]	...	...
$H_2^* + H \rightarrow H + H + H$	9.8(−12)	0.50	2.7(4)
$H_2^* + H_2 \rightarrow H_2 + H + H$	9.8(−12)	0.50	2.7(4)
$H_2^* + H_2^* \rightarrow H + H + H_2$	9.8(−12)	0.50	...
$H_2^* + O \rightarrow OH + H$	9.0(−12)	1.00	...
$H_2^* + OH \rightarrow H_2O + H$	3.6(−11)	...	...
$H_2^* + O_2 \rightarrow OH + OH$	1.0(−10)	...	...
$H_2^* + C \rightarrow CH + H$	1.2(−9)	0.50	...
$H_2^* + CH \rightarrow CH_2 + H$	2.2(−11)	0.67	...
$H_2^* + C^+ \rightarrow CH^+ + H$	9.4(−12)	1.25	...
$H_2^* \rightarrow H_2$	2.0(−7)[c]	...	...
$H_2 \rightarrow H_2^*$	[d]	...	...

NOTE.—Numbers in parentheses: see Table 2.

[a] See text for the rate of photodissociation of H_2^*.

[b] See text for the rate of collisional de-excitation of H_2^* by H_2.

[c] Radiative decay of vibrationally excited H_2.

[d] See text for the rate of UV fluorescence producing H_2^*.

© American Astronomical Society • Provided by the NASA Astrophysics Data System

1985ApJ...291..722T

TABLE 10

COSMIC-RAY IONIZATION REACTIONS

Reaction	d[a]
$H \rightarrow H^+ + e^-$	4.6(−1)
$He \rightarrow He^+ + e^-$	5.0(−1)
$H_2 \rightarrow H^+ + H + e^-$ ...	2.2(−2)
$H_2 \rightarrow H_2^+ + e^-$	9.3(−1)

NOTE.—Numbers in parentheses: see Table 1.

[a] The rate of ionization is taken to be $k = 1.6 \times 10^{-17} d$.

TABLE 11

CHARGE EXCHANGE REACTIONS

Reaction	a	c
$H^+ + O \rightarrow O^+ + H$	7.0(−10)	2.30(2)
$H^+ + S \rightarrow S^+ + H$	1.3(−9)	...
$H^+ + Si \rightarrow Si^+ + H$	9.9(−10)	...
$H^+ + Mg \rightarrow Mg^+ + H$	1.1(−9)	...
$H^+ + Fe \rightarrow Fe^+ + H$	7.4(−9)	...
$He^+ + Si \rightarrow Si^+ + He$	3.3(−9)	...
$C^+ + S \rightarrow S^+ + C$	1.5(−9)	...
$C^+ + Si \rightarrow Si^+ + C$	2.1(−9)	...
$C^+ + Mg \rightarrow Mg^+ + C$	1.1(−9)	...
$C^+ + Fe \rightarrow Fe^+ + C$	2.6(−9)	...
$S^+ + Si \rightarrow Si^+ + S$	1.6(−9)	...
$S^+ + Mg \rightarrow Mg^+ + S$	2.8(−10)	...
$S^+ + Fe \rightarrow Fe^+ + S$	1.8(−10)	...
$Si^+ + Mg \rightarrow Mg^+ + Si$	2.9(−10)	...
$Si^+ + Fe \rightarrow Fe^+ + Si$	1.9(−10)	...

NOTE.—Numbers in parentheses: see Table 2.

TABLE 12

RADIATIVE ASSOCIATION REACTIONS

Reaction	a
$H + C \rightarrow CH$.....	1.00(−17)
$C^+ + H \rightarrow CH^+$ ...	1.70(−17)
$C^+ + H_2 \rightarrow CH_2^+$ ...	6.00(−16)
$Si^+ + H_2 \rightarrow SiH_2^+$ ...	1.00(−15)

NOTE.—Numbers in parentheses: see Table 2.

TABLE 13

REACTIONS OF NEGATIVE IONS

Reactions	a	b	c
$H + e^- \rightarrow H^-$	3.0(−16)	1.0	...
$H^- + H \rightarrow H_2 + e^-$ ...	1.3(−9)	...	...
$H^- + C^+ \rightarrow H + C$ ...	2.3(−7)	−0.50	...
$H^- \rightarrow H + e^-$ ...	2.4(−7)	...	0.90[a]

NOTE.—Numbers in parentheses: see Table 2.

[a] Photodetachment reaction.

TABLE 14

REACTIONS WITH AN ACTIVATION BARRIER

Reaction	a	b	c
$H_2 + O \rightarrow OH + H$	9.0(−12)	1.0	4.5(+3)
$H + OH \rightarrow H_2 + O$	4.2(−12)	1.0	3.5(+3)
$H_2 + OH \rightarrow H_2O + H$	3.6(−11)	...	2.6(+3)
$H_2O + H \rightarrow H_2 + OH$	1.5(−10)	...	1.0(+4)
$H + O_2 \rightarrow OH + O$	3.7(−10)	...	8.5(+3)
$OH + O \rightarrow H + O_2$	4.0(−10)	...	6.0(+2)
$OH + OH \rightarrow H_2O + O$	1.0(−11)	...	5.5(+2)
$O + H_2O \rightarrow OH + OH$	1.1(−11)	...	9.2(+3)
$O_2 + H_2 \rightarrow OH + OH$	1.0(−10)	...	9.3(+3)
$H_2 + C \rightarrow CH + H$	1.2(−9)	0.50	1.4(+4)
$H + CH \rightarrow H_2 + C$	1.2(−9)	0.50	2.2(+3)
$H_2 + CH \rightarrow CH_2 + H$	2.2(−11)	0.67	8.8(+3)
$H + CH_2 \rightarrow CH + H_2$	2.2(−11)	0.67	1.3(+4)
$C^+ + H_2 \rightarrow CH^+ + H$	9.4(−12)	1.25	4.7(+3)
$H + H_2 \rightarrow H + H + H$	2.3(−11)	1.25	6.5(+4)
$H_2 + H_2 \rightarrow H_2 + H + H$	2.3(−11)	1.25	6.5(+4)

NOTE.—Numbers in parentheses: see Table 2.

© American Astronomical Society • Provided by the NASA Astrophysics Data System

1985ApJ...291..722T

migration time scale and consequently decrease the critical grain temperature. For a completely imperfect surface $T_{cr} \approx 44$ K, using the numbers quoted above.

The grain temperature in photodissociation regions is not well known. Far-infrared observations of OMC-1 yield a maximum color temperature (50–100 μm) of 65 K for grains heated by θ^1 Ori C (Werner *et al.* 1976). The actual grain temperature may be somewhat lower because of an increase in the grain emissivity with frequency. Equation (A22) provides a theoretical estimate of an average temperature of grains in photodissociation regions subjected to FUV and IR radiation. For parameters typical of nearby early-type stars (Table 2), this yields grain temperatures in the range 60–120 K. It should be noted, however, that in the same radiation field different types of grains will have different temperatures, owing to differences in absorption and emission efficiences, sizes, and composition. There is, for example, a factor of 2 difference in temperature between a 200 Å graphite grain and a 3000 Å ice grain. It is possible, therefore, for H_2 formation to stop on small graphite grains while it is still proceeding on large ice-type grains. The formation of heavier molecules on grains seems ruled out, however, in photodissociation regions near early-type stars.

In our calculations we will assume that H_2 formation in photodissociation regions proceeds at the same rate as in the diffuse interstellar medium. Other gas-phase species will evaporate before they can react on a grain surface.

APPENDIX D

THE CLOUD MODEL

For the construction of a model cloud, the plane-parallel slab is divided into a number of depth zones. At each depth z the energy balance and the chemical equilibrium have to be solved simultaneously to determine the temperature and the molecular abundances. The energy balance is given by

$$\sum_i \Gamma_i(T(z), \boldsymbol{x}(z)) - \sum_i \Lambda_i(T(z), \boldsymbol{x}(z)) = 0 , \tag{D1}$$

where the heating (Γ_i) and cooling (Λ_i) terms are described in Appendices A and B and the vector $\boldsymbol{x}(z)$ contains the molecular abundances at depth z. In a steady state, determining the molecular abundances reduces to solving m equations

$$\boldsymbol{F}(T(z), \boldsymbol{x}(z)) = \frac{d\boldsymbol{x}(z)}{dt} = 0 , \tag{D2}$$

where m is the total number of species (see Tielens and Hagen 1982). In total there are therefore $m + 1$ equations in the $m + 1$ unknowns $T(z)$ and $\boldsymbol{x}(z)$.

The nonlinear interplay of molecular abundances and temperature in the chemical and thermal equilibrium complicates the model calculations considerably. In our calculation we have separated these problems as follows. Two temperatures are chosen which bracket the solution of equations (D1) and (D2). The solution (T, $\boldsymbol{x}$) is then determined by a midpoint interation scheme. This means that at the temperature midpoint the chemical equilibrium (eq. [D2]) is solved with a Newton-Raphson method (see Tielens and Hagen 1982). With the calculated molecular abundances and the midtemperature, the residual of equation (D1) is then calculated. The iteration is then pursued in the temperature interval that again brackets the solution. The iteration is stopped when the solution repeats to $\pm 0.5\%$.

Once the temperature and molecular abundances are known, the contribution of the current depth to the emergent intensity, $\Delta I(x_{ij}, z)$, is calculated:

$$\Delta I(x_{ij}, z) = (2\pi)^{-1} \Lambda(x_{ij}, z) \Delta z , \tag{D3}$$

where the values of Λ are given by equation (B1) and Δz is the thickness of the layer. Finally, the contribution of the layer to the molecular column densities and the optical depth in the IR and millimeter emission lines and the FUV photodissociation lines and continuum are calculated (see eqs. [A7] and [B8]). The calculation is then pursued in the next depth zone.

Typically, in our numerical models at each depth 5 temperature iterations are required for 0.5% accuracy. For each temperature about 8 iterations are required in the Newton-Raphson solution of the chemical equilibrium. For 60 depth points a calculation typically takes between 3 and 10 minutes on a CDC 7600. Most of the time is used in solving the chemical equilibrium.

REFERENCES

Abramowitz, M., and Stegun, I. A. 1973, *Handbook of Mathematical Functions* (New York: Dover).
Bally, J., and Langer, W. D. 1982, *Ap. J.*, **255**, 143.
Black, J. H., and Dalgarno, A. 1976, *Ap. J.*, **203**, 132.
———. 1977, *Ap. J. Suppl.*, **34**, 405.
Blitz, L., and Shu, F. H. 1980, *Ap. J.*, **238**, 148.
Bondeybey, V. E., and Brus, L. E. 1980, *Adv. Chem. Phys.*, **41**, 269.
Boughton, W. L. 1978, *Ap. J.*, **222**, 517.
Brown, R. L., Lockman, F. J., and Knapp, G. R. 1978, *Ann. Rev. Astr. Ap.*, **16**, 445.
Burke, J. R., and Hollenbach, D. J. 1983, *Ap. J.*, **265**, 223.
Chu, Y. H., and Watson, W. D. 1983, *Ap. J.*, **267**, 151.
Clavel, J., Viala, Y. P., and Bel, N. 1978, *Astr. Ap.*, **65**, 435.
Cravens, T. E., and Dalgarno, A. 1978, *Ap. J.*, **219**, 750.
Crawford, M. K., Genzel, R., Townes, C. H., and Watson, D. M. 1985, *Ap. J.*, **291**, 755.
de Boer, K. S. 1981, *Ap. J.*, **244**, 848.
de Jong, T. 1972, *Astr. Ap.*, **20**, 263.
———. 1977, *Astr. Ap.*, **55**, 137.
———. 1980, *Highlights Astr.*, **5**, 301.
de Jong, T., Chu, S. I., and Dalgarno, A. 1975, *Ap. J.*, **199**, 69.
de Jong, T., Dalgarno, A., and Boland, W. 1980, *Astr. Ap.*, **91**, 68.
Dewdney, P. E., and Roger, R. S. 1983, *Bull. AAS*, **15**, 616.
Draine, B. T. 1978, *Ap. J. Suppl.*, **36**, 595.
Dupree, A. K. 1974, *Ap. J.*, **187**, 25.
Elitzur, M., and Watson, W. D. 1980, *Ap. J.*, **236**, 172.
Elmegreen, B. G., and Lada, C. J. 1977, *Ap. J.*, **214**, 725.
Federman, S. R. 1982, *Ap. J.*, **257**, 125.

© American Astronomical Society • Provided by the NASA Astrophysics Data System

1985ApJ...291..722T

Federman, S. R., and Shipsey, E. J. 1983, *Ap. J.*, **269**, 791.
Field, G. B., Somerville, W. B., and Dressler, K. 1966, *Ann. Rev. Astr. Ap.*, **4**, 207.
Flannery, B. P., Roberge, W., and Rybicki, G. B. 1980, *Ap. J.*, **236**, 598.
Flower, D. R., and Launay, J. M. 1977, *J. Phys. B*, **10**, 3673.
Freeman, A., and Williams, D. A. 1982, *Ap. Space Sci.*, **83**, 417.
Frerking, M. A., Langer, W. D., and Wilson, R. W. 1982, *Ap. J.*, **262**, 590.
Furniss, I., Jennings, R. E., King, K. J., Lightfoot, F. G., Emery, R. J., Naylor, D. A., and Fitton, B. 1983, *M.N.R.A.S.*, **202**, 859.
Genzel, R. 1983, private communication.
Genzel, R., Watson, D. M., Townes, C. H., Dinerstein, H. L., Hollenbach, D., Lester, D. F., Werner, M. W., and Storey, J. W. V. 1984, *Ap. J.*, **276**, 551.
Glassgold, A. E., and Langer, W. D. 1973, *Ap. J.* (*Letters*), **179**, L197.
———. 1974, *Ap. J.*, **193**, 73.
———. 1975, *Ap. J.*, **197**, 347.
———. 1976, *Ap. J.*, **206**, 85.
Graedel, T. E., Langer, W. D., and Frerking, M. A. 1982, *Ap. J. Suppl.*, **48**, 321.
Habing, H. J. 1968, *Bull. Astr. Inst. Netherlands*, **19**, 421.
Hill, J. K., and Hollenbach, D. J. 1978, *Ap. J.*, **225**, 390.
Hollenbach, D. J., and McKee, C. F. 1979, *Ap. J.*, **41**, 555.
Hollenbach, D. J., and Salpeter, E. E. 1970, *J. Chem. Phys.*, **53**, 79.
———. 1971, *Ap. J.*, **163**, 155.
Hunter, D. A., and Watson, W. D. 1978, *Ap. J.*, **226**, 477.
Jenkins, E. B., Jura, M., and Loewenstein, M. 1983, *Ap. J.*, **270**, 88.
Jenkins, E. B., and Shaya, E. J. 1979, *Ap. J.*, **231**, 55.
Langer, W. D. 1976, *Ap. J.*, **206**, 699.
———. 1977, *Ap. J.* (*Letters*), **212**, L39.
Launay, J. M., and Roueff, E. 1977*a*, *Astr. Ap.*, **56**, 289.
———. 1977*b*, *J. Phys. B*, **10**, 879.
Lee, K. T., Bowman, J. M., Wagner, A. F., and Schatz, G. C. 1982, *J. Chem. Phys.*, **76**, 3583.
Legay, F. 1978, in *Chemical and Biochemical Application of Lasers*, Vol. **2**, ed. C. B. Moore (New York: Academic), p. 43.
Lepp, S., and McCray, R. 1983, *Ap. J.*, **269**, 560.
Lester, D. F., Werner, M. W., Storey, J. W. V., Watson, D. M., and Townes, C. H. 1981, *Ap. J.* (*Letters*), **248**, L109.
Leung, C. M. 1983, *Bull. AAS*, **15**, 639.
Light, G. C. 1978, *J. Chem. Phys.*, **68**, 2831.
London, R. 1978, *Ap. J.*, **225**, 405.
Loren, R. B. 1979, *Ap. J.* (*Letters*), **234**, L207.
McKee, C. F., Storey, J. W. V., Watson, D. M., and Green, S. 1982, *Ap. J.*, **259**, 647.
Melnick, G., Gull, G. E., and Harwit, M. 1979, *Ap. J.*, **227**, L29.
Morton, D. C. 1974, *Ap. J.* (*Letters*), **143**, L35.
Münch, G., and Hippelein, H. 1982, in *Symposium on the Orion Nebula*, ed. A. E. Glassgold, P. J. Huggins, and E. L. Schucking (*Ann. NY Acad. Sci.*, Vol. **395**), p. 170.
Oppenheimer, M., and Dalgarno, A. 1974, *Ap. J.*, **187**, 231.
Oppenheimer, M., and Dalgarno, A. 1975, *Ap. J.*, **200**, 419.
Osterbrock, D. E. 1974, *Astrophysics of Gaseous Nebulae* (San Francisco: Freeman, p. 47.
Palmer, P., Zuckerman, B., Penfield, H., Lilley, A. E., and Mezger, P. G. 1967, *Nature*, **215**, 40.
Peimbert, M. 1982, *Ann. NY Acad. Sci.*, **395**, 24.
Phillips, T. G., and Huggins, P. J. 1981, *Ap. J.*, **251**, 553.
Phillips, T. G., Huggins, P. J., Wannier, P. G., and Scoville, N. Z. 1979, *Ap. J.*, **231**, 720.
Pottasch, S. R., Wesselius, P. R., and van Duinen, R. J. 1979, *Astr. Ap.*, **74**, L15.
Prasad, S. S., and Huntress, W. T., Jr. 1980, *Ap. J. Suppl.*, **43**, 1.
Roberge, W. G., Dalgarno, A., and Flannery, B. P. 1981, *Ap. J.*, **243**, 817.
Russell, R. W., Melnick, G., Gull, G. E., and Harwit, M. 1980, *Ap. J.* (*Letters*), **240**, L99.
Russell, R. W., Melnick, G., Smyers, S. D., Kurtz, N. T., Gosnell, T. R., Harwit, M., and Werner, M. 1981, *Ap. J.* (*Letters*), **250**, L35.
Sandell, G., and Mattila, K. 1975, *Astr. Ap.*, **42**, 357.
Schatz, G. C. 1981, *J. Chem. Phys.*, **74**, 1133.
Schinke, R., and Lester, W. A., Jr. 1979, *J. Chem. Phys.*, **70**, 4893.
Shull, J. M. 1978, *Ap. J.*, **219**, 877.
Solomon, P. M., and Sanders, D. B. 1980, in *Giant Molecular Clouds in the Galaxy*, ed. P. M. Solomon and M. G. Edmunds (Oxford: Pergamon), p. 41.
Spitzer, L. 1978, *Physical Processes in the Interstellar Medium* (New York: Wiley), p. 107.
Stacey, G. J., Smyers, S. D., Kurtz, N. T., and Harwit, M. 1983, *Ap. J.* (*Letters*), **265**, L7.
Stecher, T. P., and Williams, D. A. 1967, *Ap. J.* (*Letters*), **149**, L29.
———. 1972, *Ap. J.* (*Letters*), **177**, L141.
Storey, J. W. V., Watson, D. M., and Townes, C. H. 1979, *Ap. J.*, **233**, 109.
Thronson, H. A., and Lada, C. J. 1983, *Ap. J.*, **269**, 175.
Tielens, A. G. G. M. 1983, *Astr. Ap.*, **119**, 177.
Tielens, A. G. G. M., and Hagen, W. 1982, *Astr. Ap.*, **114**, 245.
———. 1985, in preparation.
Tielens, A. G. G. M., and Hollenbach, D. 1984, *Icarus*, in press.
———. 1985, *Ap. J.*, **291**, 747 (Paper II).
Treffers, R. 1983, private communication.
Van Dishoeck, E. F., and Dalgarno, A. 1984, *Ap. J.*, **277**, 576.
Watson, D., Genzel, R., Townes, C. H., Werner, M. W., and Storey, J. W. V. 1984, *Ap. J.* (*Letters*), **279**, L1.
Watson, W. D. 1972, *Ap. J.*, **176**, 103.
Watson, W. D., and Walmsley, C. M. 1982, in *Regions of Recent Star Formation*, ed. R. S. Roger and P. C. Dewdney (Dordrecht: Reidel), p. 357.
Werner, M. W. 1970, *Ap. Letters*, **6**, 81.
Werner, M. W., and Ellis, H. B. 1985, in preparation.
Werner, M. W., Gatley, I., Harper, D. A., Becklin, E. E., Loewenstein, R. F., Telesco, C. M., and Thronson, H. A. 1976, *Ap. J.*, **204**, 420.
Whithworth, A. P. 1975, *Ap. Space Sci.*, **34**, 155.

A. G. G. M. TIELENS and DAVID HOLLENBACH: Mail Stop 245-6, NASA/Ames Research Center, Moffett Field, CA 94035

© American Astronomical Society • Provided by the NASA Astrophysics Data System

1985ApJ...291..722T

THE ASTROPHYSICAL JOURNAL, 291:747–754, 1985 April 15
© 1985. The American Astronomical Society. All rights reserved. Printed in U.S.A.

PHOTODISSOCIATION REGIONS. II. A MODEL FOR THE ORION PHOTODISSOCIATION REGION

A. G. G. M. TIELENS AND DAVID HOLLENBACH
NASA/Ames Research Center, Moffett Field, California
Received 1984 July 13 accepted 1984 October 31

ABSTRACT

We have constructed a model for the photodissociation region in Orion. This model matches the observed emission in the fine-structure lines of O I 63 μm and 145 μm, C I 609 μm, and C II 158 μm and the low-lying rotational lines of CO. It also explains the extended H_2 1–0 $S(1)$ emission, the carbon recombination lines, and the C I 9850 Å line. The emission in the C I 370 μm, Si II 35 μm, and Fe II 26 μm, 35 μm lines is predicted. The model fit implies that a fairly uniform density ($\sim 10^5$ cm^{-3}) photodissociation region lies behind the Trapezium stars. The peak temperature in this region is about 500 K, and the intensity of the incident far-ultraviolet (FUV) field is approximately 10^5 times as intense as the ambient interstellar field. This model shows that the observed high brightness temperature of the C I 609 μm line can be explained by emission from the C^+/C/CO transition region. This difference with previous chemical models is due to a higher gas phase elemental abundance of carbon, to the charge exchange reactions of C^+ with S and SiO, and to carbon self-shielding.

Subject headings: interstellar: molecules — nebulae: H II regions — nebulae: Orion Nebula

I. INTRODUCTION

In a previous paper we have modeled the chemistry and heating balance in molecular clouds illuminated by an intense far-ultraviolet (FUV) (6 eV $< h\nu <$ 13.6 eV) field (Tielens and Hollenbach 1985, hereafter Paper I). The models assumed an FUV-illuminated plane-parallel slab, so that the calculation was strictly in one dimension, the depth measured in visual extinction A_v into the slab. Microturbulence with a characteristic Doppler width δv_d was assumed to dominate the pressure. Constant hydrogen nucleus density n_0 was assumed, so that the pressure was approximately constant through the slab. The numerical code solved for the equilibrium gas temperature T and the chemistry as a function of A_v. The dominant heating mechanism was found to be the photoelectric ejection of energetic electrons from grains, which transforms up to 0.04 of the incident FUV flux into gas heating. This "heating efficiency" depends on the positive charge of the grains, which in turn depends on a unitless parameter $\gamma \propto G_0 T^{0.5} n_e^{-1}$, with n_e the electron number density and G_0 the FUV flux measured in units of the "Habing field," which is taken to be 1.6×10^{-3} ergs cm^{-2} s^{-1} (Habing 1968). The emergent spectrum from the slab was calculated using an escape probability formalism for the line radiation. The predicted spectra included the fine-structure lines of O I, C I, C II, Fe II, and Si II; the low-lying rotational transitions of CO, and an estimate of the FUV–pumped H_2 1–0 2 μm vibrational transitions. The spectra depended mainly on the model free parameters n_0 and G_0. Other model parameters which generally can be derived from other observations or theoretical considerations include the gaseous elemental abundances, δv_d, the ratio of FUV opacity to optical opacity of the grains, the ratio of A_v to column density of hydrogen nuclei, and the emergent far-infrared continuum flux from dust, F_{IR}, which can be calculated from the dust temperature T_0 and the 100 μm dust optical depth $\tau_{100\,\mu m}$.

The results of the models show that the FUV creates a hot (100–1000 K) layer ($A_v < 3$) of atomic gas (H, O, C^+). This gas is heated by photoelectrons from dust grains and cooled by the O I 63 μm and C II 158 μm fine-structure lines. Around $A_v \approx$ 3–4 atomic hydrogen and ionized carbon are transformed into H_2 and C or CO, respectively. This warm (50–100 K) gas is also heated by photoelectrons from dust grains but is cooled by molecular rotation lines from CO. Beyond $A_v > 4$ carbon is mainly in the form of CO. The gas is now heated by the infrared continuum from warm ($\sim$75 K) dust grains. Ground state atomic oxygen is radiatively excited by 63 μm continuum photons, followed by collisional de-excitation by H_2 molecules which heats the gas. The gas is also heated by collisions with warm dust grains. Cooling still occurs through the CO rotational lines. Deep in the cloud ($A_v > 10$) atomic oxygen is converted into O_2.

These models are relevant not only to the gas which separates H II regions from their parental molecular cloud but also to neutral shells around planetary nebulae, bright-rimmed clouds, reflection nebulae, and regions surrounding protostars. In this paper we will apply our model to the well-studied Orion photodissociation region. Applications to the other regions are deferred to future publications.

This paper is organized as follows. Section II summarizes the observations of Orion. In § III we analyze the fine-structure observations. The emphasis is on a simple semianalytic model which highlights the essential physics. In this way values for physical parameters of this region such as density, temperature, electron density, and intensity of the incident FUV field are derived. The observations are also compared with our detailed numerical model calculations, and a best fit model is constructed. Section IV summarizes the main results.

II. THE OBSERVATIONS

The Orion complex is the nearest site of recent massive star formation. Most of the observational studies devoted to Orion are reviewed in Glassgold, Huggins, and Schucking (1982). In this section we will summarize these and more recent observations relevant to the understanding of the photodissociation region.

© American Astronomical Society • Provided by the NASA Astrophysics Data System

1985ApJ...291..722T

The Orion region has been observed in the O I 63 μm and 145 μm, C II 158 μm, and C I 609 μm fine-structure lines (Melnick, Gull, and Harwit 1979; Furniss *et al.* 1983; Ellis and Werner 1985; Werner *et al.* 1984; Stacey *et al.* 1983; Russell *et al.* 1980; Phillips and Huggins 1981). Table 1 summarizes the observed integrated intensities for these lines, as well as those of the low-lying rotational levels of CO (Phillips *et al.* 1977, 1979). The absolute calibration is uncertain by $\sim$30%. The beam sizes of the far-infrared fine-structure line measurements are all about 45″, except for the C I 609 μm measurement, which has a beam size of 2′.6. The beam size of the CO observations are about 1′.

The O I 63 μm emission in Orion has been mapped with 30″ resolution by Werner *et al.* (1984) and with 1′.65 by Furniss *et al.* (1983). The emission is extended on a 3′ scale and shows two distinct peaks. The northern one is centered on the BN/KL region and is probably associated with the wind shock (Werner *et al.* 1984). The southern peak occurs southwest of the Trapezium, slightly south of the radio continuum peak. It is about halfway between the Trapezium and a peak in the far-infrared and submillimeter continuum (Keene, Hildebrand, and Whitcomb 1982; Werner 1983; Drapatz *et al.* 1983) and in the ^{13}CO column density map (Schloerb and Loren 1982). This southern continuum source does not contain any embedded 20 μm sources brighter than 60 Jy (less than about 10% of the BN object) and probably represents a column-density enhancement (Keene, Hildebrand, and Whitcomb 1982).

In a northwest-to-southeast scan in the O I 63 μm line across the central region of the Orion Nebula, a third peak shows up at the position of θ^2 Ori A, slightly southeast of the prominent ionization bar (Ellis and Werner 1985). It coincides with a peak in the ^{12}CO as well as in the ^{13}CO brightness temperatures (Schloerb and Loren 1982).

The O I 145 μm and C II 158 μm lines have recently been observed both from the Lear Jet and from the Kuiper Airborne Observatory (KAO) (Stacey *et al.* 1983; Ellis and Werner 1985; Russell *et al.* 1980). The distribution of the O I 145 μm and C II 158 μm intensities in a scan across the Orion Nebula looks remarkably similar to that of the O I 63 μm intensity. All three show a peak at the Trapezium and at the ionization bar. These far-infrared lines are more extended and spatially uniform than the continuum.

The Orion region has also been scanned with a 2′.6 beam in the C I 609 μm line (Phillips *et al.* 1980; Phillips and Huggins 1981). The emission in this line is very extended ($\sim$25′). These observations will be discussed in more detail in § III*d*.

The molecular gas temperature as derived from ^{12}CO observations has a peak value of about 75 K in the direction of the BN/KL objects and drops to a value of about 10 K at a distance of 1 pc ($\sim$6′), although the distribution is quite irregular. Distinct patches of higher temperature and column density can be discerned in the CO maps. The ^{12}CO line is expected to become optically thick within the photodissociation region, and therefore the models are constrained to fit these observations.

The carbon radio recombination lines also originate in the photodissociation region. They indicate an electron density of about 10^2 cm^{-3} and a gas temperature in excess of 100 K (Boughton 1978). The red C I lines at 9850 and 8727 Å seem also to be associated with the neutral gas (Münch and Hippelein 1982). It has been suggested that these lines are emitted during the radiative recombination of C^+ and e (Cesarsky 1982). Recently, Treffers (1983) has observed extended H_2 1–0 $S(1)$ emission in Orion. The intensity of this emission is low, and its association with the ionization bar suggests an origin in the photodissociation region.

In addition to the above observations of fine-structure, H_2, CO, and carbon lines which we intend to model, there are a number of observations of the H II region, the photodissociation region, and the molecular cloud which can be used to constrain the model parameters.

The Orion Nebula is an H II region which is ionized by the Trapezium stars, in particular θ^1 Ori C, and to a lesser extent θ^2 Ori A. It appears as a blister on the much larger Orion molecular cloud (Zuckerman 1973; Balick, Gammon, and Doherty 1974). The luminosity of the ionizing stars is about

TABLE 1

COMPARISON OF THE MODEL CALCULATIONS WITH OBSERVATIONS TOWARD ORION

Line	Observed at θ^1 Ori C (ergs cm^{-2} s^{-1} sr^{-1})	Standard Model (ergs cm^{-2} s^{-1} sr^{-1})	Model Fit[a] (ergs cm^{-2} s^{-1} sr^{-1})
O I 63 μm	4 to 6 (−2)	7.5(−2)	4.6(−2)
O I 145 μm	3 to 6 (−3)	3.2(−3)	3.5(−3)
C II 158 μm	4 to 7 (−3)	2.6(−3)	3.8(−3)
C I 610 μm	6.7(−6)	3.5(−6)	8.8(−6)
C I 370 μm	...	1.8(−5)	3.8(−5)
Si II 34.8 μm	...	1.6(−3)	1.8(−3)
Fe II 26 μm	...	1.1(−3)	6.0(−4)
Fe II 35.4 μm	...	1.9(−4)	7.0(−5)
CO J = 1–0	6.5(−7)	4.1(−7)	4.9(−7)
CO J = 2–1	6.0(−6)	4.6(−6)	5.4(−6)
CO J = 3–2	1.9(−5)	1.8(−5)	1.9(−5)
CO J = 4–3	...	4.1(−5)	4.5(−5)
CO J = 5–4	...	7.6(−5)	4.5(−5)
CO J = 6–5	...	1.2(−4)	1.1(−4)
CO J = 7–6	...	1.5(−4)	1.3(−4)
CO J = 8–7	...	1.8(−4)	1.4(−4)
CO J = 9–8	...	1.8(−4)	1.3(−4)

NOTE.—Numbers in parentheses: 7.5(−2) = 7.5 × 10^{-2}.

[a] A possible improved fit with lower than standard dust-to-gas ratio $\delta_d = 0.5$ and a lower gas density $n_0 = 10^5$ cm^{-3} (see text).

© American Astronomical Society • Provided by the NASA Astrophysics Data System

1985ApJ...291..722T

10^5 $L_\odot$, and the stars are located at a distance of about 0.1–0.2 pc from the molecular cloud (Werner *et al.* 1976). This leads to an incident FUV flux of about $G_0 \sim 10^5$.

For the elemental abundances, $\mathscr{A}_i$, the values obtained for the heavily depleted line of sight toward ζ Oph are chosen (Morton 1974; de Boer 1981; Jenkins, Jura, and Loewenstein 1983). Note that for the carbon abundance the upper limit has been chosen (see Table 2). This value is equal to the measured carbon abundance in the Orion Nebula (Peimbert 1982) and is therefore probably more appropriate for models of the Orion photodissociation region (the oxygen abundance in Table 2 is also equal to the measured value in the H II region, as expected if the H II plasma consists of ionized molecular cloud material). The derived lower limit to the carbon abundance toward ζ Oph is half the upper limit (Jenkins, Jura, and Loewenstein 1983). As discussed in Paper I, we do not expect that carbon is depleted in the form of grain mantles in the photodissociation region.

The gas density in the central core of the H II region is about 10^4 cm^{-3}. With a gas temperature of about 10^4 K, the H II region gas pressure against the neutral gas is about 10^8 K cm^{-3}. The pressure in the photodissociation region, $P \propto n_0 \delta v_d^2$ (see Paper I), is therefore constrained to be of this order. The gas distribution in the H II region may, however, be quite clumpy, and the external pressure on the photodissociation region may differ somewhat from this value (see Peimbert 1982).

The photodissociation region gas density and pressure are also constrained somewhat by using millimeter observations of the molecular gas which lies deep in the photodissociation region and beyond, in the opaque molecular core. The somewhat dubious premise here is that the pressure and density deep in the cloud reflect the surface pressure and density. These observations reveal a ridge of high-density ($\sim 10^6$ cm^{-3}) molecular material running N-S through the BN/KL region with a gas temperature of perhaps ~ 50 K. The molecular gas density seems to decrease with a r^{-2} dependence from this region to a value of about 10^3 cm^{-3} at a distance of 1 pc (Westbrook *et al.* 1976; Goldsmith *et al.* 1980; Keene, Hildebrand, and Whitcomb 1982).

Several observations may be used to constrain the turbulent Doppler width δv_d in the photodissociation region. Unfortunately, the line width of the far-infrared fine-structure lines is less than the instrumental resolution (~ 30 km s^{-1}) except for the C I 609 μm line, which has an observed FWHM width of 5 km s^{-1}. (We ignore here the small region of shock-excited O I 63 μm emission toward BN/KL which was resolved by Werner *et al.* 1984.) This places an upper limit on δv_d of about 3 km s^{-1}. The carbon recombination lines indicate that the gas in the photodissociation region has $\delta v_d \approx 2.7$ km s^{-1} behind the Trapezium stars (Boughton 1978), although some velocity structure may be present within the fairly large beams (2'.6) of these observations (Jaffe and Pankonin 1978). In the calculations we will adopt $\delta v_d = 2.7$ km s^{-1}.

Observations which constrain the dust extinction properties are discussed in the next section. However, we note here that the far-infrared continuum observations show a maximum color temperature of the dust of about $T_0 \approx 75$ K and a maximum optical depth at 100 μm ($\tau_{100\,\mu\mathrm{m}}$) of about 0.3 (Werner *et al.* 1976).

TABLE 2

STANDARD MODEL PARAMETERS[a]

Parameter	Standard Model
n_0 (cm^{-3})	2.3(5)
G_0	1.0(5)
δv_d (km s^{-1})	2.7
$\mathscr{A}_C$	3.0(−4)
$\mathscr{A}_O$	5.0(−4)
$\mathscr{A}_{Si}$	7.9(−7)
$\mathscr{A}_S$	7.9(−6)
$\mathscr{A}_{Fe}$	2.5(−7)
$\mathscr{A}_{Mg}$	1.3(−6)
F_{IR} (ergs cm^{-2} s^{-1})	5.0(2)
T_0 (K)	75
$\tau_{100\,\mu\mathrm{m}}$	3.0(−1)
δ_d	1.0

NOTE.—Numbers in parentheses: see Table 1.

[a] The photodissociation region parameters are defined as follows: n_0 is the hydrogen nucleus density, G_0 is the incident FUV flux in units of the "Habing flux" (see Paper I), δv_d is the turbulent velocity width, $\mathscr{A}_i$ is the fractional abundance of species i, F_{IR} is the integrated far-infrared flux from the slab, T_0 is the dust temperature, $\tau_{100\,\mu\mathrm{m}}$ is the dust optical depth at 100 μm, and δ_d is the depletion of dust relative to its abundance in the diffuse interstellar medium, or $\delta_d = (A_v/N_H)/5.2 \times 10^{-22}$ mag cm^2.

III. THE MODEL

The parameters of the standard model in Paper I have been chosen to mimic the conditions expected for the photodissociation region directly behind θ^1 Ori C (Table 2). The calculated emergent line intensities for the standard model are compared with the observations in Table 1. Also shown in this table are the results of a possible best fit model. This model has a lower dust-to-gas ratio ($\delta_d = 0.5$ or $A_v/N_H = 2.6 \times 10^{-22}$ mag cm^2) and a slightly lower gas density (10^5 cm^{-3}) than the standard model ($\delta_d = 1$ or $A_v/N_H = 5.2 \times 10^{-22}$ mag cm^2, the value appropriate for diffuse clouds, and $n_0 = 2.3 \times 10^5$ cm^{-3}). As discussed below, other small changes in the parameters can also produce a good fit. As a result of this change, this model has a somewhat lower temperature throughout the atomic region than the standard model. The maximum temperature, for example, is only 550 K in the best fit model, as opposed to 1100 K in the standard model (cf. Fig. 7 of Paper I). The temperature in the molecular gas is equal to about 50 K in both cases. The behavior of the molecular abundances as a function of visual extinction in this model is quite similar to that in the standard model (cf. Fig. 9 of Paper I). The column density of most species are, however, larger by a factor of 2 because of the increased penetration depth of the FUV.

a) The O I 63 μm *Line*

The core of our interpretation of the O I 63 μm emission in Orion is that the gas is heated by electrons, photoelectrically ejected from dust grains. As much as a few percent of the energy absorbed by a dust grain can be converted into heat for the gas and ultimately into O I 63 μm emission. The remaining heat will be radiated by the grains in infrared continuum radiation. It is the identification of the heat source of the gas that will allow us to calculate the global physical parameters of the region (e.g., T, n_0, and G_0) from the observations.

As will be discussed in detail below, the average efficiency of the photoelectric heating can be obtained from the observed

© American Astronomical Society • Provided by the NASA Astrophysics Data System

1985ApJ...291..722T

total line and continuum flux. This efficiency depends on the unitless parameter $\gamma = 2.9 \times 10^{-5} G_0 T^{0.5} n_e^{-1}$, with T in K and n_e in cm^{-3} (see Fig. 5 of Paper I). Because the intensity of the incident FUV field can be determined from the dust infrared continuum and the gas temperature from an estimate of the peak intensity of the optically thick O I 63 μm line, a reasonable value of the electron density can be derived. Given the carbon abundance, this determines the gas density in the photodissociation region.

The integrated intensity of all far-infrared fine-structure lines is not much more than the O I 63 μm intensity of 5×10^{-2} ergs cm^{-2} s^{-1} sr^{-1} at the Trapezium. The integrated far-infrared continuum intensity at that position is about 1.2×10^1 ergs cm^{-2} s^{-1} sr^{-1} (Werner *et al.* 1976; Drapatz *et al.* 1983). This yields an efficiency ϵ of the photoelectric effect of about 4×10^{-3}. Actually, this efficiency should be divided by 2. In a semi-infinite plane-parallel layer, a good assumption for the O I 63 μm, the cooling radiation only escapes through one boundary. The far-infrared emission from the dust, however, is optically thin and escapes in two hemispheres. This yields for ϵ about 0.2%. Using Figure 6 from Paper I, we then estimate that $\gamma \approx 0.6$, or $G_0 T^{0.5} n_e^{-1} \approx 2 \times 10^4$ $K^{0.5}$ cm^3.

The intensity of the incident FUV field G_0 and the gas temperature T can be estimated in the following way prior to detailed model fits. The average interstellar FUV intensity on a cloud is 1.2×10^{-4} ergs cm^{-2} s^{-1} sr^{-1} (Habing 1968). The observed integrated infrared intensity toward the Trapezium (see above) implies that $G_0 = 10^5$ at that position, assuming that FUV is primarily responsible for heating the dust. The integrated intensity of an optically thick line emerging from a homogeneous (constant density and constant excitation temperature T_x) plane-parallel slab is given by

$$I \approx B_\nu(T_x)\nu(\delta v_d/c) f(\tau) , \quad (1)$$

where $B_\nu(T_x)$ is the Planck function at the frequency of the line, δv_d is the turbulent Doppler width, and the factor $f(\tau)$ arises from optical-depth effects, with τ the line-averaged optical depth (Paper I). The function $f(\tau)$ varies logarithmically with τ and is typically of order unity for $\tau \sim 5$. The O I 63 μm line becomes optically thick for hydrogen nucleus column densities $N_H > 2 \times 10^{21}$ cm^{-2} or $A_v > 1$. In our detailed model calculations, this line is always optically thick ($\tau \sim 5$) and $f(\tau) \sim 1$. Assuming $\delta v_d = 2.7$ km s^{-1} and using the observed intensity in O I 63 μm, we derive $T_x \approx 265$ K.

Using these estimates for G_0 and T_x and assuming that $T = T_x$, we find from the derived value of γ an electron density n_e of 80 cm^{-3} in the photoelectrically heated region. This is in good agreement with detailed models of the carbon recombination lines which originate in the same region (Boughton 1978). If we assume a carbon elemental abundance of 3×10^{-4} as in the models, then the gas density in the photoelectrically heated region is 2.6×10^5 cm^{-3} in order to explain the ratio of the O I 63 μm to the IR continuum intensity.

The parameters of the models are close to these estimates (Table 2). The O I 63 μm intensity calculated for the standard model is actually somewhat higher than the observed intensity (Table 1). This overestimate is caused by the increase in heating efficiency with increasing depth into the cloud (decreasing FUV field and less positively charged grains), an effect ignored in the simple analysis discussed above. This also explains the higher maximum gas temperature ($\sim$1000 K) in the standard model as compared with the 265 K estimated above. The "best fit" model has a somewhat lower value for the density $n_0 = 10^5$ cm^{-3}, in order to lower the cloud surface heating efficiency somewhat. This model therefore has a maximum temperature of about 500 K, which is closer to the "average" temperature estimated from equation (1).

In a similar way we can derive the physical parameters in the photodissociation region behind the prominent ionization bar southeast of θ^1 Ori C. The integrated O I 63 μm intensity is 4×10^{-2} ergs cm^{-2} s^{-1} sr^{-1}, and the total far infrared continuum intensity is 5.3 ergs cm^{-2} s^{-1} sr^{-1} (Werner *et al.* 1976; Ellis and Werner 1985). Therefore, an analogous analysis as described above results in a calculated heating efficiency of 0.4%, an estimated intensity of the FUV field of $G_0 \approx 4.4 \times 10^4$, a gas temperature of 230 K, an electron density of 60 cm^{-3}, and a gas density n_0 of 2×10^5 cm^{-3}. Because of the increase in the efficiency with depth into the slab, the density may have been overestimated by about a factor of 2–3. Despite the lower incident FUV field, the O I 63 μm intensity does not drop appreciably because of the increase in heating efficiency with decreasing G_0. In other words, the O I 63 μm intensity in the model is more spatially uniform than the far-infrared continuum flux, as is observed.

As an aside, it should be noted that the bar is probably an ionization front seen almost edge-on (Becklin *et al.* 1976; Werner *et al.* 1976; Schloerb and Loren 1982; Keene, Hildebrand, and Whitcomb 1982). However, the almost edge-on geometry does not appreciably alter the calculated O I 63 μm intensities, since the gas temperature is relatively constant on the surface of the cloud where O I 63 μm becomes optically thick to the observer (assuming that the photodissociation slab slightly faces the observer). In order to match calculated intensities with observed intensities, one must assume that the face of the photodissociation region fills the beam.

The derived gas density is about an order of magnitude larger than the lower limit to the density estimated from the extent of the 10 and 20 μm emission associated with the ionization bar (Becklin *et al.* 1976). With our estimated density the physical extent of the atomic region emitting the 10 and 20 μm radiation is only 10^{16} cm. The extent along the line of sight is estimated to be about 0.1 pc (Werner *et al.* 1976). This implies that we view the ionization bar at an angle of 70° rather than 90°. Alternatively, the 10 and 20 μm emission may originate from dust just inside the ionized gas, which has a lower density than the gas in the photodissociation region because of the streaming away of material from the ionization front.

The molecular data provide an insight into the overall density distribution in the molecular cloud behind θ^1 Ori C. These data indicate a density of about 10^5 cm^{-3} at a distance of 3′ from the BN/KL region (Goldsmith *et al.* 1980). The region with higher density ($\sim 10^6$ cm^{-3}) in the BN/KL region indicated by the molecular data must then be buried deeper ($A_v > 10$) inside the molecular cloud in order that the photodissociation models match the observations. In our view, the formation of the infrared cluster in the BN/KL region has produced a density gradient (r^{-2}) in the surrounding gas because of gravitational collapse. This density distribution is further modified at the front of the molecular cloud by the presence of the H II region around θ Ori C, which produces a roughly circular slab with a projected radius of about 0.45 pc (3′) in which the density is quite constant ($\sim 10^5$ cm^{-3}). At a distance of about 10′, pressure equilibrium between the H II region and the molecular cloud may not yet have been reached, possibly resulting in the propagation of a slow shock into the molecular cloud (Schloerb and Loren 1982). In Figure 1 a

© American Astronomical Society • Provided by the NASA Astrophysics Data System

1985ApJ...291..722T

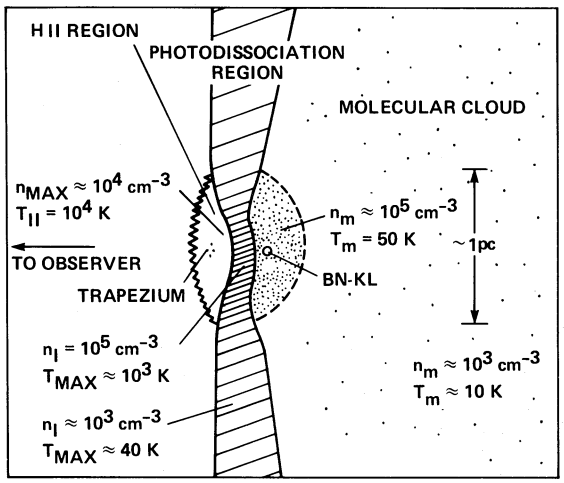

FIG. 1.—Schematic view of Orion region in the model. See text.

schematic view is given of the Orion region in our model. The high-density ($\sim 10^6$ cm^{-3}) molecular gas lies approximately within the small circle around BN/KL. Whether the gravitational collapse in the central region has been induced by the pressure of the H II region (Elmegreen and Lada 1977) cannot be ascertained from the infrared fine-structure data.

b) The C II 158 μm *Line*

The observed intensity of the C II 158 μm line is relatively easy to analyze. Because the density in the photodissociation region is much larger than the critical density, the level populations are given by the Boltzmann distribution function. Because the temperature in the C^+ zone is much larger than the excitation energy (92 K), the level populations are only weakly dependent on T. Thus, for an optically thin line, the C II 158 μm intensity is mainly dependent on the total C^+ column density. For an optically thick line the C II 158 μm intensity is given by the Planck function at the kinetic temperature (cf. eq. [1]). In Paper I a simple analytical model was used to derive the intensity of the C II 158 μm line as a function of the total C^+ column density and the temperature (see Fig. 5 in Paper I). For our best estimate of turbulent Doppler width $\delta v_D = 2.7$ km s^{-1} in the photodissociation region, the observed C II 158 μm intensity implies a temperature of at least ~ 250 K, in good agreement with values estimated from the O I 63 μm line. The observations also imply a total C^+ column density of about 5×10^{18} cm^{-2}.

The column density of C^+ is mainly determined by the penetration of FUV photons into the slab. Typically, the C^+ region extends to a grain optical depth at $\lambda \sim 1000$ Å of $\tau \approx 10$. Assuming "normal" dust properties ($\tau/A_v = 2.6$ and $A_v/N_H = 5.2 \times 10^{-22}$ mag cm^2), $N_H = 6.8 \times 10^{21}$ cm^{-2} is derived. Taking the above C^+ column densities at face value, this implies a carbon abundance of 7.5×10^{-4}, larger than the cosmic abundance value of 4×10^{-4} (Allen 1973) or the carbon abundance in the Orion H II region (Peimbert 1982).

Rather than a superabundance of carbon, the C^+ column density can be raised by two more probable causes. First, the dust in molecular clouds may not have "normal" properties. The extinction curve of the dust along the line of sight to the Trapezium stars differs considerably from the average interstellar extinction curve. The ratio of total to selective extinction, $R = A_v/E_{B-V}$, is larger, and the 2200 Å bump and the ratio of FUV opacity to A_v is smaller ($\tau/A_v \sim 1$), than in the diffuse interstellar medium (Johnson 1968; Bless and Savage 1972; Panek 1983). These differences, in dust which is presumably leftover molecular cloud material, seem to point to a larger mean size of the grains rather than the absence of small grains. The larger grain size may be caused by grain processing in the molecular cloud—for example, by coagulation of large and small grains. If the photodissociation region dust has a similar low FUV opacity, this would increase the extent of the C^+ region. Second, the large C^+ column density may be due to geometrical effects. Viewing the slab at an angle with the normal increases the observed column density, without increasing the extent of the C^+ region. In order to explain the intensities observed in Orion, the slab has to be tilted by about 60°.

These simple analytical considerations agree well with our extensive numerical calculations. The C II 158 μm intensity in the standard model falls short of the observations by about a factor of 2 (Table 2). The C II 158 μm line intensity in the possible best fit model, which has a lower dust-to-gas ratio than the standard model, is in much better agreement with the observations. It should be emphasized, however, that an equally good fit to the observations can be obtained by tilting the slab or by choosing a normal gas-to-dust ratio combined with a gray FUV dust opacity ($\tau/A_v = 1$). At present we cannot rule out any of these possibilities, and it is possible that all are operating. We do note, however, that the observed variations in the C II 158 μm line intensities in Orion are probably due to variations in geometry rather than to dust properties.

c) The O I 145 μm *Line*

The intensity in the O I 145 μm line is a complicated function of density, temperature, and optical depth in both the O I 63 μm and 145 μm lines. It is therefore difficult to interpret the observed O I 145 μm intensities in terms of a simple analytic model. Instead the full-scale numerical model calculation is needed. The intensity of the O I 145 μm line in the standard model is in reasonable agreement with the observations (Table 1). The ratio of the O I 145 μm to the O I 63 μm line may be somewhat small compared with the observations, although it should be kept in mind that the observed intensities are uncertain by about $\pm 30\%$. We note that if this observed ratio is as high as 0.1, then both transitions are optically thick (cf. the curve for $n_0 = 10^5$ cm^{-3} in Fig. 2 of Paper I). In the standard model the O I 63 μm line is optically thick but the O I 145 μm line is still optically thin. Increasing the O column density, as in the possible improved model fit (Table 2), does indeed increase the O I 145 μm/O I 63 μm line ratio. In this model the O I 145 μm line does reach an optical depth of about unity in the warm gas.

d) Origin of the C I 609 μm *and Millimeter* CO *Emission*

The C I fine-structure lines as well as the CO rotational levels originate in the warm (50–200 K) molecular gas deep in the photodissociation region. The calculated intensity of the C I 609 μm line in the standard model is about a factor of 2 lower then the observed intensity in Orion (Table 2). Because this line is optically thin ($\tau \sim 0.5$) in our model, this discrepancy is due to a C I column density which is somewhat too small. As discussed in relation to the C II 158 μm line, this may be caused by geometrical effects or to a difference in the dust properties. This discrepancy may also be attributed to a higher C/O ratio, which tends to shift the C/CO equilibrium toward C

© American Astronomical Society • Provided by the NASA Astrophysics Data System

1985ApJ...291..722T

(see Paper I). In view of the C II 158 μm results, however, the first two explanations are preferred. As exemplified by the results of the possible best fit model in Table 2, a good fit to the observations can be easily obtained.

The calculated intensities for the CO 1–0, 2–1, and 3–2 transitions are in reasonable agreement with the observations (brightness temperatures ≈ 75 K). It should be noted that the brightness temperature of the CO rotational transitions in the model increases with increasing J for low values of J. This is caused by the increase in Einstein A-value with J which makes the higher J-levels optically thick closer to the (warmer) surface. This effect may have been observed in the $J = 6$–5 transition, which is measured to have a brightness temperature of 120 K (Buhl *et al.* 1982).

The column density of neutral carbon in the photodissociation region model is about 10 times larger than previous calculations indicated (Glassgold and Langer 1975; Langer 1976, 1977; de Jong, Dalgarno, and Boland 1980). As discussed in Paper I, this is partly caused by improvements in the chemical modeling: we include charge exchange reactions between C^+ and S and SiO and self-shielding of neutral carbon. The rest of the difference is due to the choice of a higher elemental abundance of carbon in the gas phase than previous studies have assumed (cf. Paper I). This is consistent with recent determinations of the carbon depletion in the diffuse interstellar medium (Jenkins, Jura, and Loewenstein 1983). It should also be emphasized that a high carbon abundance is also needed to explain the C II 158 μm observations.

The low column densities of atomic carbon predicted by previous gas-phase chemistry models failed to provide the observed C I 609 μm intensities. The failure of these chemical equilibrium models has led to several speculations in the literature on the origin of the high atomic carbon column densities inferred from observation.

It has been suggested that the high atomic carbon column densities are caused by the lack of chemical equilibrium in molecular clouds. The chemical equilibrium time scale inside a dense cloud, where the chemistry is dominated by cosmic-ray ionization, is about 10^6 yr. Starting with an atomic cloud (i.e., all carbon in C^+), large abundances of C I are present for $t < 10^6$ yr in time-dependent models (Iglesias 1977; Gerola and Glassgold 1978; Graedel, Langer, and Frerking 1982; Tarafdar *et al.* 1985). However, this young implied age for molecular clouds is in conflict with other observations which suggest ages of 10^7–10^8 yr (cf. Bash and Peters 1976; Bash, Green, and Peters 1977). In particular, the presence of several subassociations suggest a lifetime of the Orion molecular cloud larger than 10^7 yr (Elmegreen and Lada 1977).

The nonequilibrium of the molecular cloud might be caused by turbulence. Boland and de Jong (1982) suggest that churning of atomic material from the surface to the center of the cloud leads to large amounts of C I, because of the photodissociation of CO at the surface and the long time scale for re-formation of CO in the center. However, it should be noted that an FUV radiation field capable of photodissociating CO is also capable of photoionizing C to C^+. Furthermore, the chemical equilibrium time scale in the presence of an FUV field is much shorter than the 10^6 yr quoted above for the interiors of dense clouds (a fact noted by Boland and de Jong 1982). As estimated in Paper I, the chemical equilibrium time scale in photodissociation regions is only 10^4 yr, much shorter than the turbulent circulation time scale. Consequently, photodissociation regions are expected to be in chemical equilibrium, and the carbon brought to the interior by turbulence should be mainly in the form of CO. Indeed, detailed model calculations of Boland and de Jong (1984) show atomic carbon in the photodissociation region of a dark molecular cloud, but the center is entirely CO.

Our photodissociation model for the C I 609 μm emission places the C I in chemical equilibrium at the cloud surface ($A_v < 10$). The emission is barely optically thin ($\tau \sim 1$) and originates in a warm (50 K) molecular gas. Our models predict about 10 times greater atomic carbon column densities than previous theoretical models and match the observationally inferred (optically thin) lower limits on C column densities. In the remainder of this section we argue for these lower limits on the observed C I column densities rather than the higher values favored by Phillips and Huggins (1981). They propose that C I 609 μm is very optically thick, based on a curve-of-growth analysis.

The emission from the C I 609 μm line is very extended ($\sim 25'$), and its brightness temperature is about equal to that of the ^{12}CO $J = 1$–0 line in the outer regions which lie $> 10'$ from θ^1 Ori C. In the central region the brightness temperature of the C I 609 μm line is only about one-third that of the ^{12}CO $J = 1$–0 line. In our model this behavior of the C I 609 μm line is caused by an increase in optical depth with distance from θ^1 Ori C. In the central region the C I 609 μm line has an optical depth < 1 in our model; in the outer regions this line is optically thick. This difference in optical depth is caused not by an increase in the C I column density but rather by a decreased turbulent Doppler width. The C I 609 μm line width decreases from about 5 km s^{-1} in the central region to about 2 km s^{-1} 25′ away (T. G. Phillips 1984, private communication). Therefore, in the outer regions where they are both optically thick, the ^{12}CO $J = 1$–0 and C I 609 μm lines measure essentially the kinetic gas temperature and are insensitive to n_0 and G_0.

Phillips and Huggins (1981) have suggested that the C I 609 μm line is very optically thick even in the center of the OMC-1 region. This conclusion was reached on the basis of a comparison of its line width to that of the ^{12}CO lines and its isotopes. We feel that such a curve-of-growth analysis of this complex region may be misleading. The presence of temperature, density, and turbulent or systematic velocity gradients can lead to erroneous conclusions based on line-width comparisons. For example, the C I 609 μm and ^{13}CO $J = 2$–1 lines are both optically thick in the central region ($\tau_{\rm C\,I} \sim 25$), according to the analysis of Phillips and Huggins (1981), yet their brightness temperatures are much less than the kinetic gas temperature derived from the $J = 1$–0 ^{12}CO line ($\tau \sim 80$).

In our opinion, this difficulty stems from the presence of two regions superposed on the sky: (1) the warm OMC-1 core around BN/KL, including the warm photodissociation region behind the Trapezium, and (2) the cold, lower density molecular gas behind BN/KL (see Fig. 1). These regions have quite different densities, temperatures, column densities, and intrinsic line widths. The H_2CO and CO observations, for example, show complex velocity structure (Bastien *et al.* 1981; Schloerb and Loren 1982). The H_2CO line width (FWHM) is only 1–2 km s^{-1}, which may reflect quiescent conditions much deeper into the Orion molecular cloud, far beyond the photodissociation region. Therefore, we believe that the colder quiescent region has an intrinsic line width (FWHM) of about 1–2 km s^{-1}, while the region around and in front of BN/KL has a line width (FWHM) of about 5 km s^{-1} (or $\delta v_d = 2.7$ km s^{-1}), as inferred from the carbon recombination lines. The CO

© American Astronomical Society • Provided by the NASA Astrophysics Data System

1985ApJ...291..722T

lines with high opacity (e.g., ^{12}CO $J = 2$–1 and $J = 1$–0 and ^{13}CO $J = 2$–1) originate mainly in the warm turbulent region. Those of lower opacity (e.g., ^{13}CO $J = 1$–0 and ^{12}C^{18}O $J = 1$–0 and $J = 2$–1) have a significant contribution from the cold quiescent molecular cloud. Thus, in our model, the increased width of a line does not imply greatly increased column densities, as in a curve-of-growth analysis, but rather is indicative of variations in the velocity field with depth into the cloud. It is apparent from this discussion, however, that high spectral resolution observations of the far-infrared fine-structure lines are important. The C II 158 μm and O I 145 μm lines are ideally suited for determination of δv_d, since they are generally optically thin and both arise in the photodissociation region.

Further discussion of this point must await a more thorough radiative transfer calculation than ours. However, we wish to emphasize that the ^{12}CO and C I 609 μm line intensities calculated for the photodissociation region are in reasonable agreement with the observations (Table 2). Although we have not included ^{13}CO in our chemical calculations, the following simple argument shows that the ^{13}CO line intensities can also be obtained in our model. Assuming that the ^{12}CO/^{13}CO ratio is cosmic (90) and that the kinetic temperature is constant (70 K) over the emitting region, we obtain brightness temperatures from the photodissociation region of 20 and 7 K for the ^{13}CO $J = 2$–1 and $J = 1$–0 lines, respectively. The value for the 2–1 line is in reasonable agreement with the observations. Phillips *et al.* (1979) observed a width corresponding to $\delta v_d \approx 2.9$ km s^{-1} for the ^{13}CO $J = 2$–1 line, consistent with our assumed width for the photodissociation region. The $J = 1$–0 line, however, has a model peak brightness temperature which is about a factor of 2 lower than the observation. Because of the low optical depth of this line in the photodissociation region, it may have a substantial contribution from the cold quiescent molecular cloud. This may explain the observed width of the ^{13}CO $J = 1$–0 line, $\delta v_d \approx 2.3$ km s^{-1}, which is somewhat narrower than lines which originate purely in the photodissociation region.

From this discussion it may appear that measuring the C I 370 μm line in OMC-1 will be helpful in distinguishing whether atomic carbon is mainly at the cloud surface with line opacities of order unity or whether the carbon exists throughout the cloud with correspondingly large opacities. The latter model predicts equal brightness temperatures in the lines. In our model, however, the brightness temperatures depend on the optical depths in the lines and, *a priori*, these might be expected to differ. The optical depths in the 370 and 609 μm lines are, however, quite similar, so that the brightness temperatures of the two lines are similar even in the optically thin case (i.e., both models predict about the same ratio of intensities C I 370 μm/C I 609 μm). In view of the uncertainty in the absolute calibration of submillimeter lines, it appears that measuring the C I 370 μm intensity will not settle this question.

e) C I 9850 Å

The observed intensity of the 9850 Å C I line is somewhat uncertain because of an unknown reddening correction. In our model this line originates within the region $0 < A_v < 3$. Assuming that the wavelength dependence of the dust is represented by van de Hulst curve No. 15, this corresponds to an optical depth at 9850 Å of about 0.5. Correcting the observed intensity (Münch and Hippelein 1982) by this amount of extinction results in an emitted intensity of 1.1×10^{-4} ergs cm^{-3} s^{-1} sr^{-1}. It should, however, be noted that this correction for extinction is uncertain in the photodissociation region. The calculated intensity in the standard model is about 9×10^{-5} ergs cm^{-3} s^{-1} sr^{-1}, in good agreement with this value, lending further support to the suggestion that this line originates from carbon recombination in the photodissociation region (Cesarsky 1982; Münch and Hippelein 1982).

f) H_2 1–0 *S*(1)

The extended emission in the H_2 1–0 *S*(1) line, which we attribute to FUV–pumped H_2 molecules in the photodissociation region, has an average intensity of about 2×10^{-4} ergs cm^{-3} s^{-1} sr^{-1} (Treffers 1983). This implies a column density of H_2 in the $v = 1$, $J = 3$ level of about 7.5×10^{15} cm^{-2}. Assuming that the H_2 molecules in the $v = 1$ state are distributed over the rotational levels according to the kinetic temperature of the gas (~ 500 K), we compute a total column density of H_2 molecules in $v = 1$ of about 2×10^{16} cm^{-2}. According to Shull's (1978) accurate calculations, the column density of H_2 in all $v \geq 1$ states is about 2.5 times that in the $v = 1$ state. This leads to a total "observed" column density of H_2^* of about 5×10^{16} cm^{-2}, which is in good agreement with the predicted standard model value of 4.4×10^{16} cm^{-2} (see Paper I).

It should perhaps be noted that the possible best fit model of Table 1 predicts a H_2^* column density which is about equal to that in the standard model. In both models H_2^* peaks and then rapidly falls off at $A_v > 2$, where dust and H_2 self-shielding both attenuate FUV pumping. The best fit model has a ratio A_v/N_H one-half that of the standard model, so that the extent of the H_2^* region is twice that of the standard model. However, this is offset by the abundance of H_2^*, which is one-half that of the standard model because of the factor of 2 decrease in H_2 formation on grains. If, instead, we had changed the FUV opacity of the dust to $\tau = A_v$, then again we would have increased the extent of the H_2^* region (or the penetration of the FUV) but without lowering the H_2 formation rate. Thus, in this case, the H_2^* column density would have increased by a factor of 2, as H_2 competed more effectively with the dust for FUV photons.

Finally, we note that the detection of extended emission from vibrationally excited H_2^* in Orion implies that H_2 can be formed with high efficiency on warm dust grains. It is difficult to make this more quantitative because of the possible presence of multiple dust components and different sizes, resulting in different grain temperatures in a given region (cf. Paper I).

IV. SUMMARY

We have applied our theoretical model, which calculates the energy balance and chemical equilibrium of dense molecular clouds illuminated by high FUV fields, to the photodissociation region in Orion. Our model can explain the observed intensities in the O I 63 μm and 145 μm, C II 158 μm, C I 609 μm, and the low-lying rotational transitions of CO. It also explains the extended vibrationally excited H_2 emission, the carbon radio recombination lines, and the far-red C I 9850 Å emission.

We have illustrated how the O I 63 μm, C II 158 μm, and IR continuum maps can be used, without the detailed thermochemical modeling described in Paper I, to probe the physical state of the photodissociation region. The ratio of the sum of

© American Astronomical Society • Provided by the NASA Astrophysics Data System

1985ApJ...291..722T

the integrated line strengths to the IR continuum gives an efficiency of gas to grain heating by the FUV incident on the cloud. This efficiency depends on the grain charge, which in turn depends on n_e, G_0, and T. The FUV flux G_0 can be obtained from the IR continuum; the gas temperature T can be estimated from the integrated O I 63 μm or C II 158 μm intensity together with an assumed line width. The measured efficiency, together with G_0 and T, provides the electron density if the photoelectric heating mechanism is valid. The abundance of carbon, which is constrained by the C I and C II fine-structure line strengths, then can be used to derive n_0 from n_e.

A detailed thermochemical one-dimensional model fit to the observed emission from the photodissociation region associated with the Trapezium in Orion is obtained with a gas density of $n_0 = 10^5$ cm^{-3} and an incident FUV flux 10^5 times the average interstellar value. The FUV flux implies that θ^1 Ori C. lies about 0.2 pc from the molecular cloud. The gas density in the photodissociation region is relatively constant to a distance $<3'$ from θ^1 Ori C. The dense ($\sim 10^6$ cm^{-3}) molecular ridge at BN/KL must lie buried deeper ($A_v > 10$) in the cloud. The match to the extended H_2 1–0 $S(1)$ emission implies that H_2 formation occurs efficiently on grains with temperatures $T_{gr} \sim 75$ K.

The large extent of the O I 63 μm emission is a natural consequence of the photoelectric heating mechanism. When the FUV flux drops, the positive grain charge decreases, resulting in a larger heating efficiency per FUV photon. As a consequence, the intensity of the O I 63 μm line, the dominant cooling line of the gas, does not drop as fast as the far-infrared continuum with distance from the exciting star.

Most of the C I 609 μm emission and the ^{12}CO 1–0 emission observed toward OMC-1 originates in the photodissociation region. The ^{12}CO 1–0 transition becomes optically thick at $A_v \sim 4$, and the peak brightness temperature measures the gas temperature at this depth. The C I 609 μm emission is marginally optically thin, so that its peak brightness temperature ($\sim$20 K) lies below the gas temperature. We argue that it is not necessary to invoke nonequilibrium chemistry, and therefore extremely young ages $<10^6$ years, in order to explain C I abundances observed toward molecular clouds. To explain the CO millimeter emission, we propose a two-component model with a warm foreground turbulent region (which includes the photodissociation region) and a cold background quiescent region. Some of the CO lines (e.g., ^{12}CO 1–0 and 2–1 and ^{13}CO 2–1) come from the turbulent region; others (e.g., ^{13}CO 1–0 and ^{12}C^{18}O and 2–1) come from the cold molecular cloud.

We have benefited from discussions with R. Genzel, D. Watson, and M. Werner. We would like to thank the Astronomy/Relativity Branch at NASA Headquarters for their support under NASA RTOP 188-41-53.

REFERENCES

Allen, C. W. 1973, *Astrophysical Quantities* (London: Athlone).
Balick, B., Gammon, R. H., and Doherty, L. H. 1974, *Ap. J.*, **188**, 45.
Bash, F. N., Green, E., and Peters, W. L. 1977, *Ap. J.*, **217**, 464.
Bash, F. N., and Peters, W. L. 1976, *Ap. J.*, **205**, 786.
Bastien, P., Bieging, J., Henkel, C., Martin, R. N., Pauls, T., Walmsley, C. M., Wilson, T. L., and Ziurys, L. M. 1981, *Astr. Ap.*, **98**, L4.
Becklin, E. E., Beckwith, S., Gatley, I., Matthews, K., Neugebauer, G., Sarazin, C., and Werner, M. W. 1976, *Ap. J.*, **207**, 770.
Bless, R. C., and Savage, B. D. 1972, *Ap. J.*, **171**, 293.
Boland, W., and de Jong, T. 1982, *Ap. J.*, **261**, 110.
———. 1984, *Astr. Ap.*, **134**, 87.
Boughton, W. L. 1978, *Ap. J.*, **222**, 517.
Buhl, D., Chin, G., Koepf, G. A., Peck, D. D., and Fetterman, H. R. 1982, in *Submillimeter Wave Astronomy*, ed. J. E. Beckman and J. P. Phillips (Cambridge: Cambridge University Press).
Cesarsky, D. A. 1982, *Astr. Ap.*, **113**, L7.
de Boer, K. S. 1981, *Ap. J.*, **244**, 848.
de Jong, T., Dalgarno, A., and Boland, W. 1980, *Astr. Ap.*, **91**, 68.
Drapatz, S., Haser, L., Hofmann, R., Oda, N., and Iyengar, K. V. K. 1983, *Astr. Ap.*, **128**, 207.
Ellis, H. B., and Werner, M. W. 1985, in preparation.
Elmegreen, B. G., and Lada, C. J. 1977, *Ap. J.*, **214**, 725.
Furniss, I., Jennings, R. E., King, K. J., Lightfoot, F. G., Emery, R. J., Naylor, D. A., and Fitton, B. 1983, *M.N.R.A.S.*, **202**, 859.
Gerola, H., and Glassgold, A. E. 1978, *Ap. J. Suppl.*, **37**, 1.
Glassgold, A. E., Huggins, P. J., and Schucking, E. L., eds. 1982, *Symposium on the Orion Nebula to Honor Henry Draper* (*Ann. NY Acad. Sci.*, Vol. **395**).
Glassgold, A. E., and Langer, W. D. 1975, *Ap. J.*, **197**, 347.
Goldsmith, P. F., Langer, W. D., Schloerb, F. P., and Scoville, N. Z. 1980, *Ap. J.*, **240**, 524.
Graedel, T. E., Langer, W. D., and Frerking, M. A. 1982, *Ap. J. Suppl.*, **48**, 321.
Habing, H. J. 1968, *Bull. Astr. Inst. Netherlands*, **19**, 421.
Iglesias, E. R. 1977, *Ap. J.*, **218**, 697.
Jaffe, D. T., and Pankonin, V. 1978, *Ap. J.*, **226**, 869.
Jenkins, E. B., Jura, M., and Loewenstein, M. 1983, *Ap. J.*, **270**, 88.
Johnson, H. L. 1968, in *Stars and Stellar Systems*, Vol. **7**, *Nebulae and Interstellar Matter*, ed. B. M. Middlehurst and L. H. Aller (Chicago: University of Chicago Press), p. 167.
Keene, J., Hildebrand, R. H., and Whitcomb, S. E. 1982, *Ap. J.* (*Letters*), **252**, L11.
Langer, W. D. 1976, *Ap. J.*, **206**, 699.
———. 1977, *Ap. J.* (*Letters*), **212**, L39.
Melnick, G., Gull, G. E., and Harwit, M. 1979, *Ap. J.* (*Letters*), **227**, L29.
Morton, D. C. 1974, *Ap. J.* (*Letters*), **143**, L35.
Münch, G., and Hippelein, H. 1982, in *Symposium on the Orion Nebula to Honor Henry Draper*, ed. A. E. Glassgold, P. J. Huggins, and E. L. Schucking (*Ann. NY Acad. Sci.*, Vol. **395**), p. 170.
Panek, R. J. 1983, *Ap. J.*, **270**, 169.
Peimbert, M. 1982, in *Symposium on the Orion Nebula to Honor Henry Draper*, ed. A. E. Glassgold, P. J. Huggins, and E. L. Schucking (*Ann. NY Acad. Sci.*, Vol. **395**), p. 24.
Phillips, T. G., and Huggins, P. J. 1981, *Ap. J.*, **251**, 553.
Phillips, T. G., Huggins, P. J., Kuiper, T. B. H., and Miller, R. E. 1980, *Ap. J.* (*Letters*), **238**, L103.
Phillips, T. G., Huggins, P. J., Neugebauer, G., and Werner, M. W. 1977, *Ap. J.* (*Letters*), **217**, L161.
Phillips, T. G., Huggins, P. J., Wannier, P. G., and Scoville, N.Z. 1979, *Ap. J.*, **231**, 720.
Russell, R. W., Melnick, G., Gull, G. E., and Harwit, M. 1980, *Ap. J.* (*Letters*), **240**, L99.
Schloerb, F. P., and Loren, R. B. 1982, in *Symposium on the Orion Nebula to Honor Henry Draper* ed. A. E. Glassgold, P. J. Huggins, and E. L. Schucking (*Ann. NY Acad. Sci.*, Vol. **395**), p. 32.
Shull, J. M. 1978, *Ap. J.*, **219**, 877.
Stacey, G. J., Smyers, S. D., Kurtz, N. T., and Harwit, M. 1983, *Ap. J.* (*Letters*), **265**, L7.
Tarafdar, S. P., Prasad, S. S., Huntress, W. T., Jr., Villere, K. R., and Black, D. C. 1985, *Ap. J.*, **289**, 220.
Tielens, A. G. G. M., and Hollenbach, D. 1985, *Ap. J.*, **291**, 722 (Paper I).
———. 1984, *Icarus*, in press.
Treffers, R. 1983, private communication.
Werner, M. W. 1983, private communication.
Werner, M. W., Crawford, M. K., Genzel, R., Hollenbach, D. J., Townes, C. H., and Watson, D. M. 1984, *Ap. J.* (*Letters*), **282**, L81.
Werner, M. W., Gatley, I., Harper, D. A., Becklin, E. E., Loewenstein, R. F., Telesco, C. M., and Thronson, H. A. 1976, *Ap. J.*, **204**, 420.
Westbrook, W. E., Werner, M. W., Elias, J. H., Gezari, D. Y., Hauser, M. G., Lo, K. Y., and Neugebauer, G. 1976, *Ap. J.*, **209**, 94.
Zuckerman, B. 1973, *Ap. J.*, **183**, 863.

A. G. G. M. TIELENS and DAVID HOLLENBACH: Mail Stop 245-6, NASA/Ames Research Center, Moffett Field, CA 94035

© American Astronomical Society • Provided by the NASA Astrophysics Data System